PHASE RELATIONS OF THE BIOTITES

by

DAVID ROBERT WONES

S.B., Massachusetts Institute of Technology

(1954)

SUBMITTED IN PARTIAL FULFILLMENT

OF THE REQUIREMENTS FOR THE

DEGREE OF DOCTOR OF

PHILOSOPHY

at the

MASSACHUSETTS INSTITUTE OF

TECHNOLOGY

June, 1960

Signature of Author . . . . . .
Department of Geology and Geophysics, May 14, 1960

Certified by . . . . . .
Thesis Supervisor

Accepted by . . . . . .
Chairman, Departmental Committee
on Graduate Students

PHASE RELATIONS OF THE BIOTITES

David R. Wones

Submitted to the Department of Geology and Geophysics on May 14, 1960, in partial fulfillment of the requirements for the degree of Doctor of Philosophy in Geology.

ABSTRACT

Phase relations of the biotites on the join phlogopite $\left[KMg_3AlSi_3O_{10}(OH)_2\right]$ - annite $\left[KFe_3AlSi_3O_{10}(OH)_2\right]$ have been determined at total pressures of 15,000 and 30,000 p.s.i. and at temperatures between 400°C and 900°C. Oxygen pressure was controlled by Eugster's technique of oxygen buffers, using the assemblages copper-cuprite, hematite-magnetite, nickel-nickel oxide, fayalite-quartz-magnetite, and wustite-magnetite.

Optical and lattice properties were determined for biotites on the join phlogopite-annite. Both the index of refraction and d_{060} x-ray reflection exhibit a maximum at an Fe/Fe + Mg ratio of about 0.95, and both properties vary with oxygen pressure. This indicates the presence of "oxyannite" ($KFe^{+2}Fe_2^{+3}AlSi_3O_{10}O_2$) in unspecified quantities. Crystallographic axes were determined for two intermediate biotites and the end member annite.

The position of the equilibrium annite + sanidine + magnetite + vapor was determined reversibly as a function of temperature, total pressure, and oxygen pressure. The data were extrapolated to the equilibrium annite + sanidine + hematite + vapor. Calculations were made concerning the high-temperature phase relations of annite, involving leucite and fayalite.

The intermediate biotites exhibit (at the conditions investigated) phase relations analogous to annite. Solid solution decreases the free energy of the annite molecule. The equilibrium biotite + sanidine + magnetite + vapor was investigated in detail, and the results used to determine the position of the biotite + sanidine + hematite + vapor equilibrium. Extrapolation to other total pressures than those investigated can be made by reference to hydrogen pressure.

Application of these equilibria to natural occurrences is in regard to process rather than absolute values of physical parameters. Hypotheses of igneous and metamorphic petrogenesis involving vapor equilibria may be tested by proper use of biotite phase relations. These relations also provide a simple explanation for the discordance between isotopic ages determined for biotites and other minerals from a common rock.

Thesis Supervisor: Harold W. Fairbairn
Title: Professor of Geology

TABLE OF CONTENTS

TABLES

FIGURES

FOREWORD

The experimental work presented in this thesis was conducted under the Vannevar Bush fellowship program jointly sponsored by the Massachusetts Institute of Technology and the Geophysical Laboratory of the Carnegie Institution of Washington. Prof. Gordon J. F. MacDonald of the Massachusetts Institute of Technology was the original thesis advisor because of his connection with Geophysical Laboratory as Research Associate. The author wishes to express his appreciation of the aid offered by the fellowship, and to Prof. MacDonald for his assistance in the earlier portion of this work. Prof. H. W. Fairbairn assisted in the final stages of preparation.

The work was performed under the direct supervision of Dr. Hans P. Eugster, of the Geophysical Laboratory, and it is the intention of the author to publish the results of this thesis in collaboration with Dr. Eugster. The results will be published in two papers: (1) "The Stability of Annite; Use of Oxygen Buffers in Hydrothermal Experiments" and (2) "Phase Relations of the Biotites on the Join Phlogopite-Annite."

The author is pleased to acknowledge the suggestions, criticism and assistance of Dr. Eugster at all stages of this study. By allowing the author full access to his laboratory and notebooks, Dr. Eugster greatly facilitated many aspects

of the study.

Thanks are due to A. C. Turnock for many discussions, experimental assistance, and aid in preparation of the diagrams, and also to Dr. S. P. Clark, who allowed the author use of his apparatus for some experiments at elevated temperatures.

The author also appreciates the help of Dr. J. F. Schairer and Dr. E. G. Zies, who aided in the preparation of starting materials, and is also grateful for the discussion and criticism which were freely offered by Dr. W. G. Ernst, H. Greenwood, and Dr. G. A. Chinner.

Final writing of the manuscript was done at the Geochemistry and Petrology Branch, United States Geological Survey, and the author wishes to thank Dr. D. B. Stewart, Dr. B. J. Skinner, Dr. H. Shaw, and Dr. E. H. Roseboom for their interest and criticism.

Thanks are due to Miss D. M. Thomas and Miss M. E. Imlay of the Geophysical Laboratory, who prepared the final manuscript, and to A. D. Singer, who prepared the illustrations.

Finally, the author wishes to thank his wife, Constance, who aided in the preparation of this thesis in a variety of ways.

CHAPTER I

INTRODUCTION; OBJECTIVES OF THE INVESTIGATION

1.1 Introduction.

Biotites are common in a large variety of igneous and metamorphic rocks which have formed under an equally large number of tectonic environments. For this reason the determination of phase equilibria involving biotites will yield information concerning the crystallization and recrystallization of such rocks.

There is a definite problem in selecting appropriate compositions for equilibrium studies. The biotites have a wide range of compositions, a fact amply pointed out by Jakob and Parga-Pondal (1932), Kunitz (1924), Hall (1941), Winchell (1935), Heinrich (1946), Nockolds (1947), and Foster (1957). The literature abounds with published analyses of biotites and certain generalizations can be made concerning their compositional variations.

Winchell (1951) has presented the most significant variations in biotite composition by means of a rectangular diagram having the compositions $K_2Mg_6Al_2Si_6O_{20}(OH)_4$, phlogopite; $K_2Fe_6Al_2Si_6O_{10}(OH)_4$, annite; $K_2Mg_5Al_4Si_5O_{20}(OH)_4$, eastonite; and $K_2Fe_5Al_4Si_5O_{20}(OH)_4$, siderophyllite, as the corners of the diagram. Yoder (1959) objects to the term siderophyllite, and Foster (1959, personal communication) considers eastonite to be an invalid mineral name. The writer, however, feels that Winchell's definition of the end members is preferable to that proposed by Yoder, as biotites very close to the two questioned end members have been found (Coats and Fahey, 1944; Winchell, 1935). The two substitutions concerned are the $Mg^{VI}Si^{IV} = Al^{VI}Al^{IV}$ and $Fe^{+2} = Mg^{+2}$ types, where the superscript VI indicates octahedral lattice positions and the superscript IV tetrahedral lattice positions.

Other significant substitutions in the biotite-type structure are substitution of hydroxyl groups by oxygen ("oxybiotite" [Larsen et al., 1937]), and the substitution of Al^{+3} by Fe^{+3} (lepidomelane). To a limited extent potassium can be replaced by sodium, calcium, rubidium and cesium according to the compilation of Heinrich (1946).

Partial solid solutions between biotite (trioctahedral micas) and muscovite (dioctahedral micas) have been conclusively demonstrated by Foster (1957). These intermediate series Yoder (1959) wishes to call "siderophyllite" even though that term has been used for a natural mineral of different composition. The opinion of this writer is that Winchell's terminology has proven the most useful, and the intermediate series can simply be termed biotite-muscovite solid solutions.

The major substitutions using phlogopite, $KMg_3AlSi_3O_{10}(OH)_2$, as the basic formula, are as follows:

1) $K \rightleftharpoons Na \rightleftharpoons Ca \rightleftharpoons Rb \rightleftharpoons Cs \rightleftharpoons Sr$

2) $Mg^{+2} \rightleftharpoons Fe^{+2} \rightleftharpoons Mn^{+2} \rightleftharpoons Li^{+1}$

3) $Mg^{IV}Si^{VI} \rightleftharpoons Al^{IV}Al^{VI}$

4) $Al^{+3} \rightleftharpoons Fe^{+3} \rightleftharpoons Ti^{+3} \rightleftharpoons Mn^{+3}$

5) $Si^{+4} \rightleftharpoons Ti^{+4}$

6) $3Mg^{+2} \rightleftharpoons 2Al^{+3}$

7) $(OH)^{-1} \rightleftharpoons F^{-1} \rightleftharpoons \frac{1}{2} O^{-2} \rightleftharpoons Cl^{-1}$

Because of the large varieties of substitutions, any attempt to determine biotite compositions from optical or X-ray properties can only obtain partial success. Chemical analyses remain the most satisfactory method for determining biotite compositions.

Compositions selected for this investigation were based on the previous work of Yoder and Eugster. Yoder and Eugster (1954) determined the maximum stability of phlogopite as a function of water vapor pressure

and temperature, and Eugster (1957, 1959) had tentatively worked out the stability of annite as a function of oxygen pressure, temperature, and vapor (= total) pressure. Consequently this study was undertaken to examine the phase equilibria of solid solutions between phlogopite and annite under hydrothermal conditions.

1.2 Previous Work.

Previous studies on biotites have been concerned chiefly with composition and physical properties of natural biotites. Major efforts along these lines have been those of Kunitz (1924), Grout (1924), Hall (1941), Winchell (1951), and Foster (1957).

Biotites have been the subject of a great deal of interest in metamorphic assemblages, and phase relations of biotites in metamorphic rocks have been discussed by Harker (1939), Turner (1948), Ramberg (1954), Fyfe, Turner and Verhoogen (1958), Thompson (1957), and many others.

The earliest experiments concerning the stability of biotites are those carried out by Kozu and Yoshiki (1926) and Rinne (1925). These rather crude experiments demonstrated the reversibility of the reaction biotite $\rightleftharpoons$ oxybiotite, a reaction demonstrated hydrothermally by Hellner and Euler (1957).

Biotite synthesis has been demonstrated by Roy (1949), Winkler (1954), Yoder and Eugster (1954), Eugster (1957), Wyart and Sabatier (1959), Crowley and Roy (1958), Ostrovskii (1954), and Veres, Merenkova and Ostrovskii (1955).

Yoder and Eugster (1954) carried out the first biotite stability study in their investigation of phlogopite. Eugster's (1957, 1959) work on annite was the first study on the stability of a ferrous biotite.

1.3 Objectives of this Study.

This study is primarily aimed at the determination of phase equilibria of biotites on the join phlogopite-annite and the application of these relations to natural assemblages. Certain physical properties of this solid solution series have been determined as a by-product of the primary investigation, as has information concerning the experimental technique.

The investigation has consisted of the following: 1) a reexamination of the proposed buffers of Eugster (1957) and the addition of other buffer assemblages; 2) the determination of the optical and lattice properties of biotites on the join between phlogopite and annite; 3) the determination of phase equilibria of those biotites at total pressures of 15,000 and 30,000 p.s.i. and at temperatures between 400° and 900° C; 4) extrapolations and interpolations of these results to physical and chemical conditions not investigated in this study; and 5) an attempt to demonstrate the usefulness of these results in the analysis of natural mineral assemblages containing biotites.

CHAPTER II

EXPERIMENTAL TECHNIQUES; OXYGEN "BUFFER" SYSTEMS

2.1 Experimental Techniques.

The experimental techniques used in this study are the usual hydrothermal techniques. The charges are contained in sealed gold and platinum tubes, which are in turn placed in the "cold seal" pressure vessels described by Tuttle (1949). Pressure is supplied by a 30,000 p.s.i. pump using water as a pressure medium. Pressures were measured on a bourdon type gauge calibrated against a dead weight piston gauge by F. R. Boyd of the Geophysical Laboratory. The actual pressure vessels were closed off from the reservoir system, but were opened to the system every twelve hours, and pressure deviations greater than 500 p.s.i. were noted. In most cases the variation was not noticeable.

Heat was supplied by the standard electrical furnaces, and temperatures were regulated by both on-off type regulators and variable resistance regulators. Temperatures were read by chromel-alumel thermocouples, on a Wolff potentiometer and a multiple recorder. Each entire furnace, bomb, and thermocouple unit was periodically calibrated against the melting point of sodium chloride, and occasionally against the melting point of zinc. Variations in temperature showed a maximum of 5° C, and all experimental temperatures listed in this study are given to $\pm$ 5° C as conservative limits.

The combined pressure-temperature effect for the closed bomb would be 1 per cent, or 300 p.s.i. in the case of a 30,000 p.s.i. experiment. The limits of pressure are set at $\pm$ 500 p.s.i., an extremely conservative value, one which was rarely observed on the pressure gauge.

2.2 Control of Partial Pressure of Oxygen.

The occurrence of iron in several oxidation states requires that phase equilibrium studies of systems containing iron as a component must also consider oxygen as a component. In most experimental systems a vapor phase is present as well as solid or liquid phases and this phase also may have a variable oxygen content. Hence the system has another variable besides bulk composition, temperature, and total pressure.

The new variable may be expressed as partial pressure of the component in the vapor phase, or as the composition of the vapor phase, and is a function of the chemical potential of the particular component. Partial pressure is the usual choice as this quantity is measurable, may be related to other systems, and avoids problems concerning volume and quantity.

The control of partial pressure of oxygen in the determination of phase equilibria has been fairly simple in work done at total pressures of one atmosphere. Under these conditions, a gas reaction such as

$$H_2O = H_2 + \frac{1}{2} O_2 \qquad [2.1]$$

or

$$CO_2 = CO + \frac{1}{2} O_2 \qquad [2.2]$$

will have, for a given temperature, a dissociation constant $(K)_{P,T}$ such that

$$K_{H_2O} = \frac{P_{H_2} \cdot P_{O_2}^{1/2}}{P_{H_2O}} \; ; \; K_{CO_2} = \frac{P_{CO} \cdot P_{O_2}^{1/2}}{P_{CO_2}} \qquad [2.3\ a,b]$$

where P_{H_2} represents the partial pressure of the gas species in question. If the ratio of H_2/H_2O or CO/CO_2 or even H_2/CO_2 is controlled, then the partial pressure of oxygen is specified for the given temperature and pressure.

The dissociation of a solid oxide may be expressed by a reaction such as

$$3Fe_2O_3 = 2Fe_3O_4 + \tfrac{1}{2}O_2 \qquad [2.4]$$

which will also have a dissociation constant

$$K_{HM} = \frac{a_{Fe_3O_4} \cdot P_{O_2}^{1/2}}{a_{Fe_2O_3}} \qquad [2.5]$$

where $a_{Fe_3O_4}$ represents the activity of magnetite in the solid phase. The relation between [2.4] and [2.1] and between [2.5] and [2.3a] is obvious, and demonstrates the desirability of using partial pressure of oxygen as a variable, and the use of gas mixtures to control that variable in phase equilibrium studies. This technique has been used extensively by Darken and Gurry (1945, 1946), Darken (1948), Muan (1955), and Muan and Osborne (1955).

The control of the partial pressure of oxygen under hydrothermal conditions is a result of the work of Eugster (1957). Eugster's technique involves 1) fixing the H_2/H_2O ratio of the aqueous vapor phase, and by means of a semi-permeable membrane, and 2) equilibrating that phase with the system under study. The first step in the technique is accomplished by equilibrating the vapor phase with a solid assemblage of known partial oxygen pressure, termed an "oxygen buffer." The system of interest is sealed in a platinum tube with an excess of water vapor. The oxygen buffering system is packed around this tube with excess water vapor, and the entire assembly is sealed in a gold tube. The buffer fixes the H_2/H_2O ratio of the outer water vapor, then the hydrogen passes through the platinum tube (an osmotic membrane) until an equivalent hydrogen pressure exists in the charge itself. Making the assumption of constant total pressure, the H_2/H_2O ratios of the charge and buffer are equivalent, and consequently so is the partial

oxygen pressure. The platinum membrane prevents contamination of the charge by the oxygen buffer.

Figure 1 plots the base 10 logarithm of the partial pressure of oxygen for each of the buffers used in this study as a function of reciprocal temperature. The data from which this figure is plotted are listed in table 1. These data have been compiled from a number of different sources, and table 2 is a summary of the buffer, the method used to determine its oxygen vapor pressure, and the sources of the data.

2.3 Buffers in the System Fe-O.

The buffer assemblages available in this system are iron-magnetite, iron-wüstite, wüstite-magnetite, and magnetite-hematite. The data concerning the oxygen vapor pressures of these assemblages have been determined experimentally, with the exception of the iron-magnetite assemblage. The equilibria between iron-wüstite and wüstite-magnetite were determined by Darken and Gurry (1945, 1946). Richardson and Jeffes (1948) refined the experimental data of Darken and Gurry to linear equations expressing the Gibbs Free Energy as a function of temperature. By assuming that oxygen at these temperatures and pressure behaves as an ideal gas, the expression

$$\log_{10} P_{O_2} = -\frac{\Delta G}{2.303RT} \qquad [2.6]$$

is readily derived, and is a well known expression in the theory of gas equilibria. By combining [2.6] with the linear expression for ΔG given by Richardson and Jeffes we arrive at the following expression for the partial oxygen pressure of the iron-wüstite assemblage

$$\log_{10} P_{O_2}\ (\text{atm}) = -\frac{27215}{T} + 6.56 \qquad [2.7]$$

and for the wüstite-magnetite assemblage

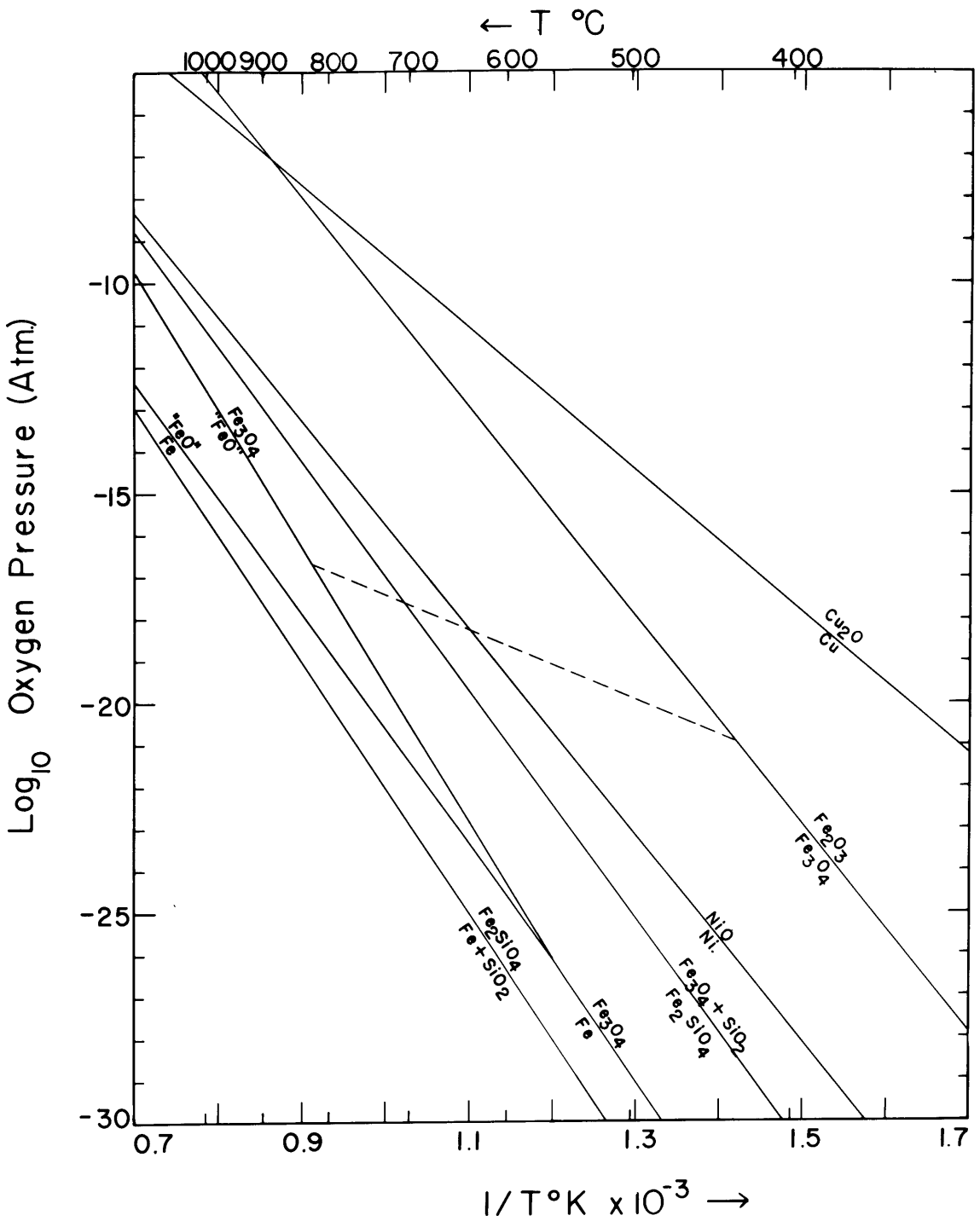

Figure 1. Plot of $\log_{10}$ oxygen pressure of systems used as buffers as a function of inverse temperature. Dashed line plots the locus of the assemblage annite + sanidine + magnetite + vapor at 30,000 p.s.i. total pressure.

Table 1. Log_{10} Oxygen Vapor Pressures of Buffer Assemblages.

T°K	Cu Cu_2O	Fe_3O_4 Fe_2O_3	Ni NiO	Fe_2SiO_4 SiO_2 Fe_3O_4	"FeO" Fe_3O_4	Fe "FeO"	Fe Fe_3O_4	Fe SiO_2 Fe_2SiO_4
400	-34.82	-47.88	-53.22	-57.96			-64.17	-67.19
500	-26.35	-35.42	-40.67	-44.31			-49.54	-52.15
600	-20.70	-27.12	-32.21	-35.21			-39.79	-42.12
700	-16.67	-21.20	-26.42	-28.71			-32.82	-34.96
800	-13.65	-16.74	-21.98	-23.84			-27.60	-29.56
833					-26.18	-26.11	-26.15	
900	-11.30	-13.28	-18.54	-20.04	-23.25	-23.68		-25.41
1000	-9.41	-10.51	-15.70	-17.01	-19.62	-20.66		-22.07
1100	-7.87	-8.25	-13.55	-14.53	-16.64	-18.18		-19.34
1200	-6.59	-6.36	-11.68	-12.46	-14.17	-16.12		-17.06
1300	-5.51	-4.76	-10.10	-10.71	-12.07	-14.38		-15.13

Table 2. Sources of Data for Oxygen Vapor Pressures of Buffers.

Buffer	Source	Method
$Cu-Cu_2O$	Maier (1929)	Experimental Determination
$Fe_2O_3-Fe_3O_4$	Norton (1955)	Experimental Determination
Ni-NiO	Bogatskii (1938)	Experimental Determination
	Wones (See Table 4)	Calculation
$Fe_2SiO_4-SiO_2-Fe_3O_4$	Muan (1955); Darken (1948); Schenck, Franz and Laymann (1932)	Experimental Determination
	Eugster (1959), Wones (See section 4.3)	Experimental Determination
	Wones (See Table 3)	Calculation
Fe_3O_4-FeO	Darken and Gurry (1945)	Experimental Determination
FeO-Fe	Darken and Gurry (1946)	Experimental Determination
$Fe-Fe_3O_4$	Norton (1955)	Calculation
$Fe-SiO_2-Fe_2SiO_4$	Darken (1948); Schenck, Franz, and Laymann (1932)	Experimental Determination

$$\log_{10} P_{O_2} \text{ (atm)} = -\frac{32730}{T} + 13.11 \qquad [2.8]$$

Norton (1955) examined the thermochemical data available for iron and magnetite and gives the following expression

$$\log_{10} P_{O_2} \text{ (atm)} = -\frac{29260}{T} + 8.980 \qquad [2.9]$$

These three equilibria intersect in the invariant four-phase point, iron, magnetite, wüstite, and vapor at a temperature of 560° C, and an oxygen pressure of $10^{-26.15}$ atm. (Foster and Welch, 1956, report a value of 570° C, but do not indicate the basis for their value.)

The magnetite-hematite buffer in this system has been studied by a number of different investigators. Norton (1955) has summed up the work of past investigators, and has also made measurements at lower temperature by a mass spectometric method. His expression for this equilibrium is

$$\log_{10} P_{O_2} \text{ (atm)} = -\frac{24912}{T} + 14.400 \qquad [2.10]$$

2.4 Buffers in the System Fe-Si-O.

The buffers in this system are iron-silica-fayalite and fayalite-magnetite-silica. Eugster (1959) has shown the uncertainties involved in the exact location of these equilibria. For the reaction iron + silica + oxygen = fayalite, Eugster used the experimental data of Schenk et al. (1932) and an extrapolation by Darken (1948). By assuming the Gibbs Free Energy a linear function of temperature, the following expression may be derived

$$\log_{10} P_{O_2} \text{ (atm)} = -\frac{30080}{T} + 8.01 \qquad [2.11]$$

The data for the reaction fayalite + oxygen = silica + magnetite has been derived from three sources. Muan (1955) has determined the partial oxygen pressure of the ternary invariant point, tridymite +

+ magnetite + fayalite + liquid + vapor at (1140° C), as 10^{-9} atm. This value combined with the data of Schenck et al. (1932) yields the following expression

$$\log_{10} P_{O_2} \text{ (atm)} = -\frac{27300}{T} + 10.29 \qquad [2.12]$$

The data presented by Eugster (1959) and this work (see section 4.3) for the mica, annite, allow a determination of the point of intersection of the partial pressure-temperature plots of the assemblage annite + sanidine + magnetite + oxygen + water. This value is 705° ± 5° C, $10^{-17.60}$ atm. oxygen pressure at a total pressure of 30,000 p.s.i. These data, combined with that of Muan, yield the expression

$$\log_{10} P_{O_2} = -\frac{27619}{T} + 10.55 \qquad [2.13]$$

This is in exceptional agreement with [2.12], and for purposes of plotting up experimental data [2.12] is used as it is the more independent of the two.

Thermochemical calculations using the sources of data given in table 3 are in close agreement with the above data. However, the calculations have a probable error of a kilocalorie, which corresponds to an order of magnitude in oxygen pressure. The calculated expression is

$$\log_{10} P_{O_2} = -\frac{27400}{T} + 10.72 \,. \qquad [2.14]$$

2.5 The Nickel-Nickel Oxide Buffer.

The oxygen vapor pressure for this assemblage has been determined both by a calculation from the existing thermochemical data, and by the actual measurement of CO/CO_2 ratios of the gas coexisting with the assemblage (Bogatskii, 1938). The thermochemical data was obtained by calorimetric methods and the sources are listed in table 4. Bogatskii approached equilibrium by oxidizing nickel metal with CO_2 and reducing nickelous oxide with CO. The excellent agreement of the two investigations is given in

Table 3. Data Used for Calculation of the Oxygen Vapor Pressure of the Quartz-Magnetite-Fayalite Assemblage.

Phase	Thermodynamic Quantity		Source
Quartz	ΔH_{298}	-210.3 Kcal/mole	Humphrey and King (1952)
	Cp		Kelley (1949)
	S_{298}	10.0 cal/°/mole	Kelley (1950)
Tridymite	ΔH_{298}	-209.6 Kcal/mole	Humphrey and King (1952)
	Cp		Kelley (1949)
	S_{298}	10.2 cal/°/mole	Kelley (1950)
Magnetite	ΔH_{298}	-267.0 Kcal/mole	Humphrey, King, and Kelley (1952)
	Cp		Coughlin, King, and Bonnickson (1951)
	S_{298}	35.0 cal/°/mole	Kelley (1950)
Fayalite	ΔH_{298}	-346.0 Kcal/mole	King (1952)
	Cp		Orr (1953)
	S_{298}	34.7 cal/°/mole	Kelley (1950)

Table 4. Data Used for Calculation of Oxygen Vapor Pressure of Ni-NiO Assemblage.

Phase	Thermodynamic Quantity		Source
NiO	ΔH_{298}	57.3 Kcal/mole	Boyle, King, and Conway (1954)
	Cp		King and Christensen (1958)
	S_{298}	9.2 cal/°/mole	Kelley (1950)
Ni	Cp		Kelley (1949)
	S_{298}	7.12 cal/°/mole	Kelley (1950)
O_2	Cp		Kelley (1949)
	S_{298}	49.01 cal/°/mole	Kelley (1950)

Table 5. Log_{10} Nickel-Nickel Oxide Oxygen Vapor Pressure.

T°K	Calculation	Bogatskii (1938)
773	-23.08	-23.50
873	-19.42	-19.82
973	-16.48	-16.50
1073	-14.08	-14.06
1173	-12.05	-12.02
1273	-10.96	-10.30
1373	-9.08	-8.84

table 5 and may be summarized by the expression

$$\log_{10} P_{O_2}\ (\text{atm}) = -\frac{24766}{T} + 8.96 \qquad [2.15]$$

2.6 The Copper-Cuprite Buffer.

The oxygen vapor pressure of the assemblage copper (Cu) and cuprite (Cu_2O) has been determined by both calculation and experimental determination. The calculations are based on the thermochemical data given in table 6, and are based on heat of formation values determined by e.m.f. measurements. The summary of Randall, Nielsen, and West (1931) shows that a multiplicity of cells determined by several authors concur to a value of about 40,000 cal. for the heat of formation.

Unfortunately, the two sets of actual vapor pressure measurements do not concur with the calculated values. The data of Maier (1929) yield a value of partial oxygen pressure about an order of magnitude higher than that determined by calculation. The data of Roberts and Smyth (1921) for the vapor pressure of liquid copper and cuprite also indicate that the vapor pressure of the assemblage is higher than that calculated.

A possible explanation could be in the non-stoichiometric composition of Cu_2O. However, the investigations of Wrigge and Meisel (1932) and those of Wagner and Hammen (1938) indicate that Cu_2O is very close to ideal composition. The high temperature work of Kiukkola and Wagner (1957) on the copper-cuprite cell also is in fair agreement with that of the low temperature e.m.f. determinations.

The value of this particular buffer assemblage lies in the fact that its vapor pressure curve crosses the curve for hematite and magnetite. The value of this "cross over" temperature is of course dependent on the vapor pressure of cuprite-copper assemblages.

Table 6. Data Used for the Calculation of Oxygen Vapor Pressure of the Copper-Cuprite Assemblage.

Phase	Thermodynamic Quantity		Source
Cu_2O	ΔH_{298}	-39.95 Kcal	Randall, Nielsen, and West (1931)
	Cp		Kelley (1949)
	S_{298}	22.44 cal/°/mole	Hu and Johnston (1951)
Cu	Cp		Kelley (1949)
	S_{298}	7.97 cal/°/mole	Kelley (1950)
O_2	Cp		Kelley (1949)
	S_{298}	49.01 cal/°/mole	Kelley (1950)

An extrapolation of Maier's data was used in calculating the oxygen vapor pressure of copper-cuprite assemblages. The expression used is

$$\log_{10} P_{O_2}\ (\text{atm}) = -\frac{16934}{T} + 7.52 \qquad [2.16]$$

Table 7 lists a comparison of oxygen pressures according to 1) calculation using the ΔH_{298} given by Makolkin (1942); 2) calculations by Richardson and Jeffes (1948); 3) calculation by Norton (1955); 4) extrapolation of the data of Kiukkola and Wagner (1957); and 5) extrapolation of the data of Maier (1929).

An attempt was made by the author to compare the vapor pressures of hematite-magnetite and copper-cuprite assemblages in silica glass tubes at various temperatures, but the high volatility of copper resulted in the formation of copper ferrite, so that such a comparison was impossible.

The affinity of copper and gold under hydrothermal conditions is so great that the actual buffer assemblages are $Cu_xAu_y + Cu_2O$ rather than $Cu + Cu_2O$. Kubaschewski and Evans (1958) give an idealized treatment for this reaction which indicates that the partial oxygen pressures of the experiments is at least an order of magnitude higher than that of the $Cu + Cu_2O$ assemblages. Consequently, experiments made with this buffer were used for their qualitative value only.

2.7 Partial Pressure of Oxygen at Elevated Pressure.

At pressures below and including one atmosphere, one may assume that oxygen behaves as an ideal gas; however, at elevated total pressures its behavior is non-ideal. At these pressures it becomes convenient to substitute fugacity for partial pressure. Fugacity has the dimension of pressure and obeys the perfect gas laws. It is related to pressure by the expression

$$f = \gamma P \qquad [2.17]$$

Table 7. Log_{10} Oxygen Vapor Pressure of the Cu-Cu_2O Assemblage.

T°K	Calculation	Richardson and Jeffes (1948)	Norton (1955)	Kiukkola and Wagner (1957)	Maier (1929)
400	-35.93	-37.09	-36.39	-37.65	-34.82
500	-27.22	-28.35	-27.85	-28.50	-26.35
600	-21.48	-22.53	-22.15	-22.40	-20.70
700	-17.36	-18.36	-18.08	-18.04	-16.67
800	-14.30	-15.24	-15.03	-14.78	-13.65
900	-11.92	-12.81	-12.65	-12.23	-11.30
1000	-10.04	-10.87	-10.75	-10.20	-9.41
1100	-8.50	-9.28	-9.20	-8.54	-7.87
1200	-7.23	-7.96	-7.90	-7.15	-6.59
1300	-6.16	-6.84	-6.81	-5.98	-5.51

when γ is the activity coefficient and is a function of total pressure and temperature.

The variation of fugacity with total pressure is easily derived from the expression for the Gibbs Free Energy

$$d\Delta G = \Delta V\, dP - \Delta S\, dT \qquad [2.17]$$

at constant temperature this expression becomes

$$d\Delta G = \Delta V_S\, dP_T + \Delta V_g\, dP_g$$

where ΔV_s = volume change of solid phases, P_T represents total pressure, ΔV_g represents the volume of gas in question, and P_g represents the pressure of the gas in question. As ΔG must remain zero at equilibrium this expression becomes

$$\int_{P_1}^{P_2} \Delta V_g\, dP_g = -\int_{P_1}^{P_2} \Delta V_s\, dP_T \qquad [2.18]$$

As the compressibilities of the solid phases are very small, the right hand term becomes simply $-\Delta V_S[P_2-P_1]$. As the fugacity assumes ideality

$$\Delta V_g\, dP_g = \frac{RT}{f_g}\, df_g \qquad [2.21]$$

and

$$\int_{f_1}^{f_2} \frac{RT}{f_g}\, df_g = RT \ln f_2/f_1 \qquad [2.22]$$

so that

$$RT \ln f_2/f_1 = -\Delta V_S [P_2 - P_1] \qquad [2.23]$$

The actual pressure may be determined by use of the activity coefficient given by Newton (1935). Table 9 lists the $\int_{P_1}^{P_2} \Delta V_S\, dP_T$ term for each of the utilized buffers at 2000 atm. total pressure, the resultant partial fugacity, and the calculated oxygen pressures at a constant temperature of 1000° K, and table 8 lists the volume data and sources of the several phases.

Figure 2 plots the base 10 logarithm of the partial oxygen pressure as a function of temperature (°C) for each of the buffer assemblages at 2000 atmospheres.

Table 8. Volumes of Phases in Buffer Assemblages.

Phase	Vol. cc/mole	Source
Cu	7.114 ± 0.002	Palache, Berman, and Frondel (1944)
Cu_2O	23.2 ± 0.4	Palache, Berman, and Frondel (1944)
Fe_2O_3	30.4 ± 0.1	Palache, Berman, and Frondel (1944)
Fe_3O_4	44.5 ± 0.3	Rooksby (1951)
$Fe_{0.947}O$	11.96 ± 0.4	Donnay and Nowacki (1954)
Fe_2SiO_4	47.4 ± 2.0	Adams (1931)
SiO_2	22.64 ± 0.03	Wyckoff (1926)
Fe	7.09 ± 0.01	Kubachewski and Evans (1958)
Ni	6.50 ± 0.05	Donnay and Nowacki (1954)
NiO	10.88 ± 0.10	Kubachewski and Evans (1958)

Table 9. $\log_{10} P_{O_2}$ at 2000 Atm. Total Pressure and 1000° K.

Buffer	$\int_1^{2000} \Delta V_s dp$ (in calories)	$\log_{10} f_{O_2}$	$\log_{10} P_{O_2}$
$Cu + Cu_2O$	856	-9.22	-9.55
$Fe_3O_4 + Fe_2O_3$	210	-10.46	-10.79
$Ni + NiO$	411	-15.61	-15.94
$SiO_2 + Fe_3O_4 + Fe_2SiO_4$	704	-16.86	-17.19
$FeO + Fe_3O_4$	528	-19.50	-19.83
$Fe + FeO$	564	-20.54	-20.87
$Fe + Fe_3O_4$	528		
$Fe + SiO_2 + Fe_2SiO_4$	555	-21.95	-22.28

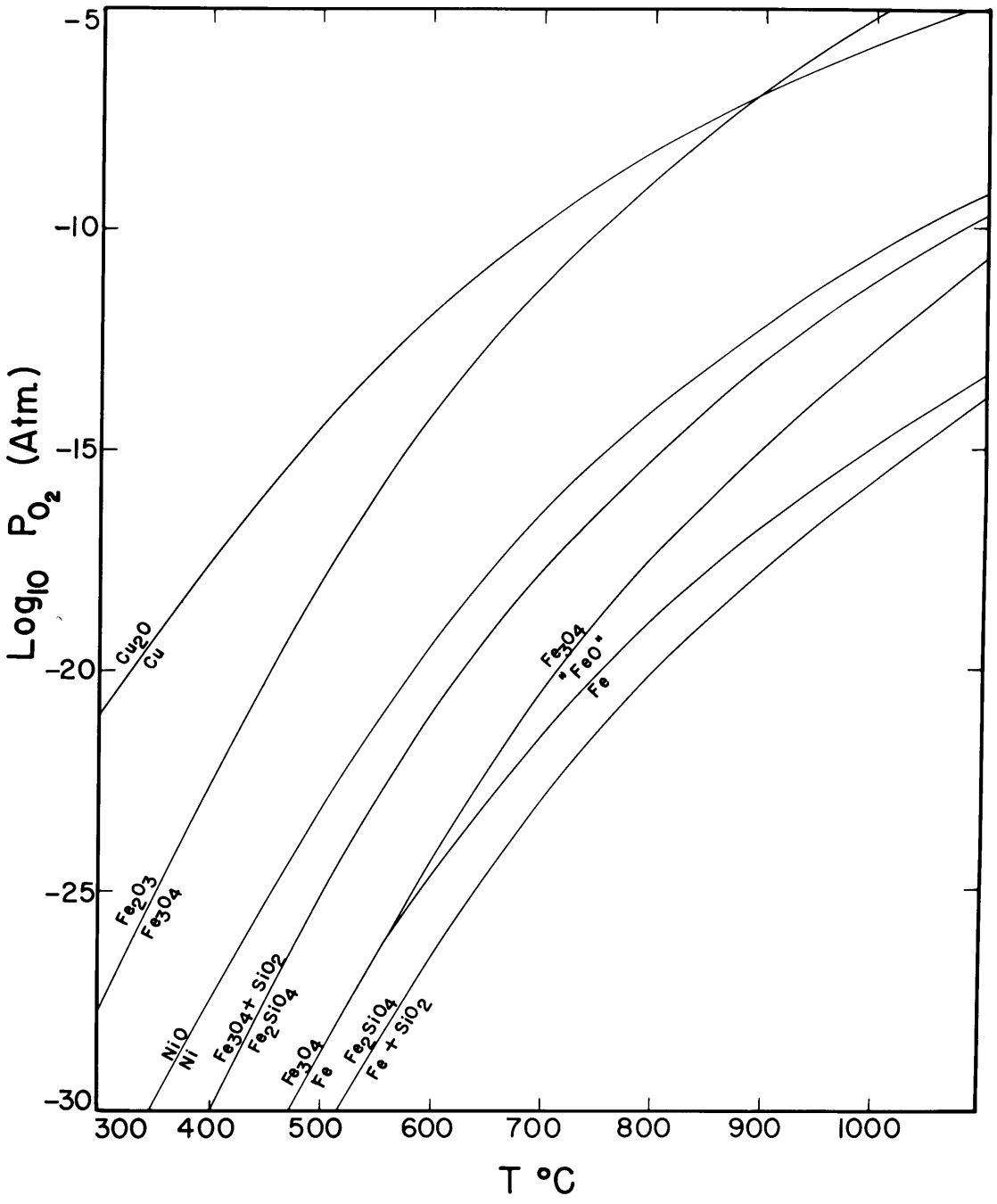

Figure 2. Plot of $\log_{10}$ oxygen pressure of systems used as buffers as a function of temperature at a total pressure of 2000 atmospheres.

2.8 Change of Quadruple Point Iron-Wüstite-Magnetite-Oxygen with Total Pressure.

This calculation is based on the Clapeyron equation

$$dT/dP = \Delta V / \Delta S \qquad [2.19]$$

for the reaction

$$0.78\ Fe + Fe_3O_4 = 4\ Fe_{0.947}O \qquad [2.20]$$

Iron Magnetite Wüstite

The volume data are taken from Kubachewski and Evans (1956) (iron), Donnay and Nowacki (1954) (wüstite), and Rooksby (1951) (magnetite). The entropy data at 298.16° K is taken from Kelley (1950) (iron and magnetite), and Humphrey, King, and Kelley (1952) (wüstite). The heat capacity data is taken from Kelley (1949) (iron) and Coughlin, King, and Bonnickson (1951) (wüstite and magnetite). The calculated slope is 0.83° C/kilobar which is negligible for this study, assuming that the compressibility and thermal expansion of the solid phases are also negligible.

2.9 Composition of the Gas Phase at Elevated Pressures.

In the experimental work presented here, the actual vapor phase present is a mixture of hydrogen and water. Knowledge of the actual composition of the gas phase is desirable for a better understanding of the actual experiment. Eugster (1959) has calculated the H_2/H_2O ratio for the water vapor in equilibrium with the iron bearing phases, using the equilibrium constant of water as given by Wagman et al. (1945), for one atmosphere total pressure.

The same approach may be made at high pressure by making three assumptions. These are 1) there are no interactions between gas species, so that the law of partial fugacities remains valid; 2) there are no new gas species formed such as H_4, O_3, H_4O_2, etc.; and 3) that the equilibrium

constant does not change with pressure.

The last assumption is valid if the calculations are made for fugacities, rather than pressures, as the equilibrium constant is defined as a function of temperature only. Any consequent shifts in that constant would be due to the non-ideal compressibilities of the involved gases, and this property is accounted for through the use of activity coefficients as discussed by Newton (1935).

The assumption regarding partial fugacities and gas species must remain unanswered for a lack of experimental data. However, as is shown in chapter 4, the experimental results of this thesis certainly indicate that these assumptions can be made safely.

An approximation of the hydrogen pressures encountered for each buffer can be made by these methods, and these pressures are listed in table 10, for a total vapor pressure of 2000 bars. Figure 3 plots the hydrogen pressure of each of the several buffers as a function of temperature at a total pressure of 2000 bars. The activity coefficients of hydrogen and water which were used are those given by Newton (1935) and Holser (1954) respectively.

2.10 Considerations Concerning the Use of Buffers.

In practice the use of the buffer technique requires two assumptions which must be evaluated. The first of these is the rapid equilibration of hydrogen pressure between buffer and charge. At temperatures above 600° C equilibrium is rapidly maintained as can be shown by the formation of hematite and magnetite from starting material containing all hematite, all magnetite, or neither (i.e., biotite). As this buffer has the lowest hydrogen pressure (other than copper-cuprite) of the ones in use, it should be the most difficult to equilibrate, and,

Table 10. Hydrogen Pressures (in Atm.) at 2000 Atm. Total Pressure.

T°K	Cu Cu_2O	Fe_3O_4 Fe_2O_3	Ni NiO	Fe_2SiO_4 SiO_2 Fe_3O_4	"FeO" Fe_3O_4	Fe "FeO"	Fe Fe_3O_4	Fe SiO_2 Fe_2SiO_4
600	4×10^{-7}	4.7×10^{-4}	0.264	6.54			737	1837
800	1.6×10^{-4}	6.6×10^{-3}	2.62	20.20			799	1773
1000	3.5×10^{-3}	1.5×10^{-2}	5.51	22.93	469	891		1606
1200	2.6×10^{-2}	2.0×10^{-2}	10.11	23.32	161	904		1417

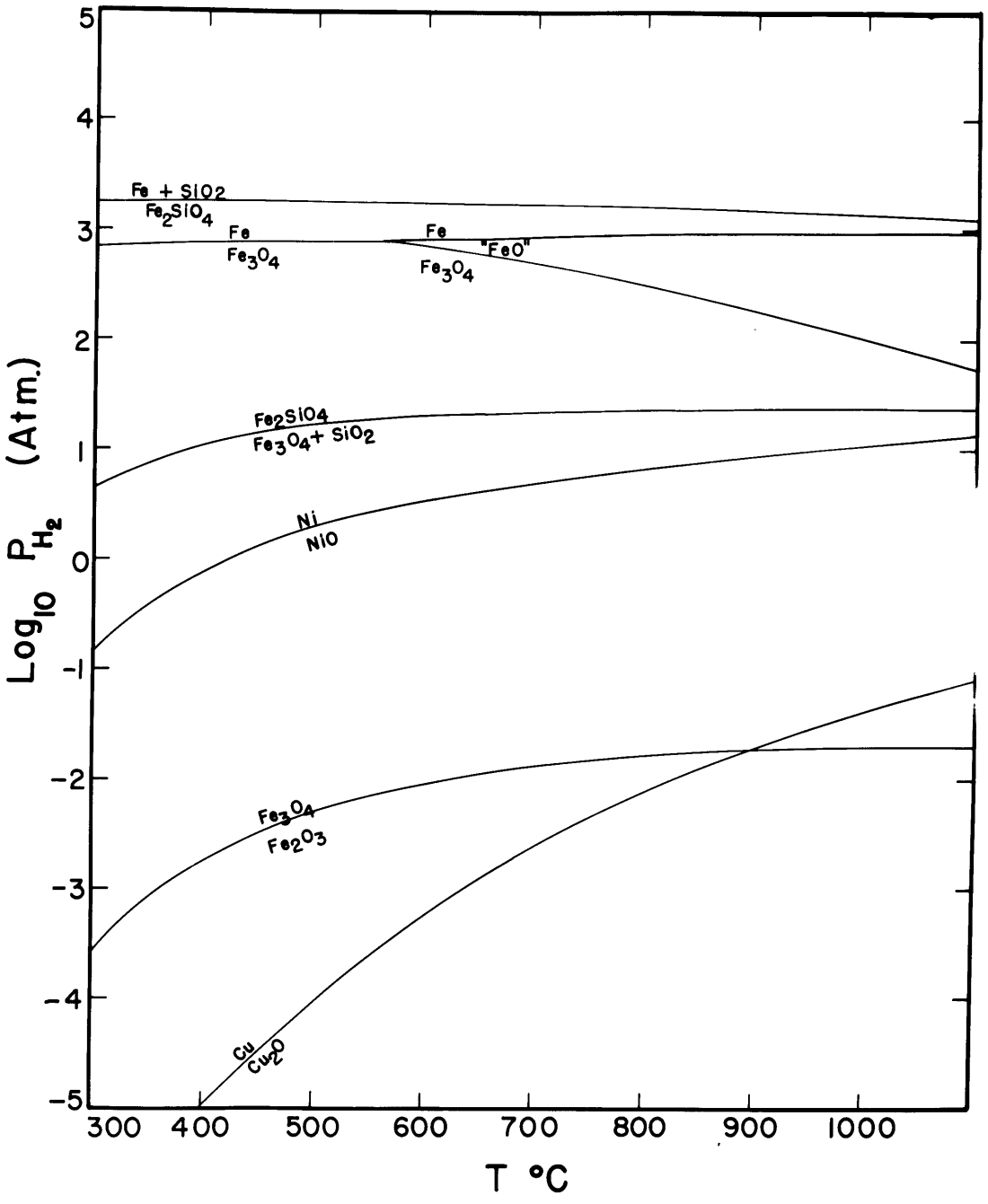

Figure 3. Plot of $\log_{10}$ hydrogen pressure of systems used as buffers as a function of temperature at a total pressure of 2000 atmospheres.

indeed, at temperatures below 600° C it appears that runs of extended duration do not necessarily equilibrate charge and buffer.

Finally, certain of the phase relations investigated may be expressed as functions of hydrogen pressure rather than oxygen pressure. In one set of experiments the inner charge contained carbon dioxide as well as water and hydrogen, and the observed equilibria were identical to those where only pure water and hydrogen were present (see section 4.11).

The second assumption requiring examination is that the equilibration of hydrogen pressures will result in equivalent oxygen vapor pressures. If the total gas pressures in the charge and buffer are the same, this assumption is a fact. However, differential solubilities of the solid phases in the charge as opposed to the buffer will affect the total vapor pressures, and, consequently, the oxygen vapor pressure.

Morey (1957) has determined the solubility of microcline and hematite at 2000 atmospheres pressure and 500° C to be 2480 ppm and 90 ppm respectively. This deviation is extremely small, but none the less is real. Hence, charges buffered by the hematite-magnetite buffer should be all magnetite. However, in this study both hematite and magnetite were observed in the interior of the charge. As the variations in partial oxygen pressure are so small, any oscillation of temperature within 0.1° C will cause the equilibrium to oscillate from hematite to magnetite and thus counteract the effect of differential solubilities.

The oxygen buffers have been shown to be equilibrium experiments in the following ways: 1) the reversibility of oxidation-reduction reactions has been unequivolcally demonstrated; 2) the assemblages within the charge (whenever phase reactions are appropriate) contain the same

phases occurring in the buffers; and 3) the data has been shown to be consistent from buffer to buffer, demonstrating both the equilibrium qualities of the buffers and the quality of the original data of the buffer assemblages.

The greatest problem in using the buffer technique is run duration. The gold tube containing the buffer is very slightly permeable to hydrogen. This means that in investigations at temperatures over 750° C the investigator must quench the run and repack the buffer every 3 to 4 days. In the apparatus used for these experiments an aqueous pressure medium was used, which in turn was "buffered" by the bomb alloy. Consequently hematite-magnetite buffers were reduced to magnetite and quartz-fayalite-magnetite mixtures were oxidized to quartz and magnetite during extended runs. The nickel-nickel oxide buffer proved quite simple to use for extended periods, indicating that the H_2/H_2O ratio of the pressure medium in the stellite bomb was very close to that of water vapor in equilibrium with Ni-NiO.

During the course of this study runs in which the buffers either were completely oxidized, reduced, or completely alloyed with the gold and platinum containers were discarded except for their qualitative value.

CHAPTER III

EXPERIMENTAL TECHNIQUE IN ESTABLISHING PHASE EQUILIBRIA; COMPOSITION OF PHASES

3.1 Technique for Determining Phase Equilibria.

The technique employed was to synthesize biotites of known composition and then subject them to various conditions of total pressure, temperature, and partial pressure of oxygen (buffer). The occurrence of new phases (K-feldspar and iron oxides) was noted, and the composition of the biotite coexisting with these phases was determined both from optical properties and $d_{(060)}$ reflection using predetermined curves.

Equilibrium was demonstrated by approaching it from two sides, once by reacting biotite with oxygen to form K-feldspar, iron oxide, and a new biotite, then by reacting a mixture of phlogopite, K-feldspar, and iron oxide (magnetite). This is the only real proof of equilibrium. It was found that in three to five days (depending upon temperature and pressure) the biotites reacted completely to form the equilibrium assemblage. Consequently the largest portion of the phase diagrams established in this study are determined from an oxidation reaction. Whenever practical two or more compositions and/or starting materials were used to verify the position of the observed equilibrium.

3.2 Reagents.

The phase assemblages produced in this study were synthesized from mixtures of several reagents. Potassium silicate glass of the composition $K_2O \cdot 6SiO_2$ was prepared and then crystallized using the technique of Schairer (1954) under his direction. This was used as the source of K_2O and SiO_2. Iron was weighed as Fe_2O_3 (J. T. Baker Lot No. 4137) or as $FeC_2O_4 \cdot 2H_2O$ (Fisher Lot No. 541312). The oxalate was analyzed by E. G. Zies

and was found to contain, by weight, Fe, 30.54 per cent; Mg, 0.21 per cent; Mn, 0.07 per cent; Na, 0.13 per cent; Ca, 0.04 per cent; and C_2O_4, 49.04 per cent.

The source of magnesium was pure MgO (J. T. Baker Lot No. 82735). Al_2O_3 was added as γ-alumina prepared by heating $AlCl_3 \cdot 6H_2O$ (Baker Lot No. 772760) at 700° C for 1 hour, a technique reported recently by Stirland, Thomas and Moore (1958). Diffraction patterns of the γ-Al_2O_3 showed only the γ-Al_2O_3 reflections and the material was optically homogeneous.

3.3 Synthesis of Biotite.

Biotites were synthesized from mixtures of these reagents or their reduced equivalents. The mixtures were weighed and then mixed by grinding under acetone in an agate mortar for 1 hour. The hematite and oxalate mixes formed in this way were used to form a third mix, referred to as an iron mix, which was formed by passing hydrogen over the mix at 700° C. The hematite and iron mixes were used as starting materials in establishing the phase relations of the biotites, but the oxalate mix was used in the synthesis of biotites in bulk quantities. Some earlier runs were made using oxalate mix as starting material. Their usefulness is described in section 4.13.

The actual synthesis of the biotites was accomplished by placing the oxalate mix in an unsealed silver capsule which in turn was surrounded by water and oxalate mix within a large sealed platinum tube. Synthesis of biotites from the oxalate mix in sealed gold tubes resulted in the formation of graphite, but the diffusion of hydrogen out of platinum tubes was sufficient to oxidize all graphite to CO/CO_2 vapors, which would be released when the capsule was opened. The water permeated the silver

foil capsule, but the leaching of iron by the outer tube was confined to the outer charge. Consequently by removing the silver foil capsule from the interior of the charge, one could easily separate the portion of the charge at constant composition. This same technique was used in the phase equilibrium experiments, and appeared to be quite satisfactory in preventing loss of iron from the system under study. Synthesis was carried out for 48 hours at 500° C and 30,000 p.s.i. The products were carefully examined for the presence of the two end members, but in almost every case only one biotite was observed. The exception was an iron mix which, at 500° C and 30,000 p.s.i. total pressure resulted in a mixture of phlogopite and annite after 48 hours.

3.4 Physical Properties of the Biotites.

The composition of the biotites produced in the phase equilibrium studies were determined by optical and X-ray techniques. The relationship between the Fe/Fe + Mg ratio and physical properties were determined from biotites of known Fe/Fe + Mg ratio equilibrated with the various buffers. The composition of the biotites is fixed in terms of all cations except hydrogen. Consequently, the synthesized biotites are solid solutions of three end members: phlogopite, $KMg_3AlSi_3O_{10}(OH)_2$; annite, $KFe_3^{+2}AlSi_3O_{10}(OH)_2$; and "oxyannite," $KFe^{+2}Fe_2^{+3}AlSi_3O_{10}(OH)_2$. The phlogopite content is constant, and known, but the annite-"oxyannite" ratio is unknown.

This problem was resolved by expressing the biotite composition in terms of the Fe/Fe + Mg ratio, and then establishing the index of refraction and d_{060} for each of the biotites in terms of buffer, temperature, and total pressure. The results are shown in figures 4 and 5 and are taken from the data of tables B through G. The values used from these

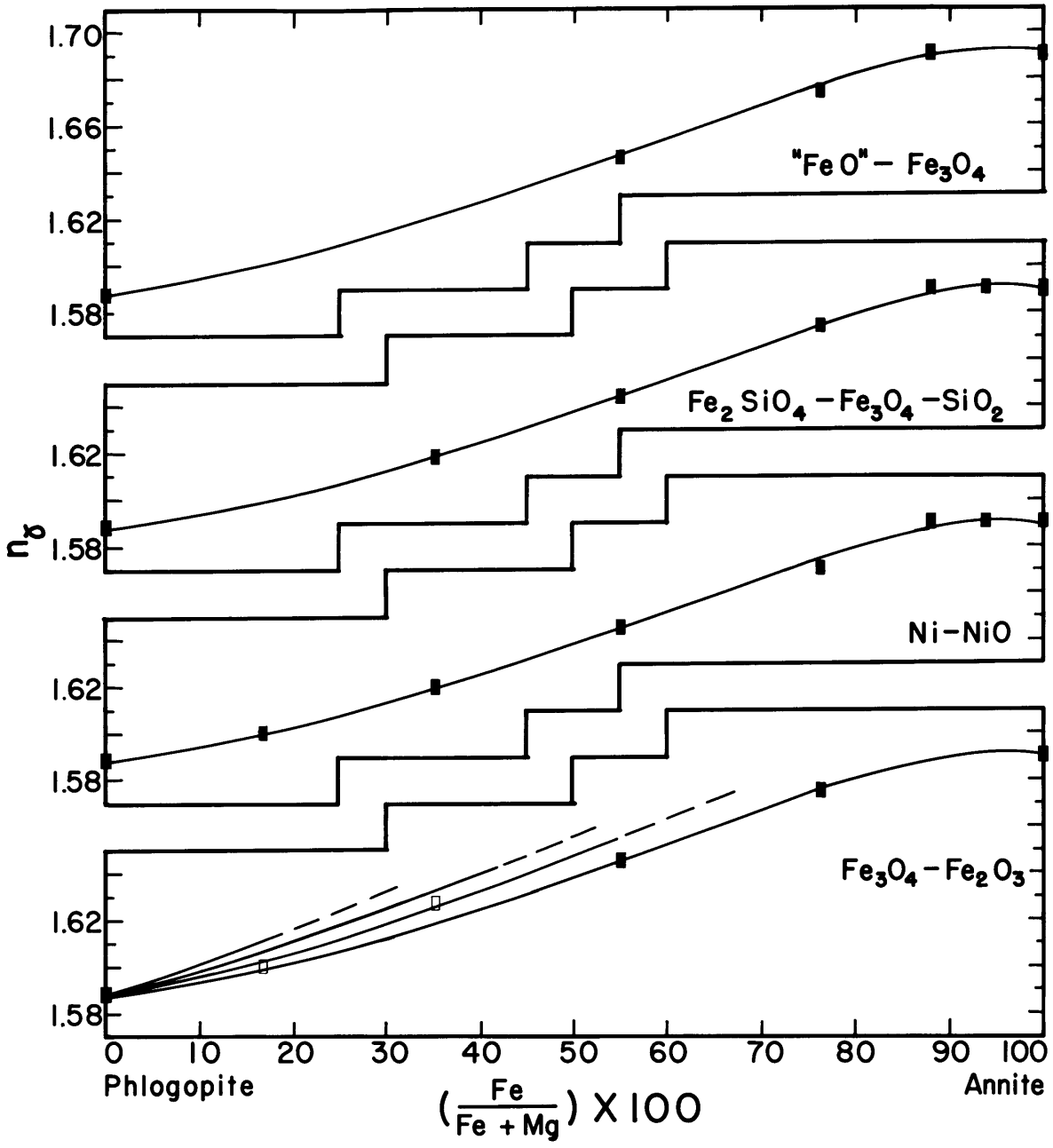

Figure 4. Plot of N_γ as a function of Fe/Fe+Mg of biotites on the join phlogopite-annite, for each of the buffer systems. For Fe_3O_4-Fe_2O_3 dark squares represent 400-500° C, open squares 600° C. Remaining curves represent 700° C and 800° C. For all other buffer systems, no systematic variation with temperature was detected.

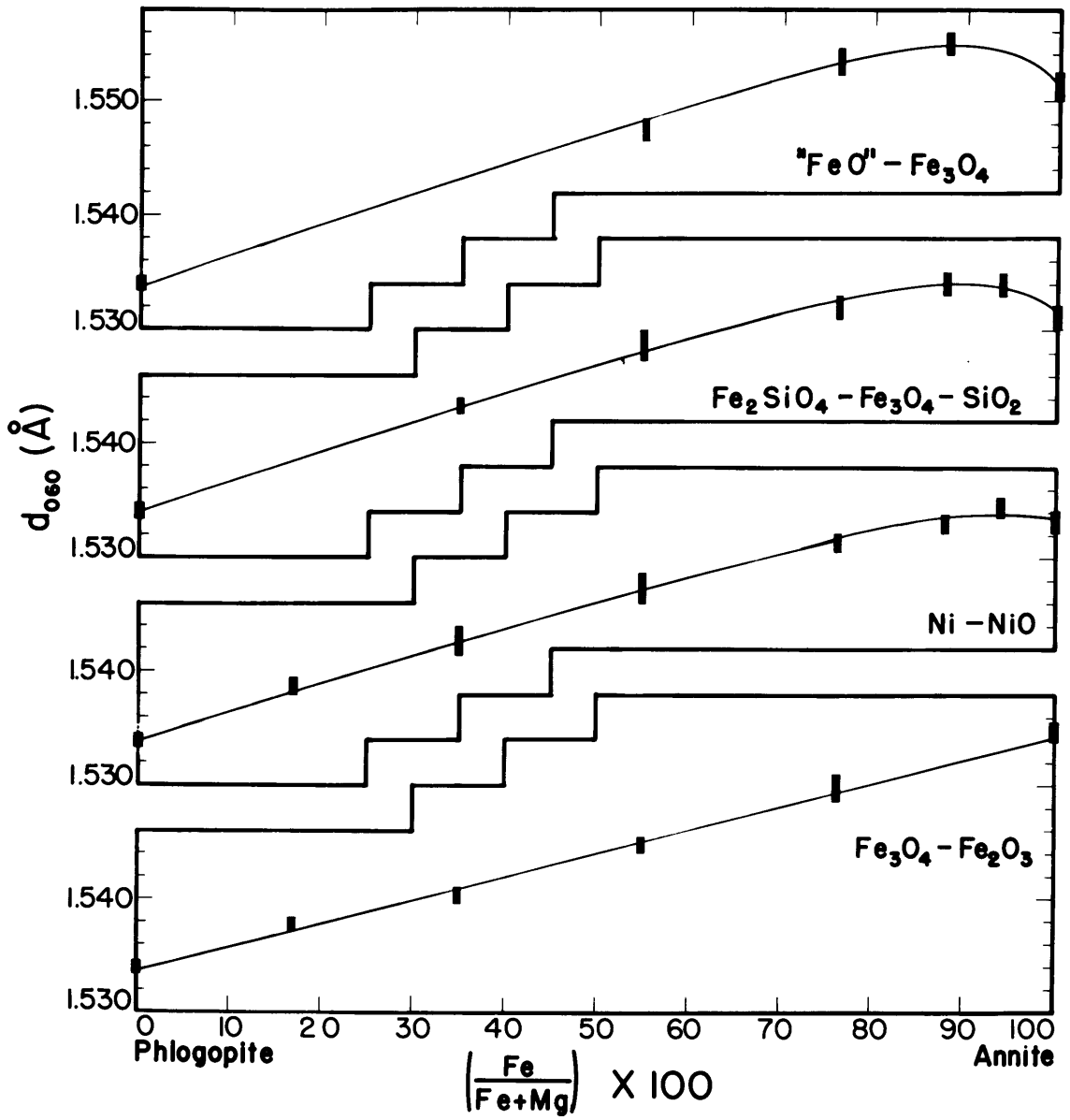

Figure 5. Plot of d_{060} (Å) as a function of Fe/Fe+Mg of biotite on the join phlogopite-annite for each of the buffer assemblages.

tables are marked with an asterisk. The symbols used in these tables are listed in table A.

As can be seen from figures 4 and 5 the properties are predominately a function of buffer (oxygen, or hydrogen, pressure) and composition. Variations due to temperature were observed only on the hematite-magnetite buffer and then for the optical properties only. Variations due to total pressure were not observed. The X-ray data only reflected variations in composition and oxygen pressure.

The reversibility of the optical properties is demonstrated by the runs listed in table 11. The first three biotites (B1570, B1579, B1576A) listed demonstrate the effect of temperature. All three represent the same starting material (biotite) equilibrated at different conditions. Runs B1543 and B1337 represent the same starting material subject to different partial oxygen pressures. Run B1563 represents B1543 re-equilibrated to more reducing conditions.

These data indicate that the hydrogen content of the lattice is indeed the important variable. The experiments of Rinne (1925) in which the index of refraction of a biotite increased when it was heated in oxygen and then returned to the original value when heated in hydrogen indicate that the indices of refraction are indeed a function of oxygen (hence, hydrogen) pressure.

Larsen et al. (1938) in their studies of the volcanic rocks of the San Juan region, Colorado, show that the ferric iron of biotites and their indices or refraction are inversely proportionate to the water content. A further study is planned by the author to resolve this problem of the oxyannite content as a function of the partial pressure of oxygen.

Table 11. N_γ of Selected Biotites Before and After Runs.

Run No.	T°C	Fe/Fe+Mg	Buffer	Before	After
B1570	700	0.169	H-M	1.593±0.005	1.602±0.003
B1579 A	800	0.169	H-M	1.593±0.005	1.610±0.003
B1576 A	800	0.169	H-M	1.593±0.005	1.613±0.003
B1245	700	0.352	H-M	1.630±0.005	1.635±0.003
B1555	600	0.352	H-M	1.616±0.004	1.627±0.003
B1543	800	0.352	H-M	1.620±0.005	1.632±0.003
B1365	700	0.169	Ni-NiO	1.595±0.005	1.600±0.003
B1372	700	0.352	Ni-NiO	1.620±0.005	1.616±0.003
B1563	700	0.352	Ni-NiO	1.627±0.003	1.619±0.003 (See B1555)
B1415	800	0.550	Ni-NiO	1.640±0.005	1.647±0.003
B1384	700	0.765	Ni-NiO	1.660±0.005	1.676±0.003
B1337	800	0.352	Q-F-M	1.620±0.005	1.618±0.003 (See B1543)
B1338	750	0.550	Q-F-M	1.635±0.005	1.644±0.003
B1335	705	0.765	Q-F-M	1.661±0.005	1.672±0.003
B1516	800	0.880	W-M	1.679±0.005	1.690±0.003

3.5 Optical Properties of Biotites.

The indices of refraction were measured on all material with individual grains $> 3\mu$. Measurements were made in white light with oils calibrated with an Abbé refractometer using a sodium vapor light source. Corrections were made for temperature changes. The routine measurements were made to $\pm$ .003, occasionally to $\pm$ .002. All values quoted in this work are $\pm$ .003.

The value of n_γ for each of the buffered systems as a function of Fe/Fe + Mg is shown in figure 4 which also includes the data on phlogopite of Yoder and Eugster (1954). The variation is regular, quite similar to that shown by Kunitz (1924) and Winchell (1951). The synthetic biotites all appear to be optically uniaxial, with the optic axis perpendicular to the basal cleavage. n_α has been measured for the series equilibrated with the nickel-nickel oxide buffer, and its value, together with the calculated birefringence is given in table 12. Also included in table 12 is extrapolated data of Winchell (1951).

The data show a maximum index of refraction at a Fe/Fe + Mg ratio of 0.95. This corresponds to a similar maximum in the d_{060} X-ray reflection.

Although this series of biotites is less aluminous than the natural biotites, these data will serve as the side of a diagram similar to that of Winchell (1951, figure 257, p. 374).

3.6 X-ray Studies.

The d_{060} X-ray reflection of the biotites is the best suited reflection for determining the composition of biotites in the system studied. It exhibits a large shift (0.020 Å) and is strong enough to be measured in the majority of cases. However, this measurement becomes very difficult,

Table 12. Optical Properties of Biotite Synthesized with Ni-NiO Buffer.

	This study				Winchell, 1951		
Fe/Fe+Mg	$n\alpha$	$n\gamma$	$n_\gamma - n_\alpha$	(Yoder and Eugster)	n_α	$n\gamma$	$n_\delta - n_\alpha$
0.000	1.548±0.003	1.588±0.003	0.040		1.535	1.565	0.030
0.169	1.564	1.600	0.036		1.540	1.580	0.040
0.352	1.575	1.619	0.044		1.570	1.625	0.050
0.550	1.598	1.646	0.048		1.594	1.651	0.055
0.766	1.616	1.676	0.060		1.612	1.671	0.059
0.880	1.622	1.681	0.059		1.622	1.682	0.060
0.939	1.628	1.691	0.063		1.627	1.687	0.060
1.000	1.629	1.689	0.060		1.630	1.690	0.060

if not impossible, when other phases are present in quantities greater than 50 per cent by volume. Figure 5 is a summary of the data plotting d_{060} (Å) as a function of Fe/Fe + Mg for each of the several buffers and includes the data on phlogopite of Yoder and Eugster (1954).

There is a maximum value at 0.95 Fe/Fe + Mg which corresponds to that exhibited by the optical data. This maximum becomes more pronounced for biotites equilibrated with quartz-magnetite-fayalite and wüstite-magnetite buffers. The decrease in d_{060} for the end member annite appears to be the major contributing factor to this maximum. The maximum is probably due to the enhanced stability of oxyannite in the biotite lattice with increased phlogopite content. The author plans to examine this question, and that of the optical data, in a future study.

In the magnesium rich biotites, there is a pronounced variation in the d_{060} spacing between buffers, and this variation does not seem to correspond to the optical data. The increase in n_γ, so pronounced when the temperature is increased on the hematite-magnetite buffered runs, is not accompanied by any measurable variation in the d_{060} spacing. However, biotites synthesized on the nickel-nickel oxide buffer have pronounced variations in the d_{060} spacing compared to those synthesized on the hematite-magnetite buffer.

The unit cell dimensions of the biotites synthesized on the nickel-nickel oxide buffer have been determined for the biotites whose compositions are 0.5501, 0.8801, and 1.00 Fe/Fe + Mg. The powder X-ray data for these biotites are given respectively in tables H, J, and K, and the unit cell dimensions and molar volumes are tabulated in table 13. As can be seen from these tables, the 1M 3T polymorphism described by Smith and

Table 13. Cell Dimensions of Biotites Synthesized with Ni/NiO Buffer (in Å).

1M Setting

Fe/Fe+Mg	a	b	c	β	Vol. (cc/mole)
0.000	5.314±0.01	9.204±0.02	10.314±0.005	99°54'±5'	149.3±2.0
0.550	5.355±0.01	9.285±0.02	10.297±0.005	99°56'±10'	151.5±2.0
0.880	5.374±0.01	9.313±0.02	10.280±0.005	99°53'±5'	152.3±2.0
1.000	5.384±0.01	9.321±0.02	10.282±0.005	100°16'±10'	152.6±2.0

Data on Phlogopite (0.000) Taken from Yoder and Eugster (1954)

3T Setting

Fe/Fe+Mg	a	c	Vol. (cc/mole)
0.000	5.314±0.01	30.480±0.01	149.6±2.0
0.550	5.355±0.01	30.426±0.01	151.6±2.0
0.880	5.379±0.01	30.378±0.01	152.7±2.0
1.000	5.381±0.01	30.321±0.01	152.6±2.0

Yoder (1956) cannot be differentiated by means of powder X-ray data. However, the 1M fit is very much the best for the annite end member. This also may be a partial explanation for the observed maximum in the b crystal axis at 0.95 Fe/Fe + Mg.

The indices of refraction, on the whole, have been shown to be more sensitive than the d_{060} data in the determination of the Fe/Fe + Mg ratio of the biotites, and can be measured easily in runs containing less than 50 per cent biotite. Most emphasis in this study has been placed on the optical data.

The technique of Gower (1957), in which the Fe/Fe + Mg ratio of biotite is determined by measuring the ratio of the 004 and 005 reflection intensities, could not be used in this study as 1) the presence of the magnetite 311 reflection would interfere with the 004 biotite reflection, and 2) the fine grained nature of the material made it extremely difficult to get the preferred orientation required by Gower's technique. The biotites observed in this study showed the same general shift Gower observed, but this variation was not pursued quantitatively.

3.7 Identification of Other Phases Occurring in the Phase Equilibria Studies.

Other phases occurring in the phase equilibrium studies are K-feldspar, magnetite, hematite, olivine, leucite and pyroxene. K-feldspar, hematite, olivine, leucite, and pyroxene were all easily identified by optical techniques. Magnetite was also observed optically, but required X-ray powder diffraction data for positive identification.

The feldspar usually forms in crystals with well developed 110, $1\bar{1}0$, and 010 faces. The orientation of the optic plane is 010 and the 2V is small, indicating high sanidine. The γ index of refraction is about

1.522 ± 002, the value reported by Tuttle (1952) for synthetic sanidine. γ of the synthetic sanidines from runs at a variety of temperatures and partial pressures of oxygen was always at the same value, indicating that there was no observed solid solution of the $KFeSi_3O_8$ end member (Coombs, 1954).

The hematite occurs as hexagonal platelets of a bright ruby red color; this identification was verified by X-ray diffraction. The determination of the composition of the magnetite proved difficult. The possible solid solutions which might be present are magnetite-hematite (Fe_3O_4 - Fe_2O_3); magnetite-hercynite (Fe_3O_4 - $FeAl_2O_4$); and magnetite-magnesioferrite (Fe_3O_4 - $MgFe_2O_3$). The work of Darken and Gurry (1945, 1946) indicates that Fe_3O_4 - Fe_2O_3 solid solutions are not important at temperatures below 1000° C, and that in the conditions prescribed by these experiments, magnetite should be a stoichiometric compound.

Turnock (1958) has defined the variation of the unit cell edge with composition. The magnetites synthesized in this study have a unit cell edge of 8.393 Å indicating no observable hercynite solid solutions.

Magnesioferrite, unfortunately, has the same unit cell edge as magnetite, and consequently the size of the unit cell edge is not useful for making compositional determinations. However, certain phase relations indicate that the magnesioferrite content of the magnetite is probably very small. The primary evidence is that in the hematite field (runs made using the Cu/Cu_2O buffer) no spinel phase was ever observed. If magnesioferrite was stable in the presence of feldspar and water, it certainly should have been observed in these runs. The other evidence is that at 800° C, 30,000 p.s.i., and using a nickel-nickel oxide buffer, a biotite whose Fe/Fe + Mg ratio (see run No. B1585) is

0.939 reacts to form biotite, sanidine, and magnetite. If all of the oxides in such a biotite reacted to form a spinel phase, and none of it went into a new biotite, then the new spinel phase would contain 20.54 mole per cent Mg Fe_2O_4. However, in the above mentioned reaction biotite makes up about 10 per cent of the reaction products, indicating that the magnetite formed is very close to Fe_3O_4 composition. It seems likely that MgO has a greater affinity for the silicate lattice than the oxide lattice.

Olivine was encountered in a few runs on the wüstite-magnetite buffer and some preliminary runs on the quartz-fayalite-iron buffer. The olivines in the former were rounded and not well formed. In the latter they have a prismatic habit. These latter experiments were very difficult to evaluate, as the affinity of iron for platinum was extremely high. The recognized assemblage was biotite-sanidine-leucite-olivine-vapor. As the iron loss of these charges was great and the partial oxygen pressures much too low for the majority of natural biotite assemblages, these assemblages were not extensively examined.

The occurrence of leucite was never definitely verified during this study. In the few regions where the reaction biotite = leucite + kalsilite + fayalite + H_2O was expected, the loss of iron to the platinum tube was sufficient that an excess of silica was available and the observed assemblage was usually sanidine + leucite + olivine. A few exceedingly small grains of apparent isotropic character were observed, and they were presumed to be leucite.

The only other solid phase observed in the course of these experiments was pyroxene. This phase would appear metastably during the early synthesis of magnesium rich biotites, but would disappear with time.

Occasionally a rupture of a platinum tube would occur, and if the quartz-fayalite-magnetite buffer was used, the reaction quartz + biotite ⇌ sanidine + glass + pyroxene + magnetite + water took place.

The presence of the vapor phase was verified when the tubes were opened. Its composition with respect to the gas species was discussed in chapter 2; its composition with respect to the other components of the system is not known.

CHAPTER IV

PHASE RELATIONS OF THE BIOTITES ON THE JOIN PHLOGOPITE-ANNITE

4.1 Presentation of the Phase Equilibria.

The biotite phase equilibria can best be presented by first describing the phase relations of the end members, and then discussing the phase relations of the intermediate members. The actual experimental data are best presented in terms of pseudo-binary joins, one join for each buffer employed. The biotites are finally discussed in terms of an isobaric space having partial pressure of oxygen, temperature, and composition as its coordinates.

4.2 Phase Relations of Phlogopite.

The maximum stability curve for phlogopite has been determined by Yoder and Eugster (1954). This curve represents the conditions at which phlogopite reacts to form leucite, orthorhombic kalsilite, forsterite, and water vapor, and, with their permission, is reproduced here as figure 6. The conditions represented here are those where total pressure is equal to water vapor pressure. At 15,000 and 30,000 p.s.i., the respective temperatures of the above equilibrium are 1050° and 1085° C. The present study did not go to temperatures above 960° C, but all evidence indicates that Yoder and Eugster's curve is essentially correct.

The effect of changes in partial pressure of oxygen on the phlogopite equilibrium are indirect. The main effect will be to vary the H_2O pressure by changing the H_2/H_2O ratio. The highest H_2 pressure generated in this study was in water vapor equilibrated with wüstite and magnetite at 30,000 p.s.i. and 800° C and had a value of about 6000 p.s.i. At 1085° C (the reaction temperature of phlogopite at

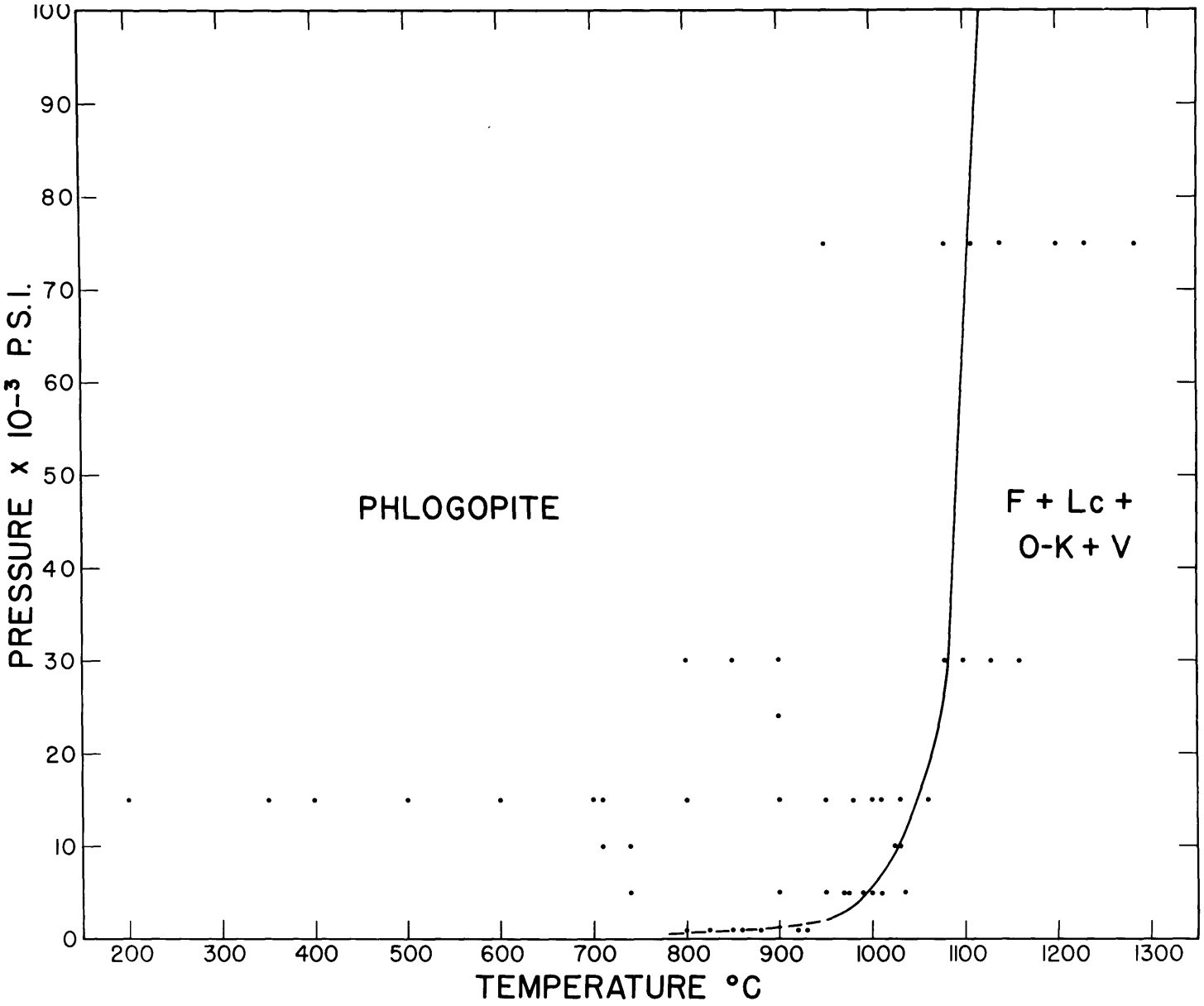

Figure 6. Phlogopite stability as a function of pressure and temperature (after Yoder and Eugster, 1954).

30,000 p.s.i.), the effective H_2 pressure is about 1500 p.s.i. This would cause a shift of about 4° C in the phlogopite equilibrium.

4.3 Phase Relations of Annite.

The general phase relations of annite were first determined by Eugster (1956) while developing the buffer technique. The problem of the phase relations of hydrous iron silicates has been discussed by Eugster using annite as an example (Eugster, 1959). The discussion of these relations here is necessary for two reasons: 1) the present study has amplified and changed some portions of the original diagram, and 2) the reader must be familiar with the phase relations of the end member in order to fully understand the phase relations of the intermediate biotites.

The phase relations of annite under a total vapor (H_2 + H_2O) pressure of 30,000 p.s.i. are shown in figure 7 as a function of the partial pressure of oxygen (P_{O_2}) and temperature. The diagram presented here is compiled from the data of Eugster (1956, 1957, 1959), experimental work done during the course of this study, and some extrapolations based on thermodynamics and the phase rule.

The bulk composition annite (+ vapor) forms several different phase assemblages, three of which are shown in figure 7. These three assemblages, which are unequivocal, are 1) annite + vapor, 2) sanidine + hematite + vapor, and 3) sanidine + magnetite + vapor. The major problems lie in the nature of the high-temperature equilibria. Two possible combinations of the high-temperature assemblages are presented in figure 8. This figure shows only the relative phase relations, as this study did not investigate equilibria at conditions with oxygen pressures lower than that of a magnetite-wüstite assemblage.

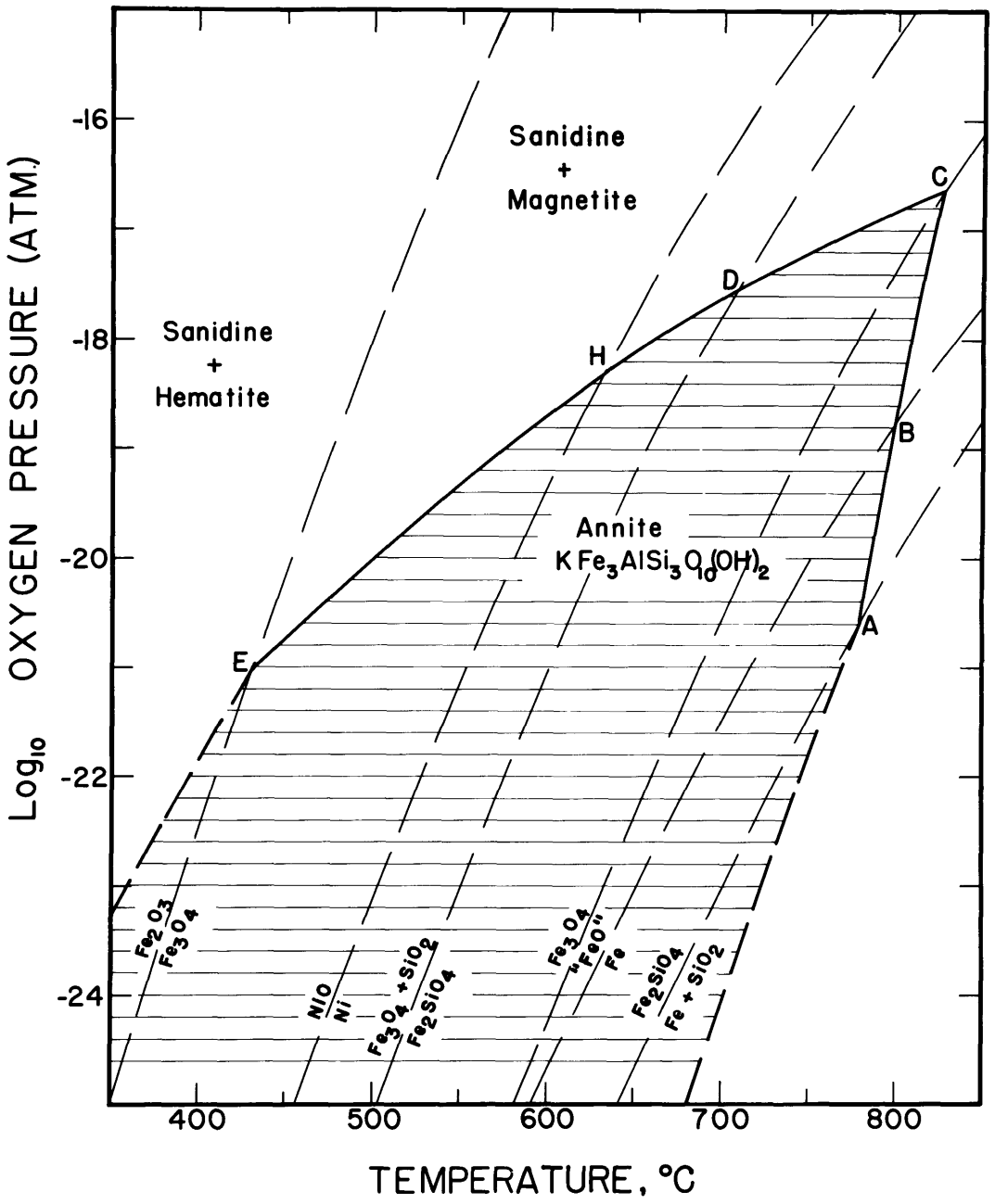

Figure 7. Stability of annite as a function of oxygen pressure and temperature at a total pressure of 30,000 p.s.i.

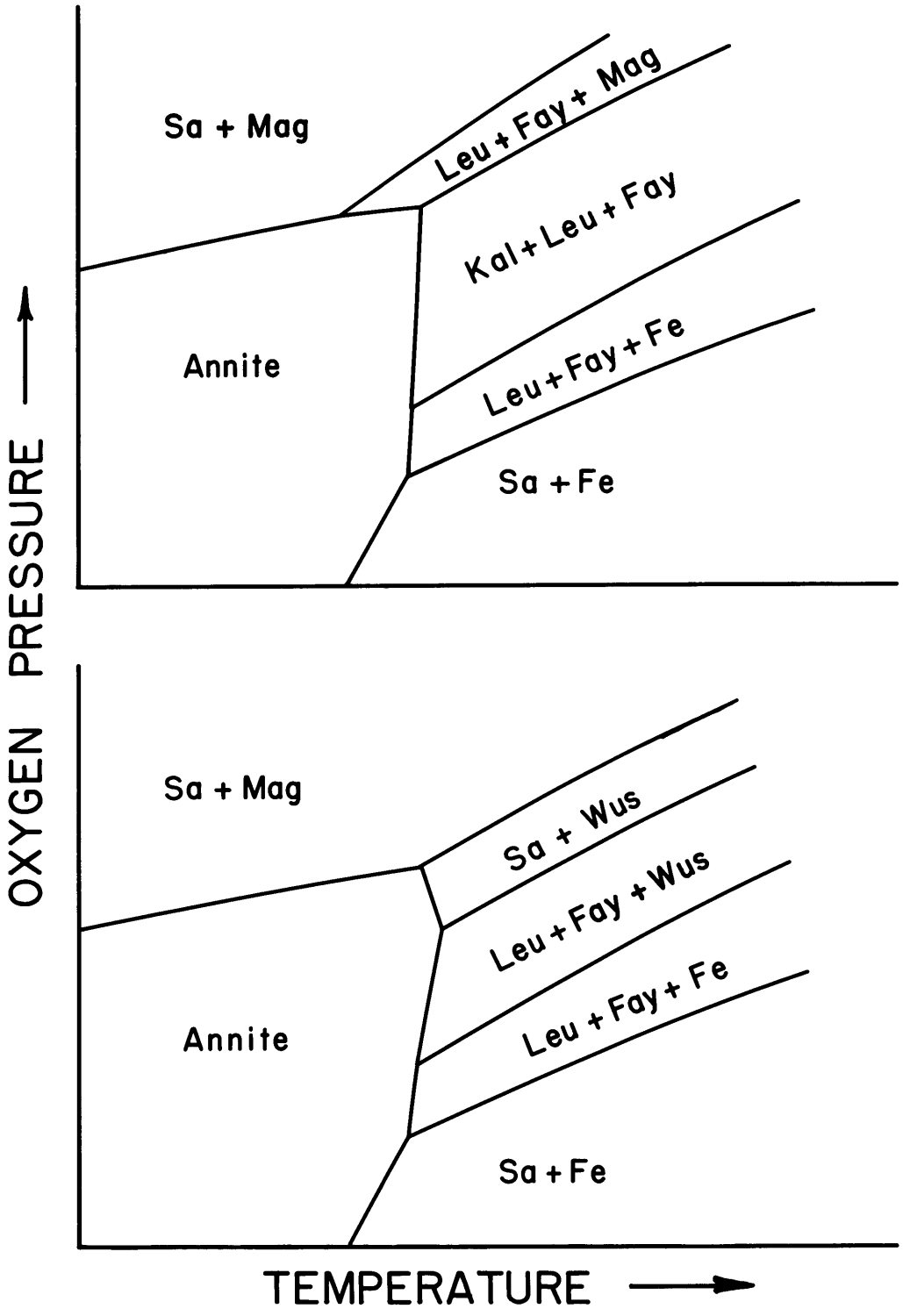

Figure 8 (a and b). Alternative hypotheses of annite phase relations as a function of oxygen pressure and temperature at constant total pressure.

Figure 8a indicates that the remaining assemblages are 4) leucite + magnetite + fayalite + vapor; 5) kalsilite + leucite + fayalite + vapor; 6) leucite + iron + fayalite + vapor; and 7) sanidine + iron + vapor. This set of assemblages is based on 1) the incompatibility of wüstite with either sanidine or leucite, and 2) the incompatibility of kalsilite and sanidine. Experimentally the only phases positively identified by the author are annite, sanidine, leucite, fayalite and magnetite. Iron has a great affinity for platinum at high temperatures and pressures; consequently, the runs made at low oxygen pressures are constantly depleted in iron, giving rise to sanidine + leucite + fayalite assemblages.

Figure 8b presents the possible alternative high-temperature assemblages which are: 4') sanidine + wüstite + vapor; 5') leucite + wüstite + fayalite + vapor; 6') leucite + iron + fayalite + vapor; and 7') sanidine + iron + vapor. The evidence for this latter configuration lies in the fact that fayalite has not been observed by the author in runs made on the wüstite-magnetite buffer, but the assemblage sanidine + magnetite + vapor has been observed. Eugster (personal communication) reports fayalite occurring frequently in his experiments.

There is sufficient thermodynamic data to calculate the partial oxygen pressure of the assemblage sanidine + magnetite + leucite + fayalite at 800° C, but the calculation is rather crude. It is merely to calculate ΔG for the reaction:

$$3KAlSi_3O_8 + 2Fe_3O_4 = 3KAlSi_2O_6 + 3Fe_2SiO_4 + O_2 \qquad [4.1]$$

sanidine magnetite leucite fayalite oxygen

at 25° C and determine the partial oxygen pressure. The extrapolation is then made to 800° C by assuming ΔH constant. The data used in the calculation are given in table 14. The data used for sanidine were

Table 14. Source of Thermodynamic Data Used in Calculating the Oxygen Vapor Pressure of the Magnetite-Sanidine-Fayalite-Leucite-Vapor Assemblage.

Phase	Quantity		Source
Magnetite	ΔH_{298}	-267 Kcal/°/mole	Humphrey, King, and Kelley (1952)
	S_{298}	35.0 cal/°/mole	Kelley (1950)
	C_p		Coughlin, King, and Bonnickson (1951)
Fayalite	ΔH_{298}	-346.0 Kcal/mole	King (1952)
	S_{298}	34.7 cal/°/mole	Kelley (1950)
	C_p		Orr (1953)
Sanidine (ferriferous orthoclase)	ΔH_{298}	-930.6 Kcal/mole	Kracek et al. (1953)
	S_{298}	52.5 cal/°/mole	Kelley et al. (1953)
	C_p		Kelley (1949)
Leucite	ΔH_{298}	-717.7 Kcal/mole	Kracek et al. (1953)
	S_{298}	44.0 cal/°/mole	Kelley et al. (1953)
	C_p		Not determined
Oxygen	S_{298}	49.01cal/°/mole	Kelley (1950)
	C_p		Kelley (1949)

actually taken from ferriferous orthoclase and consequently the calculations are even more approximate. The result at a temperature of 1100° C is $_{10}$16.4 bars, which is slightly higher than the $_{10}$-16.6 bars for wüstite-magnetite assemblages at the same temperature. Consequently, difficulty in interpreting the experimental results is to be expected. However, this calculation makes figure 8a the more probable of the two alternatives. This conclusion is certainly confirmed by the lack of natural assemblages containing wüstite.

The importance of establishing the correct assemblage at point C of figure 7-2 is very great as it is necessary to extrapolate the assemblage annite + sanidine + magnetite + vapor to point "E," which is its terminus. The data determining the position of curve E-D-C are given in table B, appendix I. For point C Eugster's value of 825° ± 5° C was used. This study ascertained the equilibrium to lie at 705° ± 5° C for the quartz-magnetite-fayalite buffer (point D) and at 635° ± 5° C for the nickel-nickel oxide buffer (point H).

The establishment of the equilibrium on the hematite-magnetite buffer (point E) proved more difficult. At 450° C a 960-hour run using annite as starting material produced sanidine + hematite + magnetite, while another run (made by Eugster) at 400° C produced very small amounts of sanidine and hematite after 3000 hours. Attempts at reversal from sanidine and magnetite were made at 430° C and 400° C. After 714 and 2000 hours respectively there was no observed reaction except for the formation of a few grains of muscovite. On the basis of these runs the equilibrium was placed at 425° ± 25° C, indicating the need for an extrapolation.

The extrapolation was made by use of the Clapeyron equation

$$\frac{d \log_{10} P_{O_2}}{d(1/T)} = \frac{-\Delta H}{2.303R} \qquad [4.2]$$

The three assumptions which must be made in order to perform this extrapolation are 1) ΔH for the reaction remains constant, 2) oxygen behaves as a perfect gas, and 3) the composition of annite does not shift appreciably towards "oxyannite."

The properties of annite given in table B indicate that annite probably does change composition somewhat between point "C" and point "E," but the exact amount cannot be ascertained at present. If the plot is made in terms of fugacity rather than pressure, oxygen is defined as an ideal gas. The change in ΔH as determined from the slope of the reaction is about 41 kcal/mole. The next problem is the determination of the deviation in ΔH for this reaction. As there is no available data on the heat content of annite, an approximation was made using the data of Kelley et al. (1954) on fluorphlogopite and combining this with heat contents of the other phases (Kelley, 1949). The result is a lowering in ΔH at lower temperatures of about 10 kcal. However, as the curve appears to be linear at higher temperatures, the extrapolation was made graphically (see figure 14). The intersection of the sanidine-magnetite-annite-vapor equilibrium with the hematite-magnetite equilibrium is at 433° C at 30,000 p.s.i. total vapor pressure and at 417° C at 15000 p.s.i. total vapor pressure.

The final problem to be resolved in the determination of the phase relations of annite is the location of the equilibrium annite + sanidine + hematite + vapor. Eugster (1956, 1959) and Wones and Eugster (1958, 1959) indicate that this equilibrium is coincident with the hematite-magnetite equilibrium. This premise is based on the occurrence of

sanidine-hematite-annite assemblages in runs buffered by hematite-magnetite assemblages at low temperatures.

However, at temperatures below 500° C both the author and W. G. Ernst (personal communication) found the diffusion of hydrogen through platinum extremely slow, so that at very low temperatures and correspondingly low hydrogen pressures the inner charge is essentially a closed system. In such a case the annite would react with water vapor and produce the sanidine-hematite-annite-vapor assemblage, at a partial pressure of oxygen somewhat above that of the hematite-magnetite buffer.

The position of the sanidine-hematite-annite-vapor assemblage has been calculated in the following manner

$$4/3KFe_3AlSi_3O_{10}(OH)_2 + 2/3\ O_2 = 4/3KAlSi_3O_8 + 4/3Fe_3O_4 + 4/3H_2O \qquad [4.3]$$

$$4/3Fe_3O_4 + 1/3\ O_2 = 2Fe_2O_3 \qquad [2.4]$$

$$4/3KFe_3AlSi_3O_{10}(OH)_2 + O_2 = 4/3KAlSi_3O_8 + 2Fe_2O_3 + 4/3H_2O \qquad [4.4]$$

By adding the ΔH's of [4.3] and [2.4] a value of 65.3 kcal is obtained for the ΔH of [4.4]. This value leads to a value of -14.3 for the slope $\left[\frac{\partial \log_{10} P_{O_2}}{\partial(1/T)}\right]$ of the sanidine + hematite + annite + vapor assemblage. As this value is less than that of the hematite-magnetite assemblage (-24.9) it demonstrates that the two assemblages have dissimilar oxygen vapor pressures.

The points established for the location of the sanidine-magnetite-annite-vapor equilibrium are given in table 15. These values are quite important as they are the ones used in the phase relations of the intermediate biotites.

The invariant points of figures 7 and 8 are actually points on univariant equilibria when the total pressure is admitted as a variable. Eugster (1959) has discussed this problem rather fully. Figure 9 is taken

Table 15. Position of the Annite-Sanidine-Magnetite-Vapor Assemblages for Various Buffer Assemblages.

Total Pressure	Fe_2O_3 Fe_3O_4	NiO Ni	Fe_3O_4 SiO_2 Fe_2SiO_4	Fe_3O_4 FeO
15,000 p.s.i.	(417°C)	617±5°C	685±5°C	790±5°C
30,000 p.s.i.	(433°C)	635±5°C	705±5°C	*825±5°C

Parentheses indicate values derived by extrapolation.

*Value obtained by Eugster (1957).

from his discussion. The loci of the univariant and divariant assemblages are functions of total pressure, partial oxygen pressure, and temperature.

The lowering of water vapor pressure lowers both the temperature and partial oxygen pressure of the assemblages involving sanidine + iron oxide + annite + vapor. In the case of the more reduced assemblages, a decrease of water vapor pressure is accompanied by a decrease in temperature and very slight deviations in P_{O_2}.

4.4 Phase Relations of the Intermediate Biotites.

The phase relations of the intermediate biotites are functions of the four variables, P_{total}, P_{O_2}, temperature, and composition. These relations are developed by first presenting isobaric temperature-composition diagrams for each of the buffer assemblages. As has been shown in chapter 2, in such a plot the partial pressure of oxygen is constantly increasing with temperature. After presenting the "T-X" diagrams the isobaric P_{O_2}-T-X relations will be discussed, and finally the variations caused by changes in the total pressure.

The assemblages encountered are 1) biotite + vapor, 2) biotite + sanidine + hematite + vapor, 3) biotite + sanidine + hematite + magnetite + vapor, 4) biotite + sanidine + magnetite + vapor, and either 5) biotite + leucite + magnetite + olivine + vapor or 5') biotite + sanidine + magnetite + wüstite + vapor. This latter represents the most reducing conditions produced during this study. The reasons for making such a limitation are geologic; wüstite assemblages are unknown geologically, and iron bearing assemblages are restricted to meteorites and certain rare basalts.

As 900° C was the maximum temperature investigated, certain inter-

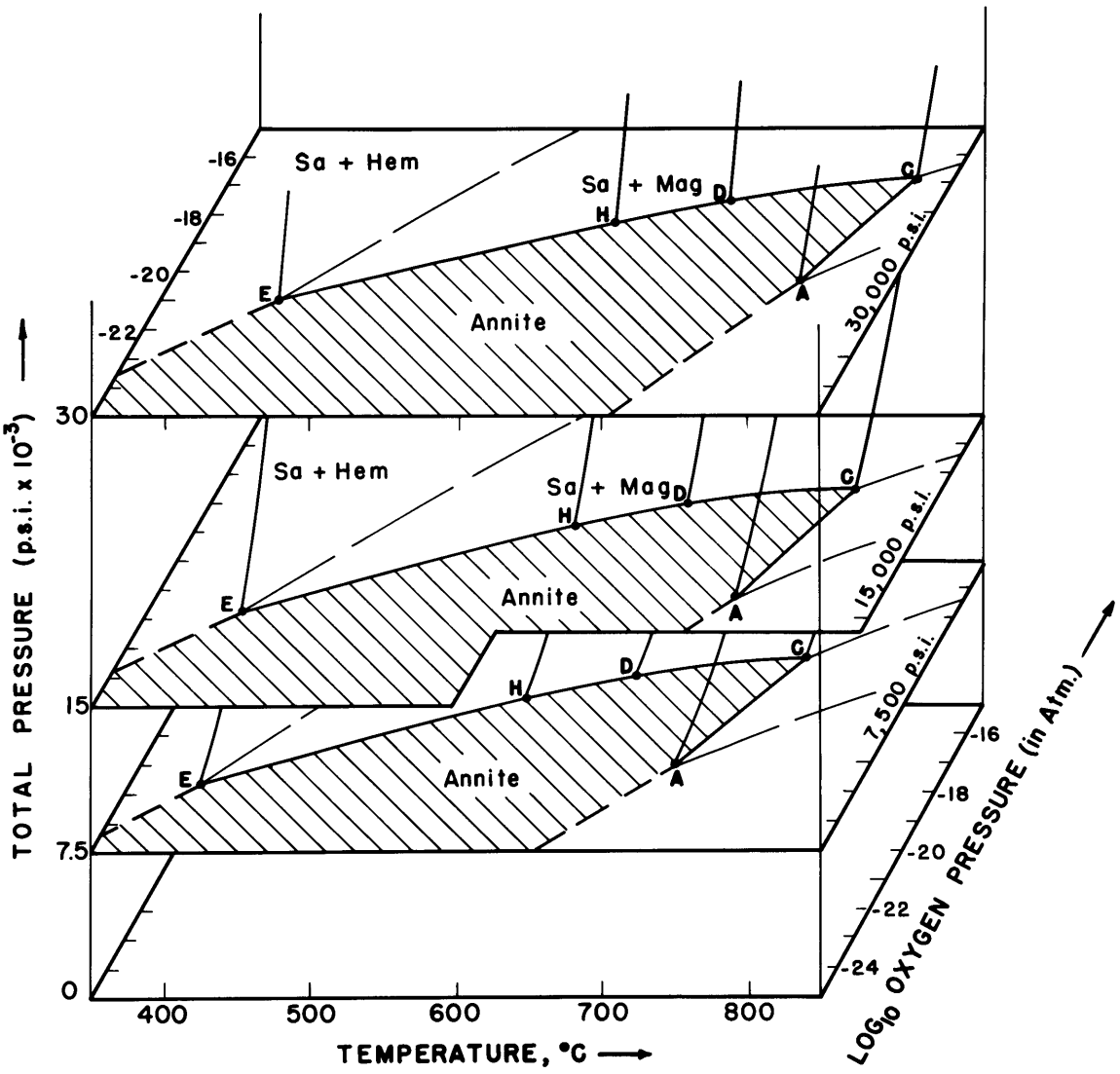

Figure 9. Stability field of annite as a function of P_{O_2}-T-P_{total} (after Eugster, 1959).

polations are made concerning the phase relations of biotites at temperatures above that value. These relations will necessarily be more complex than their low-temperature counterparts, as they include the introduction of the phases leucite, kalsilite, pyroxene and olivine in addition to biotite, sanidine and the iron oxides.

4.5 The Magnetite-Wüstite Buffer.

The phase relations of biotites at partial pressures of oxygen equivalent to the magnetite-wüstite assemblages are shown in figure 10. The actual experimental evidence upon which this figure is based is given in table C, and is summarized in table 16, which lists the criteria used in determining that diagram. The diagram represents a constant pressure of 15,000 p.s.i. and the temperatures investigated were 850° C and below.

As has been shown for annite (see section 4.3) the nature of this high-temperature assemblage is not perfectly clear. The buffer is usually formed by mixing iron and hematite in an appropriate ratio to form wüstite and magnetite. In run B1090 the experiment reached 820° C in about one-half hour and the result was a mixture of biotite, fayalite, sanidine, magnetite, and possibly some leucite. The inference was that the partial oxygen pressure was temporarily fixed at that of the wüstite-iron buffer, and that a more reduced assemblage formed. When the magnetite-wüstite buffer formed, the charge reacted to form metastable sanidine and magnetite, and finally reformed biotite. In an attempt to get around these difficulties, in runs B1467 and B1489 the run was held at 700° C for about four hours before being placed at 850° C. In the latter case only sanidine and magnetite were positively identified. Olivine and leucite were not observed optically, nor was wüstite observed in the X-ray patterns.

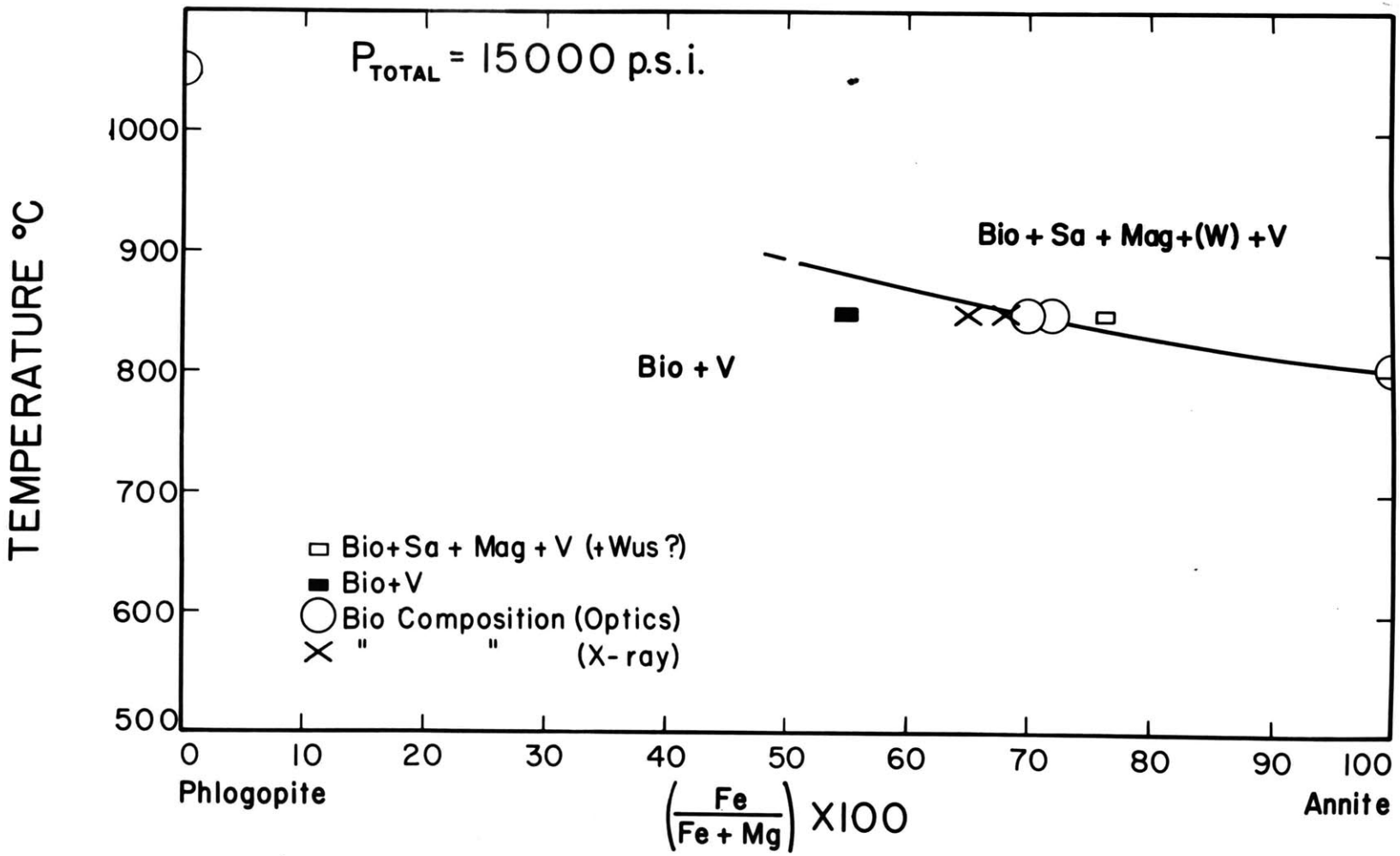

Figure 10. Stability of biotites on the join phlogopite-annite as a function of temperature and composition (Fe/Fe+Mg) at 15,000 p.s.i. total pressure, and at oxygen pressures corresponding to the magnetite-wüstite buffer. Wüstite inferred as a phase; for explanation, see text.

Table 16. Criteria Used in Establishing the Position of Biotite-Sanidine-Magnetite-(Wustite)-Vapor Assemblage.

Fe/Fe+Mg Biotite	T°C	Source
	15,000 p.s.i. total pressure	
0.00	1050	Yoder and Eugster (1954)
0.69±0.05	850	Table C; Runs B1467, B1489
1.00	790	Table B; extrapolation

No attempts were made to reverse this equilibrium, and it is presented as representing the maximum thermal stability of the assemblage biotite + sanidine + magnetite + vapor. The heavy curve in the diagram represents the composition of the biotite in equilibrium with sanidine and magnetite at 15000 p.s.i., at the appropriate temperature and partial oxygen pressure. The curve was drawn on the basis of the stability of the two end members and that, at 850° C, the biotite coexisting with sanidine and magnetite had an Fe/Fe + Mg ratio of 0.69 ± .05. In figure 10 the compositional determinations are shown, and the curve drawn through their mean.

4.6 The Quartz-Magnetite-Fayalite Buffer.

The 15,000 p.s.i. and 30,000 p.s.i. isobaric T-X diagrams representing the phase relations of the biotites at partial pressures of oxygen equivalent to the quartz-magnetite-fayalite buffer are represented in figure 11. The diagram is divided into two fields, the low-temperature field representing the assemblage biotite + vapor, whereas the high-temperature field represents the assemblage biotite + sanidine + magnetite + vapor. The phase boundary may be considered as the maximum thermal stability of biotite of a given Fe/Fe + Mg ratio at the given total pressure, and equilibrated with the quartz-fayalite-magnetite buffer. However, it may be also considered as representing the composition of the biotite coexisting with sanidine and magnetite at the stated conditions of temperature, oxygen pressure, and total vapor pressure.

This equilibrium is much better established than that of the magnetite-wüstite buffer as the temperatures are lower, making runs of longer duration a possibility, and reversibility was demonstrated. The criteria establishing the equilibrium are listed in table 17, and are taken from

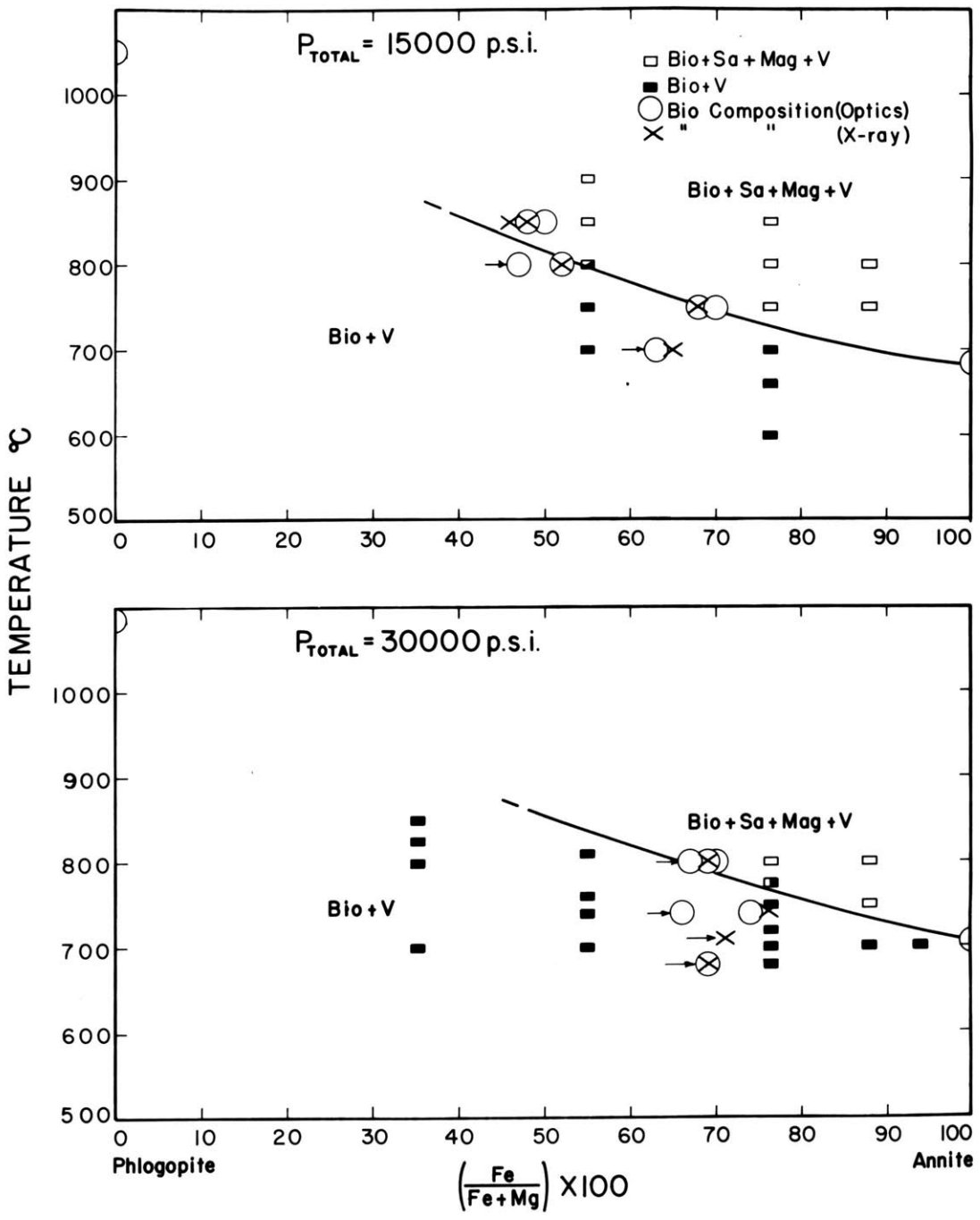

Figure 11. Stability of biotites on the join phlogopite-annite as a function of temperature and composition (Fe/Fe+Mg) at 15,000 and 30,000 p.s.i. total pressure and at oxygen pressures corresponding to the fayalite-magnetite-quartz buffer. Arrows indicate reversal runs.

Table 17. Criteria Used to Establish the Position of Biotite-Sanidine-Magnetite-Vapor Assemblages Buffered by Quartz-Magnetite-Fayalite.

Fe/Fe+Mg	T°C	Source
	Total pressure = 15,000 p.s.i.	
0.00	1050±15	Yoder and Eugster (1954)
0.52±0.05	800±5	Table D; Runs B1421, B1195, B1183
0.69±0.02	750±5	Table D; Runs B1444, B1480
0.765	725±25	Table D; Runs B1168, B1519
1.00	685±5	Table B; Runs B1536, B1534
	Total pressure = 30,000 p.s.i.	
0.00	1085±15	Yoder and Eugster (1954)
0.550	>810±5	Table D; Run B1281
0.68±0.02	800±5	Table D; Runs B1177, B1228, B1562
0.76±0.05	750±5	Table D; Runs B1271, B1438
0.765	765±15	Table D; Runs B1247, B1297
0.880	725±25	Table D; Runs B1342, B1271
1.00	705±5	Table B; Runs B1511, B1505

the experimental data of table D.

The methods used were to place biotites or their compositional equivalents at various temperatures, to ascertain the phase assemblage after the run, and to determine the composition of the biotite coexisting with the other phases. For example, at 800° C and 30,000 p.s.i. biotites with Fe/Fe + Mg ratios of 0.880 and 0.765 reacted to form the assemblage biotite + sanidine + magnetite + vapor while a biotite with a ratio of 0.550 did not react. The biotite coexisting with sanidine and magnetite was found to have a Fe/Fe + Mg composition of 0.68 $\pm$ .05. Then a mixture of phlogopite, sanidine, and magnetite corresponding to a biotite of 0.765 Fe/Fe + Mg ratio was reacted, and after 432 hours formed a biotite of 0.68 Fe/Fe + Mg coexisting with sanidine and magnetite. In figure 11 the biotites coexisting with sanidine and magnetite which were grown from a mixture of phlogopite, sanidine, and magnetite are represented by arrows.

The equilibrium is analogous to the melting diagram of a completely miscible solid solution series (i.e. plagioclase feldspars). As the temperature increases, an increasing amount of the iron rich end member becomes unstable causing the recrystallization of the biotite to a more phlogopitic composition and the formation of sanidine and magnetite. The main difference from the melting analogy is that the composition of the sanidine and magnetite are virtually unchanged as opposed to a melt, so that the "continuous reaction" merely forms more sanidine and magnetite while the composition of the biotite tends toward the phlogopite end member.

4.7 The Nickel-Nickel Oxide Buffer.

The phase relations of the biotites at partial pressures of oxygen

equivalent to the nickel-nickel oxide buffer are represented in figure 12 for total pressures of 15,000 p.s.i. and 30,000 p.s.i. The criteria which establish the position of the biotite-sanidine-magnetite-vapqr equilibrium under these conditions are listed in table 18, and details concerning the actual runs are listed in table E.

The nature of this equilibrium is identical to that of the biotites buffered by quartz-magnetite-fayalite except for the absolute values. The nickel-nickel oxide buffered assemblages lie at higher partial pressures of oxygen than their quartz-fayalite-magnetite counterparts, and, consequently, at lower temperatures. This particular buffer proved the most useful as there was a fairly wide range of temperatures which could be examined, the buffer is easy to maintain, so that runs of long duration are easily made, and reversibility was proven in three cases.

Reversible equilibrium at 30,000 p.s.i. was demonstrated at 800° C and 750° C. At 800° C oxidation reactions resulted in biotite + sanidine + magnetite + vapor assemblage with a biotite of Fe/Fe + Mg ratio of 0.58 $\pm$ .03. The reversal reaction of phlogopite + sanidine + magnetite resulted in a biotite of 0.56 $\pm$ .02 Fe/Fe + Mg ratio. At 750° C the oxidation and reduction biotite products contained 0.65 $\pm$ .05 and 0.61 $\pm$ .02 respectively.

The equilibrium at 15,000 p.s.i. was reversed at 850° C, the compositions of the oxidized and reduced assemblage biotites were, respectively, 0.44 $\pm$ .03 and 0.40 $\pm$ .02.

Information concerning the magnesioferrite content of the magnetites coexisting with sanidine and biotite was obtained from the runs made with the nickel-nickel oxide buffer. Run B1585 from table 3-4 was made at 800° C, 30000 p.s.i. using an iron mix equivalent to a biotite of 0.939 Fe/Fe + Mg composition. After 160 hours the assemblage contained biotite

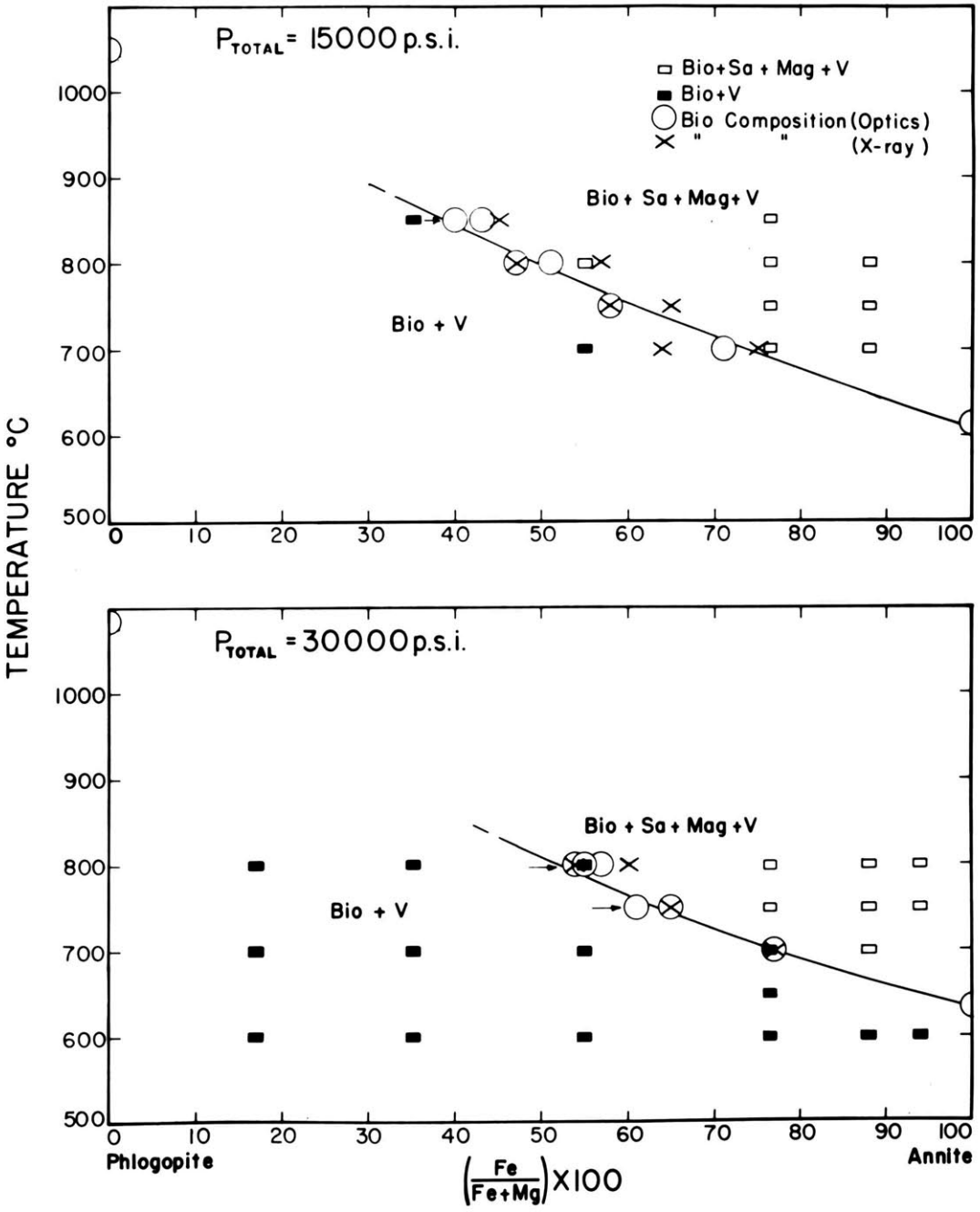

Figure 12. Stability of biotites on the join phlogopite-annite as a function of temperature and composition (Fe/Fe+Mg) at 15,000 and 30,000 p.s.i. total pressure and at oxygen pressures corresponding to the nickel-nickel oxide buffer. Arrows indicate reversal runs.

Table 18. Criteria Used to Establish the Position of Biotite-Sanidine-Magnetite-Vapor Assemblages Buffered by Nickel-Nickel Oxide.

Fe/Fe+Mg	T°C	Source
	Total pressure = 15,000 p.s.i.	
0.00	1050±15	Yoder and Eugster (1954)
0.43±0.03	850±5	Table E; Runs B1473, B1430
0.50±0.05	800±5	Table E; Runs B1419, B1441
0.58±0.05	750±5	Table E; Run B1434
0.71±0.06	700±5	Table E; Runs B1465, B1422
1.00	615±5	Table B; Runs B1529, B1535, B1533
	Total pressure = 30,000 p.s.i.	
0.00	1085±15	Yoder and Eugster (1954)
0.54±0.01	800±5	Table E; Runs B1383, B1565, B1367
0.63±0.03	750±5	Table E; Runs B1523, B1580, B1524
0.76±0.05	700±5	Table E; Run B1390
1.00	635±5	Table B; Runs B1482, B1476, B1527

+ sanidine + magnetite + vapor. If the assemblage had been sanidine and spinel the magnesioferrite content of that spinel would have been 20.54 mole per cent. As the run contained about 10 per cent biotite (visual estimate) the magnesioferrite content of the spinel phase must have been quite low.

4.8 The Hematite-Magnetite Buffer.

The biotite + sanidine + hematite + magnetite + vapor assemblages encountered under the experimental conditions are of importance in that they form a boundary limit to the biotite-sanidine-magnetite assemblages and also form an assemblage readily observed and defined in rocks.

The experimental data are presented in figure 13 and are given in detail in table F. The phase boundary in these diagrams is similar to that of figures 10 through 12 except that in this case it separates the fields biotite + vapor and biotite + sanidine + magnetite + hematite + vapor. The criteria used to establish this curve are given in table 19.

The equilibrium presented here was quite difficult to obtain. The rate of equilibrium between the buffer and charge is extremely slow, and frequently the interior charge would contain only biotite + sanidine + hematite + vapor with no observed magnetite. In runs either containing a large amount of iron or made at high temperatures this problem was not nearly so acute. Apparently the interaction of water and charge temporarily defines the oxygen pressure, and gives rise to assemblage with higher oxygen pressures than the buffer. Consequently it appeared that many of the runs first crystallized an oxidized assemblage and then gradually reduced that assemblage to the true equilibrium. The consequence of this problem is that the equilibrium curves are not known with the same precision as the quartz-magnetite-fayalite and nickel-nickel oxide buffered systems.

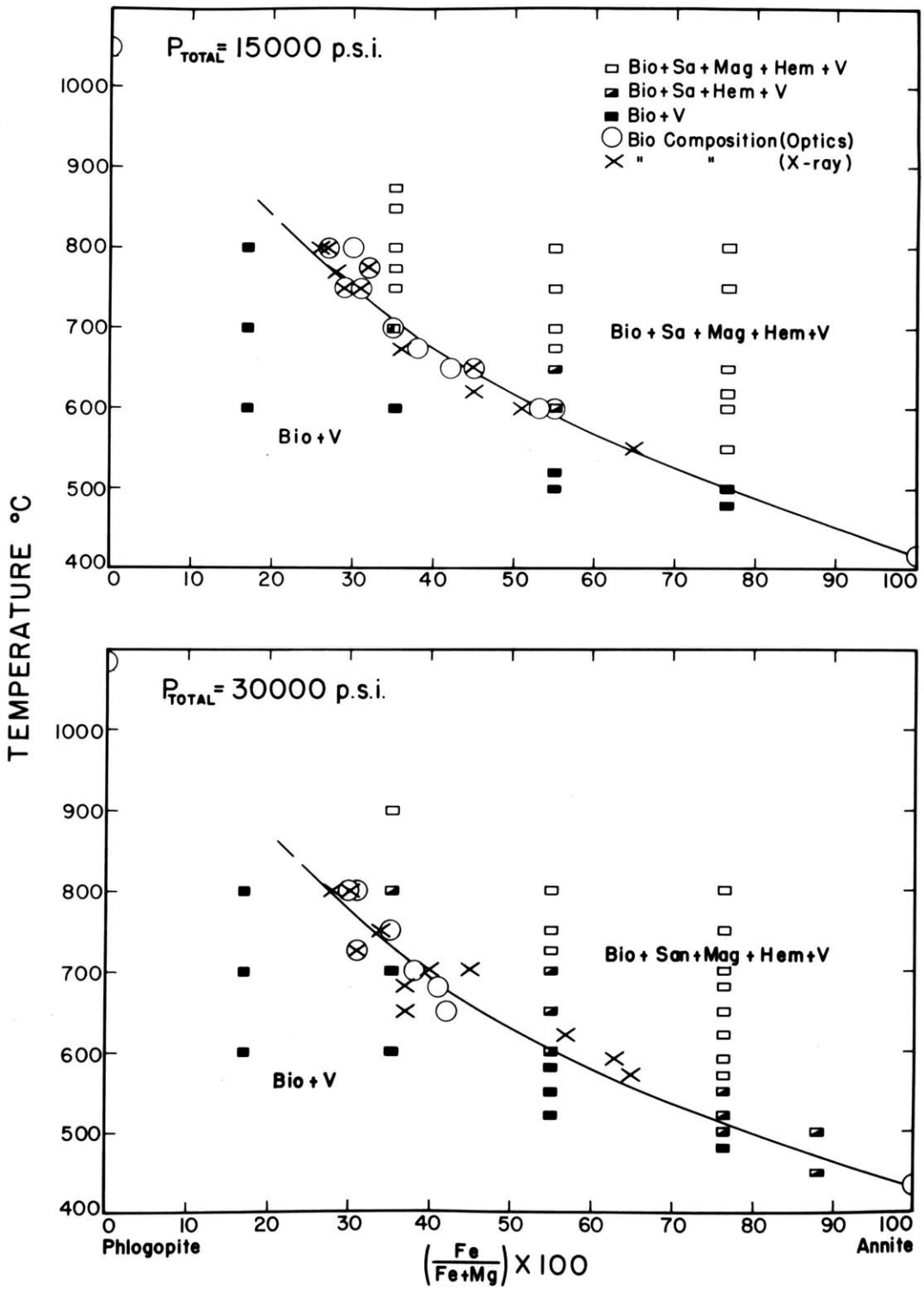

Figure 13. Stability of biotites on the join phlogopite-annite as a function of temperature and composition (Fe/Fe+Mg) at 15000 and 30,000 p.s.i. total pressure and at oxygen pressures corresponding to the hematite-magnetite buffer.

Table 19. Criteria Used to Establish the Position of Biotite-Sanidine-Magnetite-Hematite-Vapor Assemblages.

Fe/Fe+Mg	T°C	Source
	Total pressure = 15,000 p.s.i.	
0.00	1050±15	Yoder and Eugster (1954)
0.27±0.04	800±5	Table F; Runs B1551, B1184
0.30±0.02	750±5	Table F; Runs B1556, B1548
0.35±0.02	700±5	Table F; Run B1552
0.37±0.02	675±5	Table F; Run B1575
0.44±0.02	650±5	Table F; Run B1567
0.52±0.02	600±5	Table F; Run B1024
0.65±0.05	550±5	Table F; Run B1027
1.00	(417)	Section 4.3; this work
	Total pressure = 30,000 p.s.i.	
0.00	1085±15	Yoder and Eugster (1954)
0.30±0.02	800±5	Table F; Runs B1510, B1542, B1573, B1543
0.36±0.02	750±5	Table F; Runs B1554, B1004
0.38±0.05	700±5	Table F; Runs B1179, B1541
0.57±0.05	620±5	Table F; Run B1025
0.63±0.05	590±5	Table F; Run B1026
0.65±0.05	570±5	Table F; Run B1037
1.00	(433)	Section 4.3; this work

The large temperature effect, however, means that data can be collected over wider ranges than is true for the other equilibria and provides a better possibility of establishing the position of the equilibrium.

Attempts at reversals were made, but in every case the run was extended to such a length that the buffer was reduced to magnetite by the diffusion of hydrogen through the outer gold tube.

This equilibrium marks a boundary to the assemblage biotite + sanidine + magnetite + vapor. At higher partial pressures of oxygen (or lower temperatures at constant oxygen pressure) the assemblage becomes biotite + sanidine + hematite + vapor. The occurrence of this assemblage in runs buffered by hematite-magnetite assemblages indicates either 1) the biotite + sanidine + hematite + vapor assemblage coincides with the hematite-magnetite assemblage, or 2) the inner charge has not been equilibrated with the buffer. As has been seen in the case for the end member, annite, the thermodynamic arguments indicate that hypothesis (2) is more probable. It is shown in a later section that this argument also holds true for the intermediate members.

4.9 The Copper-Cuprite Buffer.

In hopes of determining the position of the biotite-sanidine-hematite-vapor equilibrium, the copper-cuprite buffer was employed. However, the experimental difficulties involved were formidable, and the attempt was temporarily abandoned. The problem was twofold: 1) the copper alloyed so rapidly with the gold and platinum tubing that the buffer was in fact a Cu_xAu_y - Cu_2O (see section 2.6), and 2) the equilibration of hydrogen between buffer and charge was an even more formidable problem here than with the hematite-magnetite assemblages.

The experiments indicate that biotite + sanidine + hematite + vapor assemblages do exist. However, the quantitative aspects of such assemblages are not known, except by thermodynamic extrapolation.

4.10 Summary of Experimental Results. Interpolation. Extrapolation.

The experimental results presented in sections 4.3 through 4.9 have determined the stability limits of the intermediate biotites at conditions where magnetite is the stable iron oxide, and at certain specified conditions of temperature, total pressure, and partial pressure of oxygen. In the application of those results to natural assemblages it shall be seen that another more useful way of expressing these data is by using them to define the composition of biotite coexisting with sanidine and magnetite under certain specified conditions.

The composite results are presented in figure 14. This figure plots the logarithm of the partial oxygen pressure of biotite + sanidine + magnetite + vapor assemblages as a function of biotite composition, total vapor pressure, and temperature. The plot is made in terms of the inverse temperature so that the partial oxygen vapor pressure curves will be linear. It can be readily seen from figure 14 that such a linearity does exist, although there are discrepancies between the curves and the experimental points. These are ascribed both to the experimental slack and to the uncertainties in the location of the buffer curves.

The points in figure 14 were taken from the curves of figures 10 through 13. The black circles represent points taken within the actual experimental data; the open circles represent those points taken from the extension of the phase boundaries in figures 10 through 13. The solid curves in figure 14 represent the data at 30,000 p.s.i., the broken curves the data at 15,000 p.s.i.

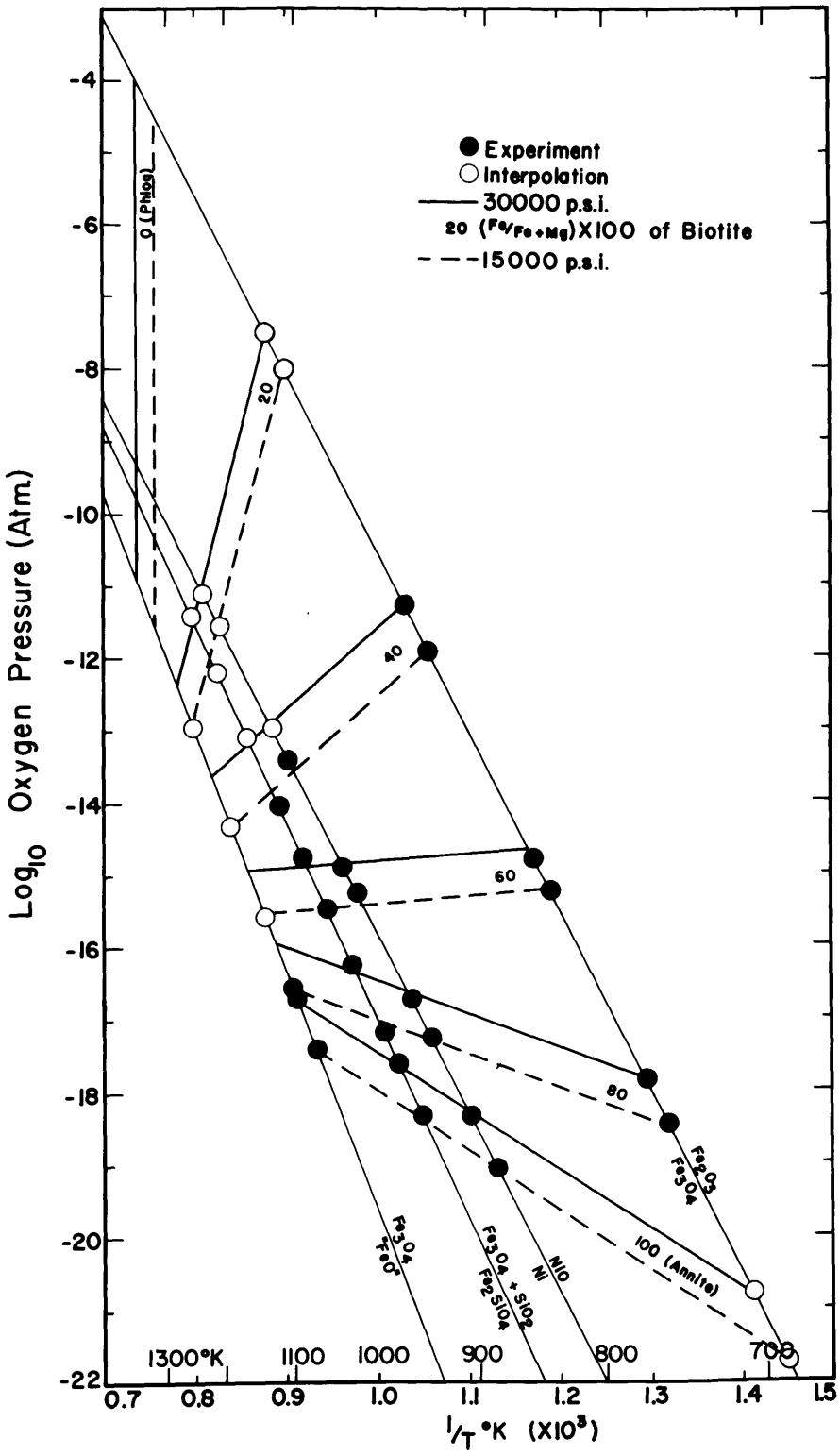

Figure 14. Locus of biotite-sanidine-magnetite-vapor assemblages as functions of oxygen pressure, temperature, composition, and total pressure. Biotite of Fe/Fe+Mg content less than that indicated for curves is stable in the magnetite field below that curve.

The loci of the biotite + sanidine + magnetite + vapor assemblages are listed in table 20. In addition to a tabulation of the temperatures at which biotites of a given composition coexist with sanidine, magnetite, and vapor the values for the slope $\left[\frac{\partial \log_{10} P_{O_2}}{\partial (1/T)}\right]$ of the specific biotite assemblages are given. These slopes can be used to determine the locus of the biotite + sanidine + hematite + vapor assemblages, as they will allow the determination of the partial molar enthalpy of the annite end member in the biotite. Then by the technique of section 4.3, the slopes of the biotite-sanidine-hematite assemblage can be determined. These slopes are also given in table 20.

These slopes are all greater than that of the hematite-magnetite assemblage, indicating that the biotite-sanidine-hematite-vapor assemblages do not coincide with the hematite-magnetite assemblage, but represent a separate equilibrium which is a function of total pressure, temperature and oxygen pressure.

4.11 High-Temperature Phase Relations of the Biotites.

The high-temperature phase relations of the biotites were not investigated directly during this study, but suggestions can be made concerning the nature of these relations. Of necessity, the first step is the resolution of the anhydrous assemblages which are equivalent to biotite in composition, with the exception of oxygen. The four parameters of interest in defining these assemblages are 1) total pressure, 2) temperature, 3) partial pressure of oxygen, and 4) composition in terms of Fe and Mg.

At moderate total pressures (1-10,000 atmospheres) and temperatures (sub-solidus), the critical parameters will be partial pressure of oxygen and composition. The phases encountered in the system will

Table 20. Locus of Biotite-Sanidine-Magnetite-Vapor and Biotite-Sanidine-Hematite-Vapor Equilibria (°C)

Biotite Composition (Fe/Fe+Mg)	"FeO" Fe_3O_4	Fe_2SiO_4 Fe_3O_4 SiO_2	Ni NiO	Fe_3O_4 Fe_2O_3	$\left[\frac{\partial \log_{10} P_{O_2}}{\partial (1/T)}\right]$ Bio-Sa-Mag	$\left[\frac{\partial \log_{10} P_{O_2}}{\partial (1/T)}\right]$ Bio-Sa-Hem
			Total pressure = 30,000 p.s.i.			
0.20	—	992	972	873	$+48.75 \times 10^{-5}$	$+23.94 \times 10^{-5}$
0.40	—	904	862	700	$+11.00 \times 10^{-5}$	-0.95×10^{-5}
0.60	—	820	768	582	$+0.10 \times 10^{-5}$	-8.36×10^{-5}
0.80	—	752	686	500	-4.50×10^{-5}	-11.30×10^{-5}
1.00	825	705	635	433	-8.25×10^{-5}	-13.80×10^{-5}
			Total pressure = 15,000 p.s.i.			
0.20	948	970	956	850	$+48.75 \times 10^{-5}$	$+23.94 \times 10^{-5}$
0.40	934	878	850	678	$+11.10 \times 10^{-5}$	-0.90×10^{-5}
0.60	875	792	750	570	$+0.10 \times 10^{-5}$	-8.36×10^{-5}
0.80	828	726	670	484	-4.60×10^{-5}	-11.36×10^{-5}
1.00	791	685	615	417	-8.50×10^{-5}	-13.96×10^{-5}

be sanidine, leucite, kalsilite, olivine, pyroxene, hematite, magnetite, and vapor. The five components necessary to define these phases are $KAlO_2$, SiO_2, MgO, Fe, and O_2.

The phase relations are most easily understood by reference to a tetrahedral configuration of the four components $KAlO_2$, MgO, SiO_2, and "FeO" as presented in figure 15. Assuming that the iron oxides may be present at the "FeO" apex regardless of their oxygen content (a projection from the oxygen apex of the five-component hyperprism of which the tetrahedron in figure 15a is the base), all of the aforementioned phases can be represented in the tetrahedron of figure 15a. The heavy line labeled P-A represents the anhydrous compositions equivalent to biotites on the join phlogopite-annite.

Figures 15b-e represent isobaric, isothermal tetrahedra at various oxygen isobars increasing from figures 15b to 15e. The assumptions made in constructing this set of diagrams are 1) no melt is present, 2) leucite and magnesioferrite are incompatible, 3) sanidine and magnesioferrite are incompatible, 4) sanidine and kalsilite are incompatible, 5) sanidine and forsterite are incompatible, 6) the fayalite content of olivine decreases with an increase of oxygen pressure above that of the quartz-fayalite-magnetite assemblage, 7) the fayalite content of the olivines decreases at oxygen pressures below that of the quartz-fayalite-iron assemblage, 8) the fayalite content of olivine is extremely low at partial oxygen pressures equivalent to the hematite field of stability, and 9) figure 8a represents the true phase relation of annite. Of these premises, Schairer (1954) has ample testimony that assumptions 4 and 5 are true, while the work of Muan and Osborne (1955) indicated that 6, 7, and 8 are true. Premises 1, 2, and 3 have been assumed merely to simplify the diagram.

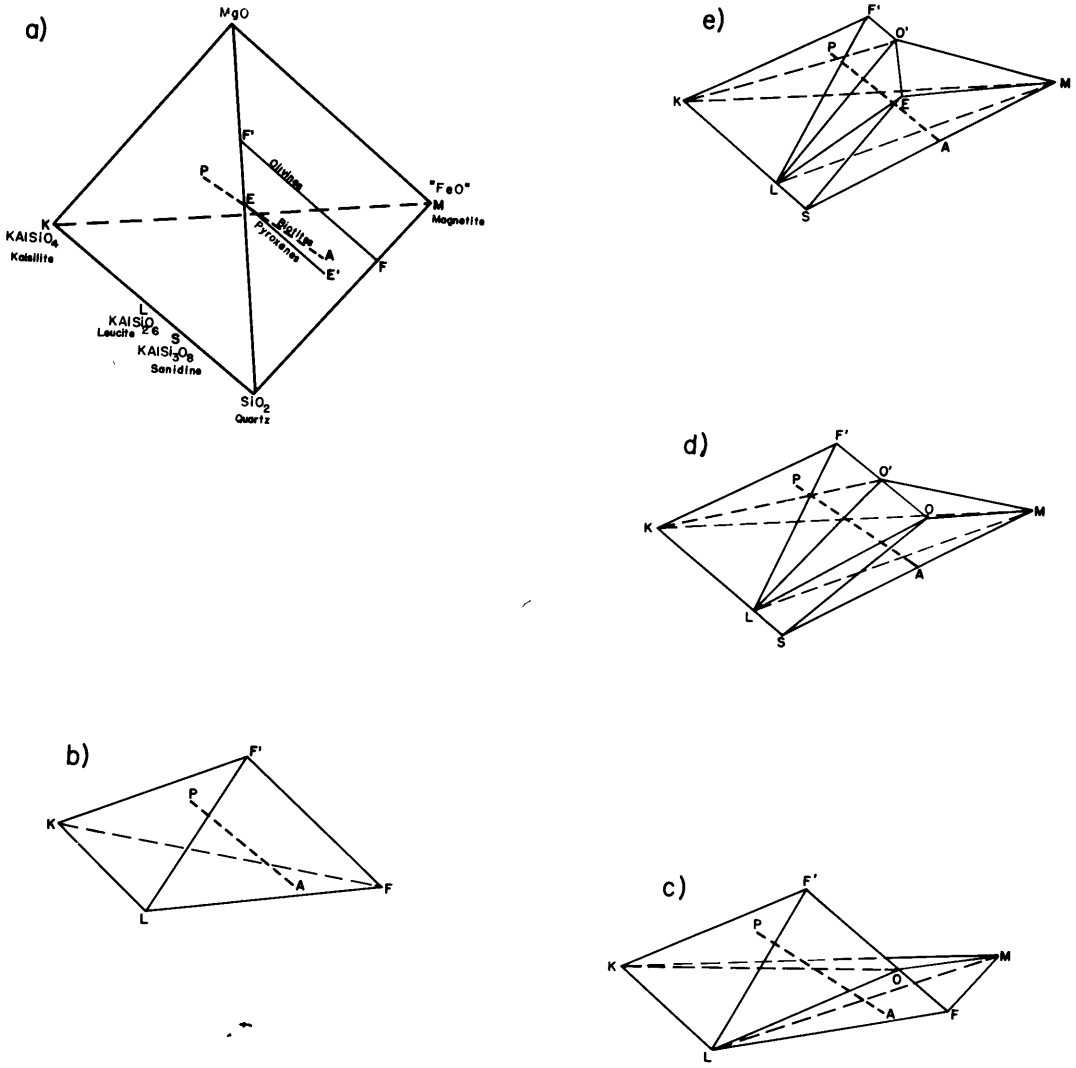

Figure 15. Proposed phase assemblages in the system $KAlSiO_4$-SiO_2-MgO-Fe-O. Compositions are presented as a tetrahedron projected from the oxygen apex of the hyperprism. Phase assemblages are isothermal; oxygen pressure increases from 15b to 15e.

Figure 15b represents the phase relations of compositions on the join "phlogopite-annite" at conditions under which the anhydrous equivalent of annite is kalsilite + leucite + fayalite. As the anhydrous equivalent of phlogopite is kalsilite + leucite + forsterite, all biotite compositions will form the three-phase (plus the ubiquitous vapor) assemblage kalsilite + leucite + olivine. In going from annite to phlogopite compositions, the assemblages encountered are all represented by triangles having a common base at K-L and apices which fall along the edge F-F' of the resultant tetrahedron. The composition of the olivine is dependent on the bulk composition of the assemblage.

Figure 15c represents slightly higher partial pressures of oxygen where the assemblage kalsilite-fayalite-oxygen reacts to form the assemblage leucite-magnetite. The volume representing the phase assemblages of interest is now a composite of tetrahedra rather than a simple tetrahedron. Starting with the annite compositional equivalent at point A and progressing toward point P, the first series of assemblages are leucite-magnetite-olivine assemblages represented by a series of triangles having a common base along line L-M, and apices falling along O-F. As in figure 15b the composition of the olivine is determined by the bulk composition of the assemblage.

At the plane L-O-M, however, the biotite equivalent assemblage changes to a four-phase assemblage kalsilite-leucite-magnetite-olivine. The olivine remains constant for all bulk compositions, and changes in the Fe/Fe + Mg ratio merely change the ratio of the phases present, not their composition. At compositions more magnesian rich than the plane K-O-L, the assemblages are kalsilite-leucite-olivine, represented by triangles having a common base on line K-L and apices falling along line O-F'.

Figure 15d represents an oxygen pressure where fayalite is no longer stable and the annite composition is represented by the assemblage sanidine-magnetite. In this case, the first assemblage encountered after sanidine-magnetite is sanidine-magnetite-leucite-olivine. The olivine in this assemblage has a fixed composition and changes in Fe/Fe + Mg ratio merely change the amounts of the several phases, not their compositions. When the Fe/Fe + Mg ratio of the biotite equivalent composition reaches surface L-O-M, the sequence towards the pure magnesium side is equivalent to figure 15c.

The assemblages represented in figure 15e contain a new phase, pyroxene. This results from partial pressures of oxygen at which the fayalite content of the stable olivine is so low that sanidine and olivine are an incompatible pair. Consequently, the first magnesium bearing assemblage encountered is sanidine-leucite-magnetite-pyroxene. This is a four-phase assemblage which is adjacent to another four-phase assemblage leucite-olivine-magnetite. More magnesium rich assemblages follow the pattern of figure 15c.

This whole group of assemblages can be projected onto a P_{O_2}-X diagram such as figure 16. This represents the relative relations of the assemblages as either oxygen pressure or Fe/Fe + Mg ratio vary. As this diagram is a projection, both three-and four-phase assemblages are plotted as areas. The difference in the two assemblages is merely that in four-phase assemblages the composition of the pyroxenes and/or olivines is fixed, in three-phase assemblages they are not. The assemblage on the left represents the anhydrous equivalent of phlogopite (kalsilite + leucite + forsterite) and is unaffected by changes in oxygen pressure. The lower portion of the diagram is more or less a mirror image of the upper portion

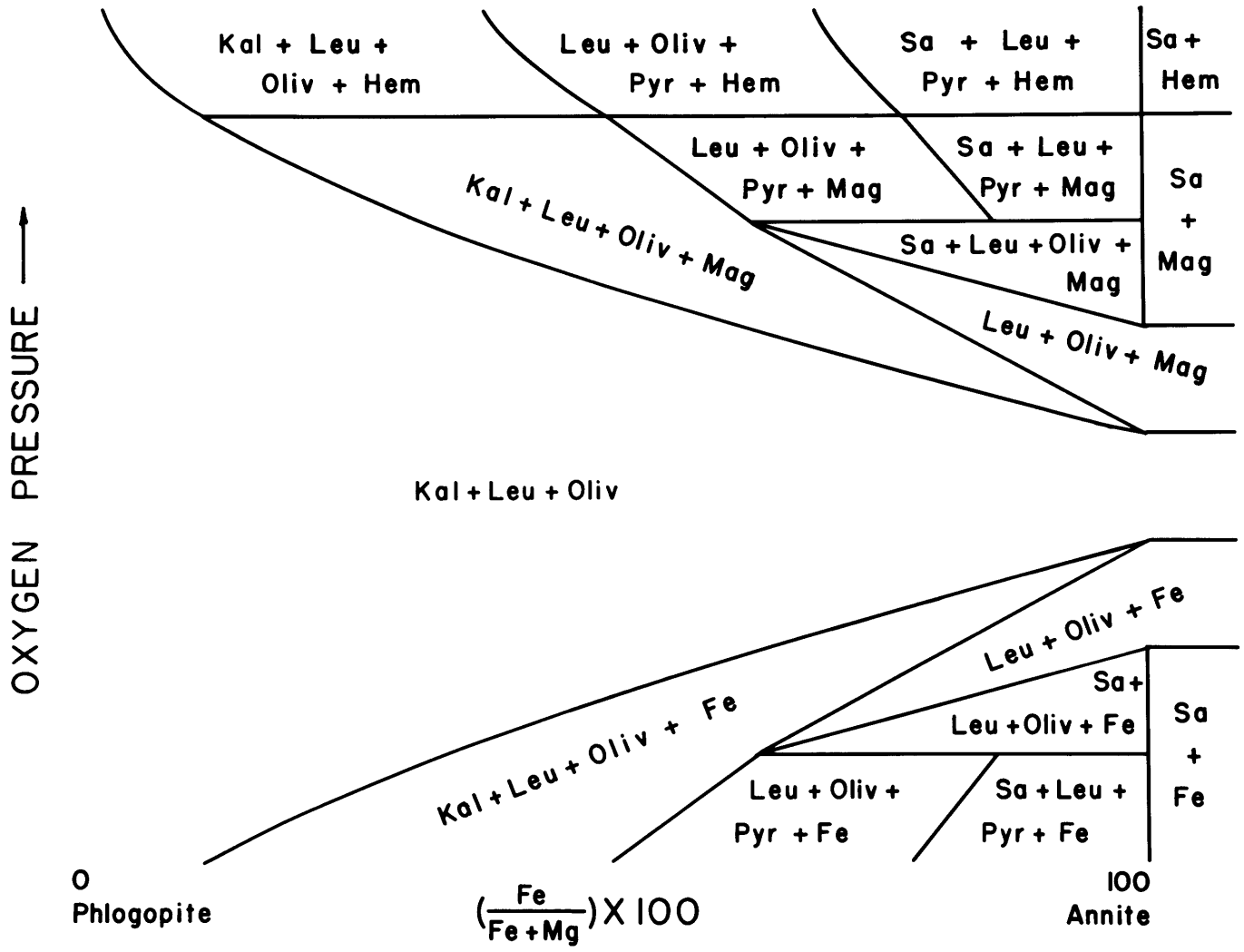

Figure 16. Proposed isothermal phase relations of the anhydrous compositions corresponding to the biotites on the join phlogopite-annite as a function of oxygen pressure and composition.

and has been derived as such.

The addition of H_2 to these diagrams will result in a highly complex series of assemblages. It has been seen in the previous portions of this study that MgO has a large affinity for the biotite structure, and that, in the presence of sanidine and magnetite, or sanidine and hematite, the phlogopite molecule would not react to form other phases at temperatures up to and including 900° C at 15,000 p.s.i. total pressure. Consequently, it seems probable that the large number of biotite assemblages which would be expected to form occur in a relatively small temperature range.

4.12 Biotite Phase Relations in the P_{O_2}-T-X Space

Figure 17 is a schematic representation of the biotite phase relations as a function of partial pressure of oxygen, temperature, and composition at constant total pressure. The diagram shows a multi-faceted volume within which biotite-vapor is the stable phase assemblage. The surfaces ruled with P_{O_2} isobars represent biotites coexisting with the indicated anhydrous assemblages at the specified temperature and oxygen pressure. Surface Y-X-L'-M-H'-N-Y represents an oxygen isobar arbitrarily selected as a cut-off pressure.

Surface C-C'-E'-E represents the composition of biotite coexisting with sanidine, magnetite, and vapor. The curves of figures 10 through 13 represent projections of the intersection of surface C-C'-E'-E with the P_{O_2}-T surfaces of the buffer assemblages on the temperature-composition plane. Curve E-E' is the composition of biotites coexisting with sanidine, hematite, and magnetite, and represents one boundary of the surface. There is a conjugate surface to C-C'-E'-E which represents the composition of magnetite coexisting with the biotite. The data cited in

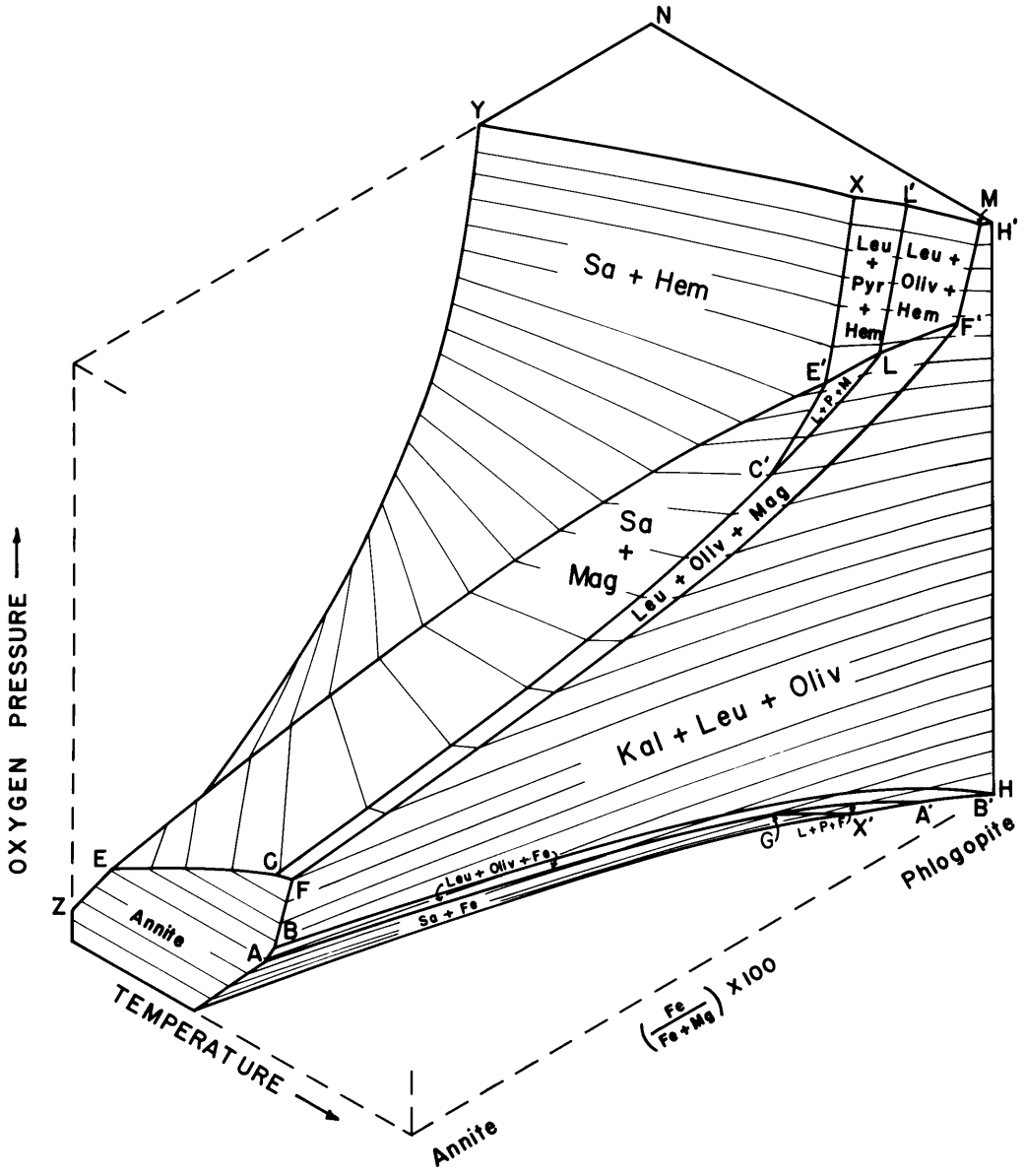

Figure 17. Proposed isobaric stability limits of biotites as a function of temperature, oxygen pressure, and composition. Various surfaces are labeled according to the phases coexisting with biotite and vapor of the given composition at the given temperature and oxygen pressure.

chapter 3 indicated that the magnesium content is fairly low, so that such a surface would originate at curve E-C and extend upward practically adjacent to the annite side of the diagram. The most interesting feature of surface C-C'-E-E' is the change in $\left(\frac{\partial P_{O_2}}{\partial T}\right)_{X,P}$ from a positive sense at annite composition, decreasing to zero at an Fe/Fe + Mg of about .60 and then becoming increasingly negative until its termination. The high-temperature and high Mg assemblages were not encountered in this study, and indications are that surfaces C'-E'-L, E'-L-L'-X, and L-F'-M-L' are all condensed into a very small temperature inverval.

Surface E-E'-X-Y-Z represents those biotites coexisting with sanidine and hematite and has been determined by the extrapolations mentioned in section 4.10. Like surface C-C'-E'-E, it has a positive $\left(\frac{\partial P_{O_2}}{\partial T}\right)_{X,P}$ at annite composition, zero at about .40 and increasingly negative until its termination. The conjugate hematite has a negligible magnesium content, and the surface representing hematite composition will be practically coincident with the annite side of the diagram.

The remaining surfaces represent biotites coexisting with the various assemblages of figure 16. These surfaces will have conjugates representing the compositions of the olivines, pyroxenes, and oxides coexisting with biotite. Surface F-B-B'-H-H'-M-F'-F represents biotites coexisting with kalsilite, leucite, and olivine. The $\left(\frac{\partial P_{O_2}}{\partial T}\right)_{X,P}$ is practically infinite as all phases are reduced. There is a slight positive slope due to 1) ferric iron in annite, and 2) effect of H_2 pressure on a reaction involving H_2O as the primary gas species.

The lower surfaces represent conditions where iron is the stable iron bearing phase and is, qualitatively, a mirror image of the magnetite assemblages.

Two types of T-X projections are shown in figure 18 (a and b) and

these correspond to 1) partial oxygen pressures equivalent to an iron-wüstite assemblage, and 2) partial oxygen pressures equivalent to a nickel-nickel oxide assemblage.

In the first case, for any Fe/Fe + Mg ratio, an increase in temperature causes no effect until the lower curve is reached. At this point, however, biotite of a given composition reacts to form kalsilite, leucite, and an olivine of greater iron content. As the temperature increases, the biotite decreases in quantity and becomes more magnesium rich, as does the olivine, until the upper curve is reached, at which point the biotite is completely gone, and kalsilite-leucite-olivine-vapor is the resultant assemblage.

In the second diagram, the relations are considerably more complex. The lower portion of the diagram is the part which was determined experimentally. In the iron rich portion of the system, as temperature is increased, the biotite reacts to form more magnesium rich biotite, sanidine, and magnetite. As the temperature increases this reaction will continue at the expense of the biotite (annite end member) until the temperature of the first reaction point is reached.

At this point the remaining biotite reacts with sanidine and magnetite to form olivine and leucite. Whether or not all the biotite reacts is dependent on the bulk composition of the assemblage. For more magnesium rich portions the biotite forms a similar "reaction series" at higher temperatures, only with leucite, olivine, and magnetite rather than with sanidine and magnetite.

As the temperature continues to increase, another reaction point is reached where biotite reacts with leucite, olivine, and magnetite to form kalsilite-leucite-olivine-magnetite assemblages. For magnesium rich com-

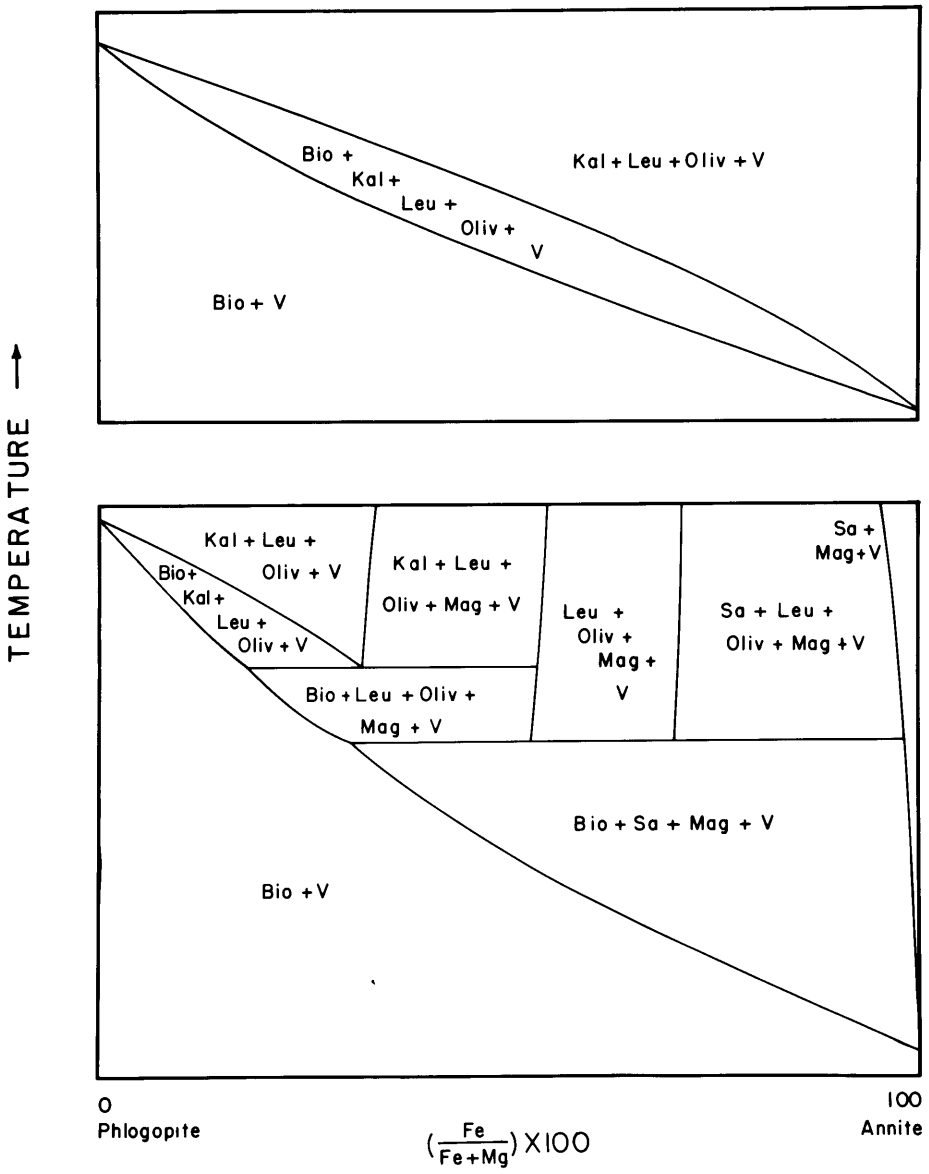

Figure 18. Proposed isobaric phase relations of biotites as a function of temperature and composition. Upper diagram represents oxygen pressures equivalent to wustite-magnetite assemblages; the lower diagram, nickel-nickel oxide.

positions, a reaction very similar to that observed for wüstite-magnetite assemblages continues until the temperature at which phlogopite reacts to form kalsilite, leucite, and forsterite. In all cases this reaction represents the maximum temperatures at which biotite is stable.

These diagrams emphasize the fact that at isobaric conditions, the maximum temperature at which biotite is a stable phase is dependent on oxygen pressure and bulk composition. The diagrams also point out the fact that biotites participate in a "continuous reaction series" and biotite composition within given assemblages is a function of temperature and oxygen pressure as well as bulk composition.

It would seem desirable to check and see that the proposed assemblages in figure 17 do not violate the phase rule. The number of effective components encountered in the study is not constant, as certain assemblages may be described in terms of four or five components while others require six. The six components encountered in the system are $KAlO_2$, SiO_2, MgO, Fe, O, and H. In the magnetite-hematite-sanidine-vapor assemblage and the iron-sanidine-vapor assemblage, the two components $KAlO_2$ and SiO_2 are reduced to the single component $KAlSi_3O_8$. Finally, in the biotite-vapor assemblage the components are $KFe_3AlSi_3O_{10}(OH)_2$, $KMg_3AlSi_3O_{10}(OH)_2$, O, and H.

The parameters which may vary are 1) pressure, 2) temperature, 3) composition of biotite, 4) composition of olivine, 5) composition of pyroxene, 6) composition of spinel, and 7) composition of vapor phase. The latter parameter, when combined with pressure, will yield the variable, oxygen pressure.

Assuming that figure 17 is a correct representation of the biotite composition phase relations, table 21 lists the variancy of the several

Table 21. Variancy of Biotite Phase Relations.

Assemblage	Components	Variancy
1) Bio + Vapor	4	4
2) Bio + Sa + Mag + Vapor	5	3
3) Bio + Sa + Hem + Vapor	5	3
4) Bio + Sa + Mag + Hem + Vapor	5	2
5) Bio + Sa + Fe + Vapor	5	3
6) Bio + Leu + Oliv + Mag + Vapor	6	3
7) Bio + Leu + Oliv + Hem + Vapor	6	3
8) Bio + Leu + Oliv + Hem + Mag + Vapor	6	2
9) Bio + Leu + Oliv + Fe + Vapor	6	3
10) Bio + Sa + Leu + Oliv + Mag + Vapor	6	2
11) Bio + Sa + Leu + Oliv + Hem + Vapor	6	2
12) Bio + Sa + Leu + Oliv + Mag + Hem + Vapor	6	1
13) Bio + Sa + Leu + Oliv + Fe + Vapor	6	2
14) Bio + Leu + Kal + Oliv + Mag + Vapor	6	2
15) Bio + Leu + Kal + Oliv + Hem + Vapor	6	2
16) Bio + Leu + Kal + Oliv + Mag + Hem + Vapor	6	1
17) Bio + Leu + Kal + Oliv + Fe + Vapor	6	2
18) Bio + Leu + Kal + Oliv + Vapor	6	3
19) Bio + Sa + Leu + Pyr + Mag + Vapor	6	2
20) Bio + Sa + Leu + Pyr + Hem + Vapor	6	2
21) Bio + Sa + Leu + Pyr + Mag + Hem + Vapor	6	1
22) Bio + Sa + Leu + Pyr + Fe + Vapor	6	2
23) Bio + Sa + Leu + Pyr + Oliv + Mag + Vapor	6	1
24) Bio + Sa + Leu + Pyr + Oliv + Hem + Vapor	6	1
25) Bio + Sa + Leu + Pyr + Oliv + Fe + Vapor	6	1
26) Bio + Sa + Leu + Pyr + Oliv + Hem + Mag + Vapor	6	0

assemblages. Assemblage (1) with its variancy of four is represented by a volume in figure 17, whereas (2) and (3) are represented by surfaces C-C'-E'-E and E-E'-X-Y-Z respectively. Assemblage (4) is represented by the curve E-E'.

If the olivines which are stable in the presence of hematite and magnetite are compatible with sanidine, assemblages (11), (12), (24) and (26) will not be realized except metastably.

It must be reiterated that figure 17 represents only schematic relations at elevated temperatures, and is the result of deduction based on experimental evidence at low temperatures and the phlogopite composition.

4.13 Effect of Total Pressure. Introduction of the Hydrogen Variable.

As is so graphically demonstrated in figure 14, a decrease in total vapor pressure is accompanied by decreases in the temperature and partial oxygen pressure of a given equilibrium. The net effect is much the same as that found for non-iron bearing hydrous silicates. However, the absolute quantities of temperature and partial oxygen pressure may vary quite widely for a given composition and total vapor pressure. Consequently, this is a "trivariant" assemblage, and it is necessary to define three of the four variables in order to define equilibrium. The four variables in question are total pressure, temperature, composition of biotite, and partial pressure of oxygen. However, this last variable can be thought of as the composition of the gas phase, and it becomes necessary to define the total pressure and the partial pressure of one of the three gas species H_2, H_2O, or O_2.

If one takes the reaction

$$2KFe_3AlSi_3O_{10}(OH)_2 + O_2 = 2KAlSi_3O_8 + 2Fe_3O_4 + 2H_2O. \qquad [4.3]$$
annite + oxygen = sanidine + magnetite + water

and adds the reaction [2.1] one arrives at the following reaction

$$KFe_3AlSi_3O_{10}(OH)_2 = KAlSi_3O_8 + Fe_3O_4 + H_2 \qquad [4.5]$$

annite = sanidine + magnetite + hydrogen

In this case the reaction has been reduced to a simple single species gas reaction.

Plotting this result on log f_{H_2} - 1/T plots for biotites of specified composition (Fe/Fe + Mg = .20, .40, .60, .80, 1.00) yields figure 19. The importance of this result cannot be over stressed, for the hydrogen pressures of the several buffers overlap due to the change in total pressure, and yet the biotite phase equilibria demonstrate the linearity required of the Clapeyron equation.

This data can be used to extrapolate to low pressures (1 atm) in its present form. However, it must be remembered that the reaction [4.5] only occurs between the wüstite-magnetite phase boundary and the magnetite-hematite phase boundary.

It can be easily shown that the equilibrium does not shift appreciably with total pressure using the methods suggested by Thompson (1955). For the reaction in question

$$d\Delta G = -\Delta S dT + \Delta V_{solid}\, d\, P_{tot} + \Delta V_{H_2}\, d\, P_{H_2} \qquad [4.6]$$

Assuming that the partial hydrogen pressure remains constant, then for a state of equilibrium

$$dT/d\, P_{tot} = \frac{\Delta V_{solid}}{\Delta S} \qquad [4.7]$$

For the reaction in question, it is known that the partial molar volume of annite is 153 cc/mole (table 13), and the total volume of sanidine (108.3 cc) and magnetite (44.5 cc) to be 152.8 cc/mole, thereby yielding a volume change of 0.2 cc/mole for the above reaction [4.5]. As there is no data on the entropy of annite, an approximation was made by

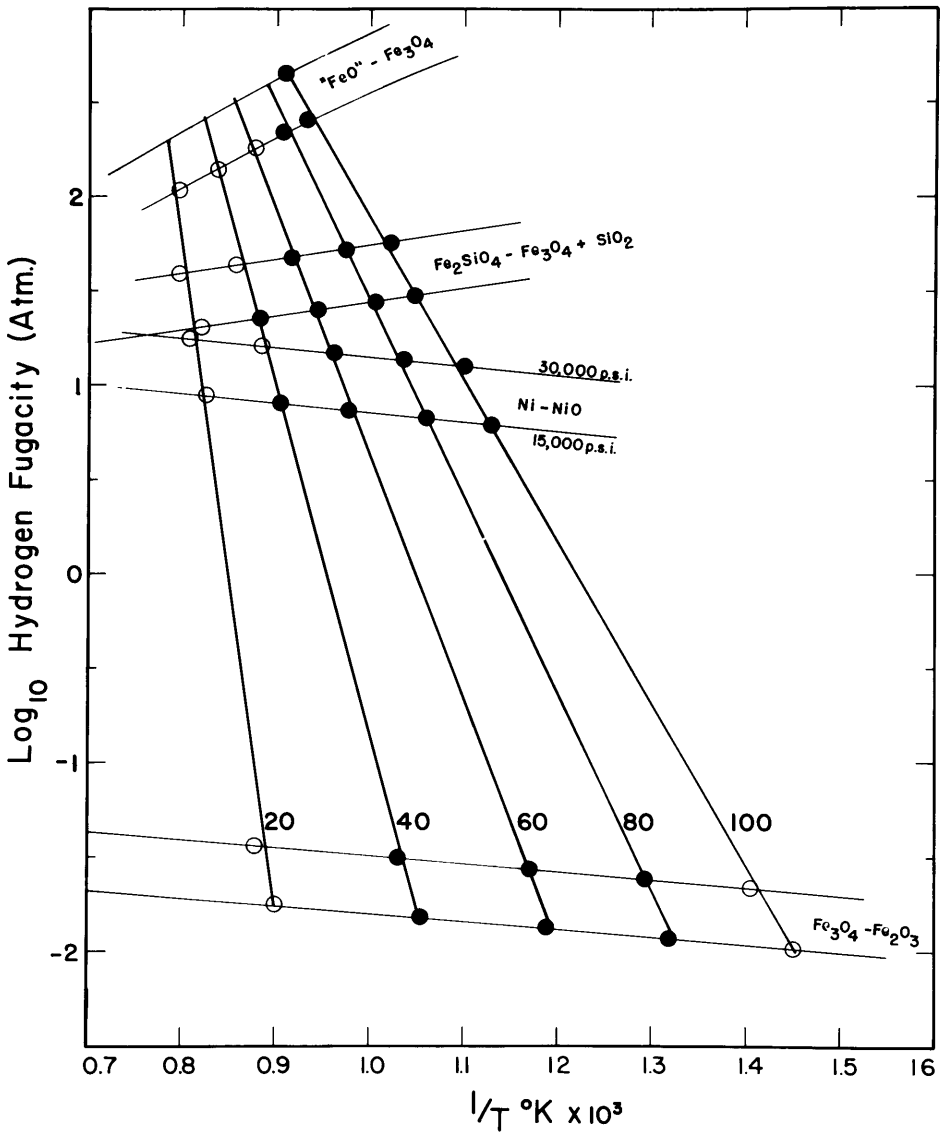

Figure 19. Hydrogen vapor pressure of the assemblage biotite-sanidine-magnetite-vapor as a function of temperature and biotite composition. Heavy lines represent stability limits of biotites of given Fe/Fe+Mg ratio. Light lines are hydrogen fugacities of water-hydrogen mixtures coexisting with the buffers at given pressures. Solid circles represent points realized experimentally. Open circles represent extrapolated points.

taking the entropy value for flurophlogopite at 1000° K (Kelley et al., 1959) and adding 21 cal/°/mole as average amounts for the substitutions of 3Fe for 3Mg and adding 2 cal/°/mole for the substitutions of 2(OH) for 2F. The resultant value of ΔS is 40 cal and hence dT/dP is 0.5° C/1000 bars indicating that the extrapolations to one atmosphere can be made by merely extrapolating figure 15.

The bulk of these extrapolations has been dependent on the Clapeyron equation of the form discussed in section 4.3. Yoder and Eugster (1954) in their work on muscovite attempt to use the form

$$\frac{dP}{dT} = \frac{\Delta S}{\Delta V} \qquad [4.12]$$

which is only as good as the slope concerned in the reaction. As was pointed out previously this study finds the form of [4.2] much more useful than [4.12] because of the larger volume of data.

At higher pressures, the compressibilities of the several solid phases should cause shifts in the position of the equilibria. However, the values of the compressibilities are all on the order of 10^{-5} cc/bar and consequently are not important at pressures below 10,000 atmospheres. The compressibility of the gas phase, although large, does not enter into consideration for this extrapolation as it is the fugacity, not pressure, which is being calculated. Consequently, it is necessary to know the activity coefficients of water and hydrogen at elevated temperatures and pressures if equilibrium is to be established in terms of actual pressures rather than fugacity.

The most important result, however, is that this clearly demonstrates the relatively low hydrogen pressures required at moderately high temperatures for ferrous biotites to remain stable. The wide variations in the character of volcanic biotites is easily understood as variations in

rates of quenching, combined with wide variations in the ability of the volcanic material to maintain hydrogen vapor pressure, will result in fresh biotite, oxybiotite, or sanidine-iron oxide pseudomorphs. This data certainly substantiates the earlier qualitative work of Rinne (1925), Kozu and Yoshiki (1926).

Unfortunately, the stoichiometry of the other biotite reactions is not as simple. For hematite reactions, oxygen must be added, while for olivine reactions water or water and hydrogen mixtures is evolved. Consequently these reactions require the definition of P_{O_2} and either P_{H_2O} or P_{H_2}.

The analysis given here allows a final check on the validity of the buffer technique, and in an unexpected way. Mixes made up of oxalate were used in early runs, but the generation of carbon dioxide into the gas phase was thought to nullify the results, as it would cause an unknown decrease in the partial vapor pressure of water in the vapor phase. However, the hydrogen pressure should be the same, if the semi-permeable membrane of platinum was operating properly.

The results from the oxalate runs are so nearly equivalent to the runs using pure biotite that it is extremely difficult to differentiate the two runs where all else is constant. However, if hydrogen pressure, rather than oxygen pressure,is the more critical variable, then this phenomenon is exactly what would be expected. As long as magnetite is the stable iron oxide, then the oxalate mix runs should yield results equivalent to the biotite runs. Table 22 compares the results of oxalate and biotite runs at equivalent temperatures, buffers, and total pressures.

Table 22. Comparison of Biotite Assemblages Crystallized from Oxalate Mix with Those Crystallized from Synthetic Biotite.

Comp.	T°C	Buffer	Assemblage	n_γ Biotite	
				Oxalate	Biotite
			Total pressure = 30,000 p.s.i.		
0.169	700	H-M	Bio-Vap	1.608±0.003	1.609±0.003
0.550	800	QFM	Bio-Vap	1.645	1.644
0.765	680	HM	Bio-Sa-Mag-(Hem)-Vap	1.643	1.641
0.765	800	QFM	Bio-Sa-Mag-Vap	1.660	1.659

CHAPTER V

GEOLOGIC APPLICATIONS

5.1 Occurrence of Biotite in Igneous Rocks.

The occurrence of biotite in igneous rocks representing wide ranges in bulk composition has been amply demonstrated throughout the geologic literature, but more specifically by Heinrich (1946) and Nockolds (1947). Figure 20 is adapted from Heinrich's data and clearly represents the tendency of biotite compositions (in terms of $MgO/FeO/Fe_2O_3$) to "cluster" according to specific rock types. The over-all pattern demonstrates that the biotites found in ultramafic rocks are high in MgO content, whereas those found in granitic rocks and pegmatites are relatively high in FeO + Fe_2O_3 content. Biotites from dioritic and granodioritic rocks have intermediate compositions.

These compositional variations found within the biotites undoubtedly reflect the bulk compositions of the rocks in question to a fair degree; these variations also reflect the effect of temperature on biotite stability. The more ultramafic rocks are conceded to have been emplaced at higher temperatures than the granitic rocks, and the variations in biotite compositions in these rocks, when compared to the biotite phase relations presented in chapter 4, certainly are in accordance with such temperature variations.

However, for the biotite equilibrium data to be more useful, the presence of a reaction assemblage is required. In such a case, the biotite composition is independent of the bulk composition of the rock and is the result of other parameters such as temperature, pressure, or partial oxygen pressure. In general, the relation defining biotite phase relations in igneous rocks may be expressed as:

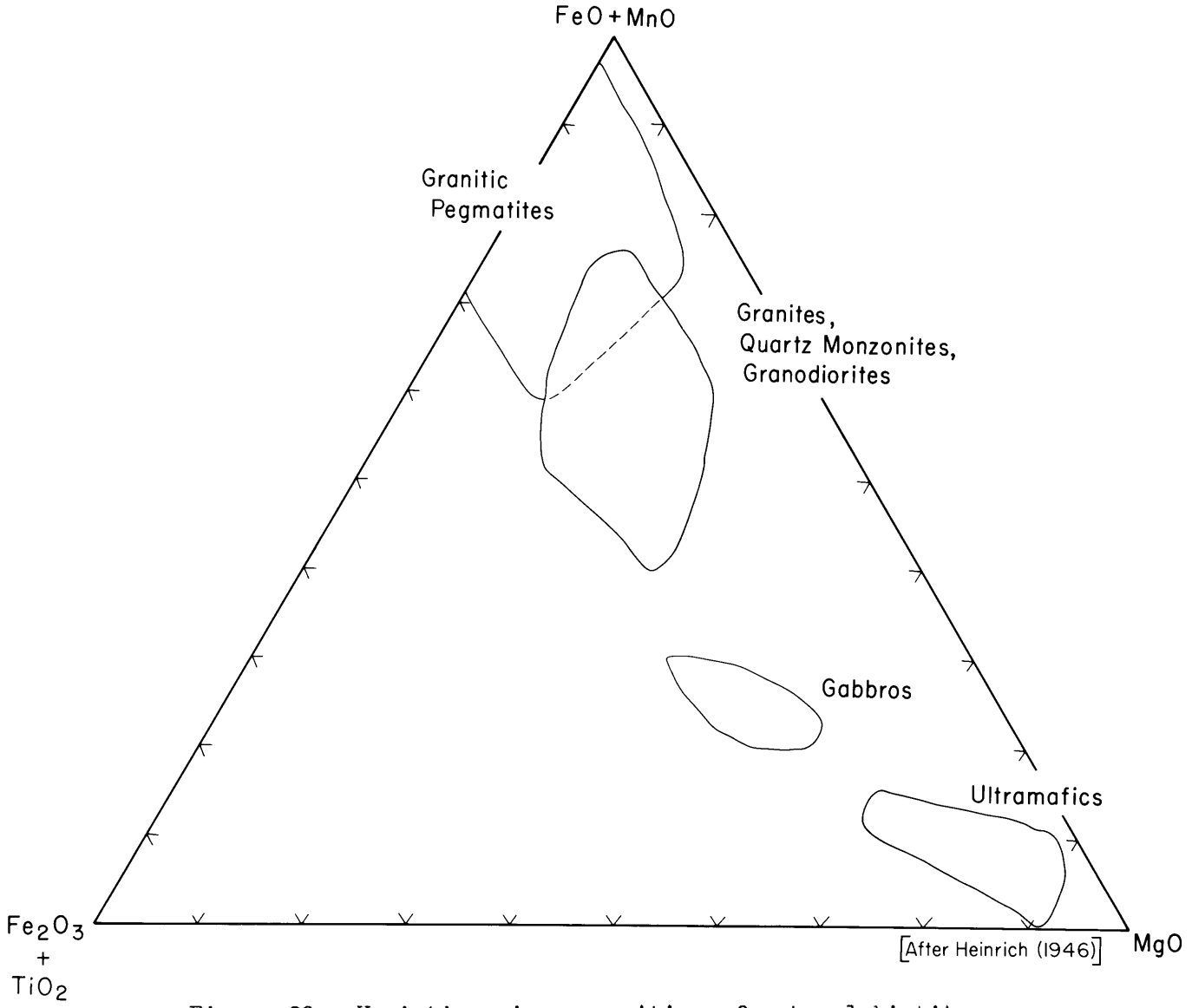

Figure 20. Variations in composition of natural biotites occurring in various igneous rocks (after Heinrich, 1946).

K-feldspar/feldspathoid + ferromagnesian mineral + water (+ oxygen) =

biotite (+ oxygen) (+ quartz).

For the experimental results of sections 4.4-4.9 the specific reaction observed was

$$KAlSi_3O_8 + Fe_3O_4 + H_2O = KFe_3AlSi_3O_{10}(OH)_2 + 1/2\ O_2 \qquad [4.1]$$

In sections 4.10-4.13 the effects of total pressure, temperature, and partial oxygen pressure on such an equilibrium were discussed in some detail.

The combined effect of water vapor pressure and temperature on biotite assemblages has been discussed by Yoder and Eugster (1954) using the example of the alkaline volcanics of Uganda as described by Holmes (1942). These volcanics are, in part, made up of the assemblage kalsilite-leucite-olivine. However, bombs and xenoliths of equivalent bulk composition frequently contain phlogopite. Furthermore, certain of the volcanic rocks have phlogopite forming at the kalsilite-olivine boundaries. The interpretation given by Yoder and Eugster is that the magma was at high water pressure and temperature, and was originally crystallizing phlogopite. Upon extrusion, the water pressure was decreased, but the temperature remained high, causing phlogopite to react to form kalsilite-leucite-olivine, As the magma cooled, phlogopite once more became stable, although at lower water vapor pressure, and the high-temperature assemblage reacted to form phlogopite.

The effect of pressure on the stability of the iron bearing biotites is considerably more complex, as oxygen pressure must be introduced as an additional variable. Larsen et al. (1937) describe variations in the compositions of biotite phenocrysts in the volcanic rocks of the San Juan

region, Colorado. Larsen found that the biotites varied widely in their FeO/Fe_3O_3 ratios, and that the higher the Fe_2O_3 ratios the lower the water content.

The biotites in bombs and inclusions had the lowest Fe_2O_3 contents, whereas the volcanic sequences varied widely in biotite Fe_2O_3 composition culminating in iron oxide pseudomorphs after biotite. If the biotite reaction is considered in terms of hydrogen pressure (see section 4.12), then the wider variations described by Larsen could represent variability in 1) hydrogen pressure and 2) water pressure. The hydrogen pressure required for stability of a given biotite in reference to the K-feldspar-magnetite reaction at one atmosphere total pressure varies from about one atmosphere to 10^{-5} atmospheres. Consequently, the biotite should remain stable as long as it is unexposed to the atmosphere. In a volcanic sequence, the biotites may be 1) contained in a bomb or inclusion and remain stable, 2) be exposed to the atmosphere for varying lengths of time, causing great variety in the hydrogen contents of biotites, or 3) be exposed continually to the atmosphere and be oxidized to K-feldspar-hematite assemblages.

The phacoliths of the northwest Adirondacks (Buddington, 1929) also emphasize the importance of water (or hydrogen) pressure in the formation of biotite. These rocks contain a K-feldspar-magnetite assemblage and are intruded into graphitic marbles. The presence of graphite indicates low partial pressures of oxygen, and the lack of biotite indicates that the water (or hydrogen) content of the phacolith was extremely low during crystallization.

Biotite assemblages should provide a great deal of information in problems where a variety of igneous rocks are thought to be related to a common

magma. If such is the case, then the vapor phase along the isotherms should be constant throughout the magma as to pressure and composition. The variation of the composition of biotite coexisting with K-feldspar and iron oxides should provide information of the homogeneity of the vapor phase in equilibrium with the plutonic mass in question.

The question of homogeneity in plutonic masses suggests the problem of differentiation and the role of biotite assemblages in such problems. The data of chapter 4 certainly suggest that biotites will take part in a continuous "reaction series," and that the sequence of mafic minerals is a problem of oxygen pressure as well as cooling. The presumed effect of cooling is to cause more iron rich biotites to form, but such will be the case only if the oxygen pressure is lowered at the same time, or if the bulk composition has an Fe/Fe + Mg ratio of less than 0.40 (see figure 17). Otherwise cooling could cause the formation of sanidine and magnetite at the expense of biotite.

The question becomes much simpler if hydrogen pressure is considered as the important variable and reference is made to figure 19. As the temperature falls, and the hydrogen pressure remains constant, biotite, sanidine, and magnetite will react to make a more iron rich biotite. However, if the hydrogen pressure were to decrease, then the biotite could react on cooling to form a more magnesium rich biotite as well as sanidine and magnetite. If a magma is water saturated and begins to crystallize while cooling, there will be an expulsion of water (H_2O) which will tend to decrease the hydrogen pressure of the gas phase in equilibrium with the magma, resulting in sanidine and magnetite rather than biotite as the final ferromagnesian crystallization product.

The classic work of Nockolds (1940) and Nockolds and Mitchell (1948)

on the caledonian intrusives indicates that various rock types could be formed by cooling and differentiating a single magma. In this study Nockolds and Mitchell demonstrate that the late stage biotites are more iron rich than the earlier ones, and as the biotite in question coexists with K-feldspar and magnetite, the hydrogen pressure is maintained at high enough values that the temperature effect is the dominant factor.

Grout (1924), in his description of the magnetite pegmatites of Minnesota, provides a possible example of a magmatic differentiation in which K-feldspar and magnetite represent the final crystallization products. The pegmatites described by Grout are closely related to granite and contain quartz-microcline-plagioclase-biotite with inner zones containing magnetite but little or no biotite. If this inner zone represents the last stage of the differentiate, presumably the hydrogen pressure was too low (oxygen pressure too high) to permit the formation of iron rich biotite. The expulsion of water from the crystallizing magma would certainly have such an effect. The biotite phase relations applied to such a case indicate that for these pegmatites a magmatic origin and a late stage vapor phase are compatible with a single process.

Biotite assemblages and their proper interpretation can yield substantial data concerning the origins of igneous rocks. Although biotite-K-feldspar-magnetite assemblages are "trivariant," they can be used as indicators of equilibrium, or if reasonable estimates of temperature and total pressure can be made, they can supply data concerning the composition of magmatic gas phases, a problem recently reviewed by Holland (1959) and Krauskopf (1959).

5.2 Occurrence of Biotite in Metamorphic Rocks.

The use of biotite in pelitic schists as an indicator of metamorphic grade was demonstrated by Barrow (1893) in the Scottish highlands. This concept was amplified by Harker (1939) and placed into the scheme of metamorphic facies (Turner, 1948; Fyfe, Turner and Verhoogen, 1958).

Unfortunately the present study does not apply directly to the general problem of pelitic schists, as only biotite compositions were investigated, whereas the pelitic schist contains a great deal of Al_2O_3 and SiO_2 in addition to biotite. However, the present study lends itself to some indirect applications to metamorphic problems.

The reaction studied intensively in chapter 4 was:

$$KFe_3AlSi_3O_{10}(OH)_2 + 1/2\ O_2 = KAlSi_3O_8 + Fe_3O_4 + H_2O \qquad [4.1]$$

biotite + oxygen = feldspar + magnetite + water

The addition of Al_2O_3 and SiO_2 will yield a reaction such as:

$$KFe_3AlSiO_{10}(OH)_2 + 1/2\ O_2 + Al_2SiO_5$$

biotite + oxygen + Al-silicate =

$$KAl_3Si_3O_{10}(OH)_2 + Fe_3O_4 + SiO_2 \qquad [5.1]$$

muscovite + magnetite + quartz

For such a reaction, oxygen pressure is very important and should be a determining factor in the composition of the resultant mineral assemblage.

Thompson (1957), in presenting a graphical analysis of the pelitic schists, treats Fe_2O_3 as a separate component and indicates that the net effect of oxidation is merely to change the Fe^{+2} available to the silicate assemblage. Figure 21, a and b, are AFM diagrams constructed in accordance with Thompson's suggestions. H_2O is treated as a mobile component, quartz (SiO_2) is ubiquitous, and Fe_2O_3 is present as hematite,

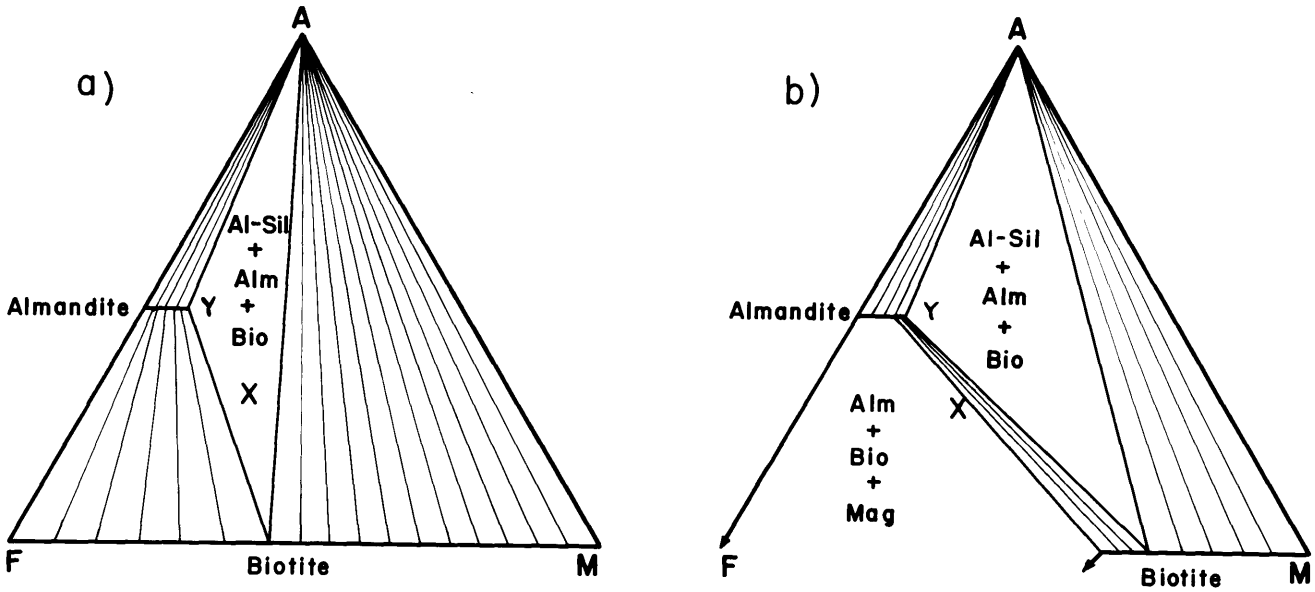

Figure 21. AFM diagrams patterned after Thompson (1957) demonstrating the effect of oxygen pressure on biotite stability and consequent effect on stable phase assemblages.

magnetite, or both. The remaining components K_2O, FeO, MgO, and Al_2O_3 may be presented in a tetrahedral configuration. The AFM diagrams of figure 21 result from a projection through the muscovite corner of such a tetrahedron.

Figure 21a represents the appropriate mineral assemblages at a partial oxygen pressure at which all biotites are stable. The observed assemblages at points Y and X are quartz-muscovite-Al-silicate-garnet-biotite-(oxide). Figure 21b represents the appropriate mineral assemblage at the same temperature and total pressure, but at oxygen pressures high enough that biotites with Fe/Fe + Mg ratios greater than 0.40 are unstable. The assemblage at Y remains the same, but the composition of the biotite is entirely different from the assemblage in figure 21a. At composition X the stable assemblage has become quartz-muscovite-garnet-biotite-oxide.

Variations very similar to these have been studied by Chinner (1958) in a sequence of rocks at Glen Clova, Scotland. Chinner found that the modal proportion of the minerals varied directly with the $2Fe_2O_3/2Fe_2O_3$ + FeO ratio of the rock, and these in turn correlated with primary sedimentary layers. Figure 22 summarizes the effects of oxidation (hence, increased oxygen pressure) on the assemblage. The iron content of the biotites in Chinner's area decreases as the oxidation ratio increases.

This indicates that individual rock units may preserve their unique partial oxygen pressure throughout several grades of metamorphism. This implies that the H_2/H_2O ratio of coexisting water vapor will vary from horizon to horizon. If this is the case, then one concludes that there was no significant circulation of water vapor in the sequence at Glen Clova.

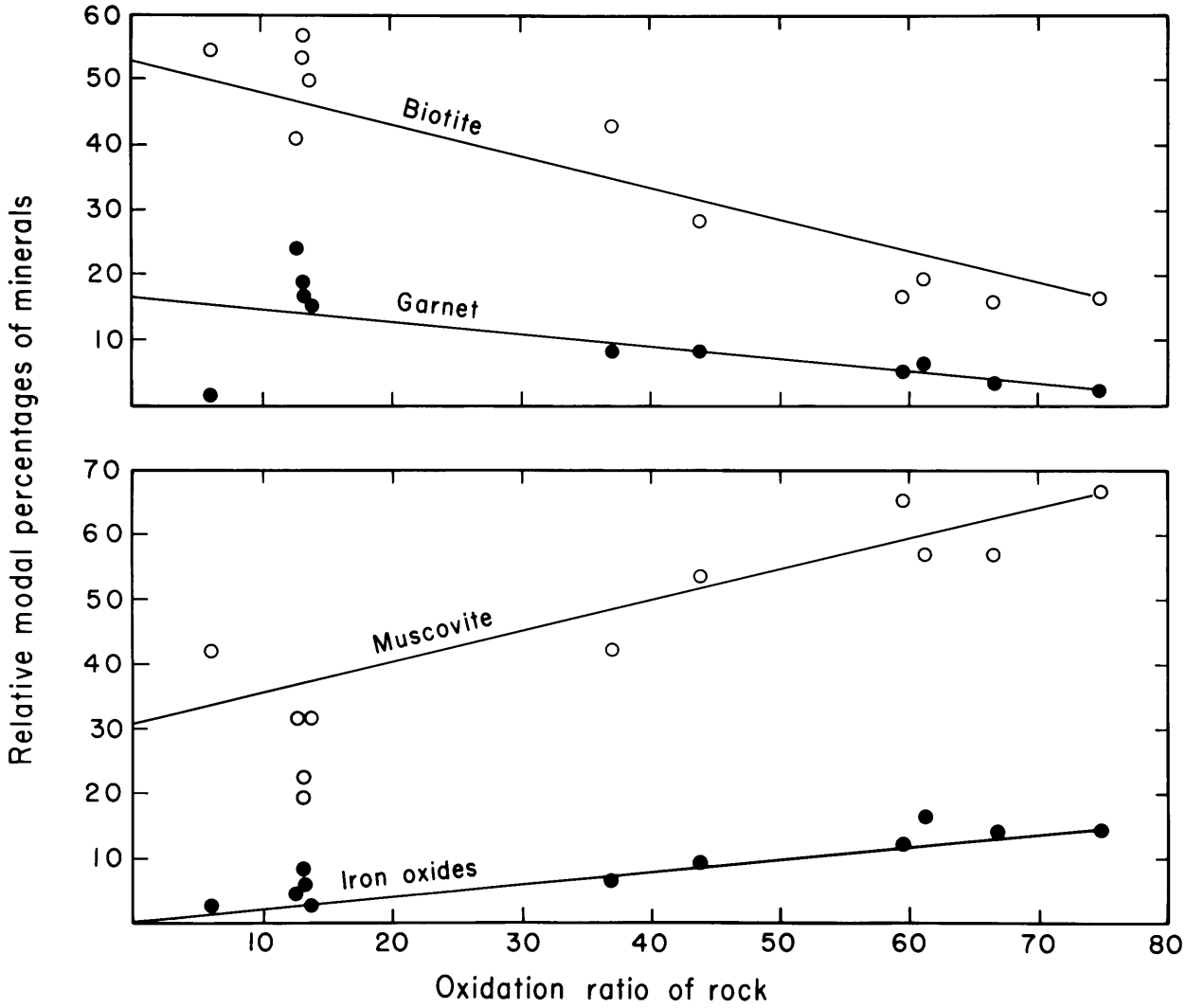

Figure 22. Modal variations of biotite mineral assemblages at Glen Clova, Scotland, as a function of the oxidation ratio of the rock (after Chinner, 1958).

This is suggestive of another problem, that of the granite gneisses. These rocks of granitic-granodioritic composition have a characteristic layered appearance, and as such, have had a multiplicity of suggested origins. One such suggestion (Harris, 1959) is that pelitic and quartzose sediments have been metasomatized by an aqueous alkaline fluid. If such a fluid has metasomatized a sequence of sedimentary rocks, it should also have brought all adjacent rock units to the same partial oxygen pressure.

The biotite-K-feldspar magnetite assemblages might be used as a check on such hypotheses. If adjacent layers have differing assemblages as regards the Fe/Fe + Mg ratio of biotites coexisting with sanidine and magnetite, and the layers can be shown to be isothermal and isobaric, then they could not have coexisted with a common aqueous fluid, and a metasomatic process is highly unlikely. However, if the biotite compositions are nearly identical, then metasomatism is still a possibility, and the problem of origin remains unresolved.

Biotites may also be used to give information regarding metamorphic gradients (i.e., in thermal aureoles). However, such use requires the consideration of the effect of variations in water vapor pressure and oxygen pressure. Once again, by reducing the problem to one of hydrogen pressure, it can be seen that in permeable rocks, at equivalent total pressure, gradients in the Fe/Fe + Mg ratio of biotites coexisting with sanidine and magnetite would undoubtedly reflect thermal gradients.

5.3 Occurrence of Biotite in Sulfide Mineral Assemblages.

The interaction of host rocks with vein minerals and the consequent "wall rock alteration" has been discussed by many investigators (Lovering, 1949; Sales and Meyer, 1949; Kerr, 1955; and Schwartz, 1959). In addition to those previously discussed there are two new factors affecting the

stability of biotite in such an environment. The first is the stability of biotite in acidic or basic vapors, a problem discussed by Hemley (1959) in terms of the mineral, muscovite. The essential effect is partial solubility of the mineral in an aqueous fluid leaving an aluminum silicate residuum.

The second problem is the stability of biotite in a sulfur rich environment. This type of equilibrium may be expressed as a reaction by adding

$$2KFe_3AlSi_3O_{10}(OH)_2 + O_2 = 2KAlSi_3O_8 + 2Fe_3O_4 + 2H_2O$$
$$\text{annite + oxygen = K-feldspar + magnetite + water} \qquad [4.1]$$

and

$$2Fe_3O_4 + 6S_2 = 6FeS_2 + 4O_2$$
$$\text{magnetite + sulfur = pyrite + oxygen} \qquad [5.2]$$

to obtain

$$2KFe_3AlSi_3O_{10}(OH)_2 + 6S_2 = 2KAlSi_3O_8 + 6FeS_2 + 3O_2 + 2H_2O \qquad [5.3]$$
$$\text{annite + sulfur = K-feldspar + pyrite + oxygen + water}$$

For reaction [5.3] there exists an equilibrium constant such that

$$K = \frac{P_{O_2}^3 \cdot P_{H_2O}^2 \cdot a_{FeS_2} \cdot a_{KAlSi_3O_8}}{P_{S_2}^6 \cdot a_{KFe_3AlSi_3O_{10}(OH)_2}} \qquad [5.4]$$

The activity of annite can be determined from the data of chapter 4, and as the other two solid phases are stoichiometric in the regions of interest, compositions of biotites coexisting with K-feldspar and pyrite (or pyrrhotite) could provide information concerning the sulfur vapor pressure of given natural assemblages.

A similar treatment can be introduced for carbonate equilibria:

$$KFe_3AlSi_3O_{10}(OH)_2 + 3CO_2 = KAlSi_3O_8 + 3FeCO_3 + H_2O \qquad [5.5]$$

5.4 Use of Biotite in Isotopic Age Determinations.

The recent work of Tilton et al. (1958) on the isotopic ages of the

various component minerals of the Baltimore Gneiss (Baltimore, Maryland) indicates that the ages of the biotites are considerably younger than the zircons and feldspars from the same rock samples. The biotite age (300 m.y.) corresponds to the Appalachian orogeny and metamorphism whereas the zircon and feldspar yield a Pre-Cambrian age (1200 m.y.)

This study has shown that biotites coexisting with K-feldspar and magnetite will recrystallize to a new composition if temperature, water vapor pressure, or oxygen pressure vary from the conditions of the original crystallization.[1] However, minerals such as feldspar, muscovite, and zircon are much less likely to recrystallize during a metamorphic event, as the biotites will have chemical as well as mechanical energy differences contributing to recrystallization.

The results demonstrate that biotite age data must be interpreted in the light of the mineral paragenesis as well as the geologic environment. Rocks in which biotite does not coexist with its reaction products (phlogopitic marbles, quartz-plagioclase-biotite gneiss) should yield biotite ages in concordance with other mineral ages from the same rock. Rocks in which the biotites do coexist with their reaction products should yield biotite ages reflecting the most recent metamorphic event, an event whose age may or may not be reflected by the other mineral ages.

---

[1] Dr. C. A. Hopson (personal communication) has stated that the assemblage biotite-magnetite-K-feldspar is present in all specimens of the Baltimore Gneiss selected for age determinations.

CHAPTER VI

RESULTS; SUGGESTIONS FOR FUTURE WORK

6.1 Summary of Results.

a) The usefulness and quantitative accuracy of the buffer techniques has been demonstrated at moderate temperatures (500° to 900° C) and pressures (15,000 to 30,000 p.s.i.).

b) Data concerning the phase relations of annite, $KFe_3AlSi_3O_{10}(OH)_2$, has been obtained in regard to both location and nature of the reaction assemblages.

c) The investigation has determined the phase relations of the biotites on the join phlogopite-annite as functions of composition, temperature, total vapor pressure, and partial pressure of oxygen.

d) The optical and lattice properties of the biotites on the join phlogopite-annite were determined and demonstrated variations with oxygen pressure.

e) The biotites demonstrated complete miscibility between phlogopite and annite, and although they represent neither an ideal nor regular solution, their extensive properties behave continuously.

f) Methods of extrapolating the experimental data have been demonstrated.

g) Schematic diagrams have been prepared concerning the proposed phase relations at higher temperatures.

h) Possible uses of biotite phase equilibria in problems of igneous and metamorphic petrogenesis have been suggested.

i) Certain anomalies concerning the use of biotite in isotopic age determinations may be resolved by the biotite phase relations.

j) Potential use of biotite in problems of ore genesis has been suggested.

6.2 Suggestions for Future Work

a) The following laboratory and theoretical studies should prove worthwhile:

1) Correlation of Fe_2O_3 content of biotites on the join phlogopite-annite with their physical properties and conditions (temperature, oxygen pressure) of formation.

2) Liquidus relations of the biotites.

3) Phase relations of aluminous biotites.

4) Phase relations of biotite-Al_2O_3-SiO_2 systems.

5) Extrapolation of biotite data to systems containing sulfur and carbon dioxide.

b) Suggestions for future field studies are:

1) Correlation of biotite assemblages within an igneous complex with the equilibrium diagrams.

2) Examination of metamorphic terrains (both regional and contact) to determine the extent of gas equilibrium.

3) Correlation of the isotopic ages of biotites and phlogopites from adjacent schists (or igneous rocks) and marbles. Such studies might elucidate whether the recrystallization of biotite is predominately a function of stress or chemical disequilibrium.

APPENDIX I

Tables recording experimental data.

A. Abbreviations used in Tables B-G.

B. Runs determining the stability and properties of annite.

C. Runs buffered by wustite-magnetite buffer.

D. Runs buffered by quartz-fayalite-magnetite.

E. Runs buffered by nickel-nickel oxide.

F. Runs buffered by hematite-magnetite.

G. Runs buffered by copper-cuprite.

Table A. Abbreviations Used in Tables B–G.

B	Biotite
S	Sanidine
M	Magnetite
H	Hematite
O	Olivine
L	Leucite
(F)	Fayalite (Less than 1%)
W	Wustite
Py	Pyroxene
SA	Synthetic annite
$SB_{16.93}$	Synthetic biotite (Fe/Fe+Mg = 0.1693)
P	Phlogopite
SAN/MAG	Mixture of sanidine and magnetite
FeMix	Mixture of $K_2O \cdot 6SiO_2$, γ-Al_2O_3, MgO and Fe
H Mix	Mixture of $K_2O \cdot 6SiO_2$, γ-Al_2O_3, MgO and Fe_2O_3
n.d.	Not determined
*	Biotites used to determine optical and lattice properties as a function of composition

Table B. Runs Determining the Stability and Properties of Annite.

Run No.	Starting Material	Buffer	T°C	Time (hr)	Products	n_γ	$d_{(060)}$
			Runs made at 30,000 p.s.i.				
B1501	FeMix	H-M	480	96	B+S+M	n.d.	1.5511±0.0010
B1537	SA	H-M	450	960	B+S+M+H	1.675±0.003	n.d.
B1538	SAN/MAG	H-M	430	714	S+M	-	-
H762*	SA	H-M	400	3000	B+(S)+(H)	n.d.	1.5547±0.0006
B1582 B	SAN/MAG	H-M	400	2325	S+M	-	-
B1522	SA	Ni-NiO	640	283	B+S+M	1.666	1.5521±0.0008
B1482	SAN/MAG	Ni-NiO	640	328	S+M	-	-
B1476	SA	Ni-NiO	640	708	B+S+M	1.689	1.5459±0.0018
B1527	SAN/MAG	Ni-NiO	635	144	B+S+M	1.675	n.d.
B1512*	SA	Ni-NiO	620	142	B+(S)	1.689	1.5530±0.0006
B1388*	SA	Ni-NiO	600	136	B	1.688	1.5540±0.0016
B1492*	FeMix	Ni-NiO	600	67	B+(S)	n.d.	1.5535±0.0009

Table B (cont'd)

Run No.	Starting Material	Buffer	T°C	Time (hr)	Products	n_γ	$d_{(060)}$
B1500	FeMix	Q-F-M	740	96	S+M	-	-
B1504	FeMix	Q-F-M	720	231	B+S+M	n.d.	1.5492±0.0010
B1511	SA	Q-F-M	710	209	B+S+M	1.679	1.5487±0.0007
B1498*	FeMix	Q-F-M	700	75	B	n.d.	1.5518±0.0005
B1505	SAN/MAG	Q-F-M	700	227	B+S+M	1.689±0.003	1.5481±0.0007
H950*	SA	Q-F-M	UNK	UNK	B	n.d.	1.5511±0.0010
B1559	SA	W-M	820	44	B+(S)+(F)	1.687±0.002	1.5523±0.0010
B1493	FeMix	W-M	820	40	B+(S)	n.d.	n.d.
			Runs made at 15,000 p.s.i.				
B1529	SA	Ni-NiO	620	163	B+S+M	n.d.	n.d.
B1535	SAN/MAG	Ni-NiO	620	210	S+M	-	-
B1533	SAN/MAG	Ni-NiO	610	160	B+S+M	n.d.	n.d.
B1536	SA	Q-F-M	690		S+M	-	-
B1534	SAN/MAG	Q-F-M	680		B+S+M	n.d.	n.d.

Table C. Runs Buffered by Wustite-Magnetite Buffer.

Run No.	Starting Material	T°C	Time (hr)	Products	$\pm\gamma$	d(060)	Fe/Fe+Mg (Biotite)
				Runs made at 15,000 p.s.i.			
B1085	$SB_{55.01}$	850	69	B+S	1.644±0.003	n.d.	0.550
B1461*	$SB_{55.01}$	850	177	B	1.648	1.5479±0.0007	0.550
B1090	$SB_{76.53}$	820	69	B+O+M+S+L(?)	1.675	n.d.	0.765
B1467	$SB_{76.53}$	850	94	B+S+M	1.670	1.5516±0.0005	0.74/0.68
B1489	$SB_{76.53}$	850	96	B+S+M	1.666	1.5507±0.0010	0.71/0.65
				Runs made at 30,000 p.s.i.			
B1516*	$SB_{88.01}$	800	73	B+(S)	1.690	1.555±0.0010	0.880

Table D. Runs Buffered by Quartz-Fayalite-Magnetite.

Run No.	Starting Material	T°C	Time (hr)	Products	$n\gamma$	$d_{(060)}$	Fe/Fe+Mg (Biotite)
				Runs made at 30,000 p.s.i.			
B1350*	$SB_{35.21}$	700	92	B	1.617±0.003	n.d.	0.352
B1337*	$SB_{35.21}$	800	89	B	1.618	1.5439±0.0006	0.352
B1330*	$SB_{35.21}$	825	118	B+(S)	1.617	n.d.	0.352
B1373	$SB_{35.21}$	850	132	B+(S)	1.612	1.5429±0.0006	<0.352
B1410*	$FeMix_{55.01}$	700	136	B	1.644	1.5478±0.0006	0.550
B1108*	$SB_{55.01}$	740	80	B+(S)	1.648	1.5487±0.0004	0.550
B1347*	$FeMix_{55.01}$	740	92	B+(S)	1.644	1.5488±0.0010	0.550
B1340*	$FeMix_{55.01}$	750	89	B+(S)	1.644	1.5493±0.0007	0.550
B1338*	$SB_{55.01}$	750	89	B+(S)	1.644	1.5485±0.0002	0.550
B1326	$SB_{55.01}$	760	92	B+(S)	1.648	1.5505±0.0006	0.550
B1280	$SB_{55.01}$	790	42	B+(S)	1.641	n.d.	0.550
B1233	$SB_{55.01}$	800	127	B+(S)	1.644	n.d.	0.550
B1281	$SB_{55.01}$	808	42	B+(S)	1.644	1.5446±0.0003	0.550

Table D (Cont'd)

Run No.	Starting Material	T°C	Time (hr)	Products	n_γ	$d_{(060)}$	Fe/Fe+Mg (Biotite)
B1141*	$SB_{76.53}$	680	169	B+(S)	1.673±0.003	n.d.	0.765
B1105	$(H\ Mix)_{76.53}$	690	89	B+S+M	1.655	n.d.	0.63
B1231	$(H\ Mix)_{76.53}$	690	142	B+S+M	1.663	1.5512±0.0006	0.70/0.69
B1131*	$SB_{76.53}$	690	189	B+(S)	1.670	1.5530±0.0007	0.765
B1261*	$(FeMix)_{76.53}$	700	48.5	B+(S)	1.675	n.d.	0.765
B1038*	$SB_{76.53}$	700	84	B+(S)	1.675	1.5527±0.0010	0.765
B1238	$(P+S+M)_{76.53}$	700	232	B+S+M	1.659	1.5499±0.0005	0.68/0.62
B1335	$SB_{76.53}$	705	449	B+S	1.672	1.5515±0.0005	0.75/0.71
B1232	$(H\ Mix)_{76.53}$	710	142	B+S	n.d.	1.5512±0.0003	0.71
B1132	$SB_{76.53}$	710	189	B+S	1.670	n.d.	0.75
B1313	$SB_{76.53}$	720	300	B+S	1.673	1.5520±0.0006	0.76/0.73
B1246	$(P+S+M)_{76.53}$	725	168	B+S+M	1.649	1.5490±0.0004	0.60/0.58
B1294*	$(FeMix)_{76.53}$	730	93	B+(S)	1.674	1.5532±0.0010	0.765
B1297*	$SB_{76.53}$	730	167	B+S	1.676	1.5505±0.0010	0.765
B1255	$(P+S+M)_{76.53}$	750	24	B+S+M	1.645	1.5485±0.0005	0.56

Table D (Cont'd)

Run No.	Starting Material	T°C	Time (hr)	Products	n_γ	$d_{(060)}$	Fe/Fe+Mg (Biotite)
B1254	$(P+S+M)_{76.53}$	750	48	B+S+M	1.645±0.003	1.5487±0.0006	0.56/0.57
B1252	$(P+S+M)_{76.53}$	750	122	B+S+M	1.646	1.5484±0.0004	0.57/0.56
B1251	$(P+S+M)_{76.53}$	750	195	B+S+M	1.646	1.5514±0.0006	0.57/0.70
B1237	$(P+S+M)_{76.53}$	750	241	B+S+M	1.659	1.5475±0.0008	0.67/0.52
B1275	$SB_{76.53}$	757	74	B+S	1.670	1.5512±0.0006	0.75/0.70
B1256	$SB_{76.53}$	775	66	B+(S)	1.680	1.5522±0.0009	0.765
B1247	$SB_{76.53}$	775	96	B+S+M	1.677	1.5499±0.0008	0.76/0.63
B1236	$(P+S+M)_{76.53}$	775	231	B+S+M	1.646	1.5472±0.0012	0.57/0.52
B1262	$(FeMix)_{76.53}$	800	46.5	B+S+M	1.664	1.5522±0.0008	0.71/0.74
B1177	$SB_{76.53}$	800	65	B+S+M	1.661	1.5499±0.0010	0.68/0.62
B1228	$SB_{76.53}$	800	142.5	B+S+M	1.659	1.5490±0.0006	0.67/0.58
B1189	$(P+S+M)_{76.53}$	800	250	B+S+M	1.640	n.d.	0.52
B1562	$(B+S+M)_{76.53}$	800	432	B+S+M	1.661	n.d.	0.68
B1270*	$SB_{88.01}$	700	48	B+(S)	1.690	1.5541±0.0005	0.880
B1345*	$SB_{88.01}$	705	113	B+(S)	1.692	1.5543±0.0008	0.880

Table D (Cont'd)

Run No.	Starting Material	T°C	Time (hr)	Products	n_γ	$d_{(060)}$	Fe/Fe+Mg (Biotite)
B1342*	$(FeMix)_{88.01}$	705	113	B+(S)	1.694±0.003	1.5541±0.0002	0.880
B1271	$SB_{88.01}$	750	48	B+S+M	1.669	1.5527±0.0014	0.74/0.76
B1438	$(FeMix)_{88.01}$	750	117	B+S+M	1.666	1.5512±0.0010	0.72/0.70
B1272	$SB_{88.01}$	800	48	B+S+M	1.663	1.5510±0.0018	0.70/0.69
B1586*	$(FeMix)_{95.93}$	600	140	B+(S)	1.689	1.5539±0.0010	0.939
				Runs made at 15,000 p.s.i.			
B1058	$SB_{55.01}$	700	138	B+S	1.638	1.5494±0.0010	$<$0.550
B1124*	$SB_{55.01}$	700	142	B+S	1.642	1.5486±0.0007	0.550
B1460*	$(FeMix)_{55.01}$	700	177	B+(S)	1.642	1.5486±0.0007	0.550
B1074	$SB_{55.01}$	720	64	B+S	1.638	1.5500±0.0007	$<$0.550
B1125*	$SB_{55.01}$	720	141	B+S	1.648	1.5480±0.0005	0.550
B1103	$SB_{55.01}$	735	67	B+S	1.641	1.5470±0.0005	0.510
B1305	$(FeMix)_{55.01}$	750	91	B+(S)	n.d.	n.d.	(0.55)
B1464	$SB_{55.01}$	800	94	B+(S)	1.644	1.5465±0.0010	0.55/0.52
B1445	$(FeMix)_{55.01}$	850	105	B+S	1.636	1.5487±0.0014	0.49/0.55

Table D (Cont'd)

Run No.	Starting Material	T°C	Time (hr)	Products	n_γ	$d_{(060)}$	Fe/Fe+Mg (Biotite)
B1481	$SB_{55.01}$	850	129	B+S+M	1.644±0.003	1.5497±0.0008	0.55/0.60
B1517	$SB_{55.01}$	900	6	B+S+M	1.643	1.5450±0.0004	0.54/0.42
B1110	$SB_{76.53}$	600	162	B+S	n.d.	1.5516±0.0007	<0.765
B1244	$(P+S+M)_{76.53}$	600	229	B+S+M	1.660	1.5489±0.0008	0.67/0.58
B1130	$SB_{76.53}$	660	209	B+(S)	1.668	1.5518±0.0005	0.75
B1196	$(P+S+M)_{76.53}$	660	250	B+S+M	1.648	1.5490±0.0004	0.59/0.58
B1168	$SB_{76.53}$	700	48.5	B+S	1.671	n.d.	0.74
B1191	$(P+S+M)_{76.53}$	700	250	B+S+M	1.655	1.5505±0.0004	0.64/0.65
B1519	$SB_{76.53}$	750	86	B+S+M	1.663	1.5501	0.70/0.63
B1444	$(FeMix)_{76.53}$	750	105	B+S+M	1.660	1.5511±0.0008	0.68/0.68
B1480	$SB_{76.53}$	750	141.5	B+S+M	1.658	1.5510±0.0014	0.66/0.68
B1240	$(P+S+M)_{76.53}$	775	229	B+S+M	1.635	1.5478±0.0010	0.49/0.53
B1183	$SB_{76.53}$	800	49.5	B+S+M	1.640	1.5473±0.0007	0.52/0.52
B1195	$(P+S+M)_{76.53}$	800	250	B+S+M	1.633	n.d.	0.47
B1446	$(FeMix)_{76.53}$	850	105	B+S+M	1.633	1.5462±0.0007	0.47/0.47

Table D (Cont'd)

Run No.	Starting Material	T°C	Time (hr)	Products	$n\gamma$	$d_{(060)}$	Fe/Fe+Mg (Biotite)
B1457	$SB_{88.01}$	750	177	B+S+M	n.d.	1.5494±0.0008	0.60
B1421	$FeMix_{88.01}$	800	89	B+S+M	1.640±0.003	n.d.	0.52
B1436	$(FeMix)_{88.01}$	800	123	B+S+M	1.639	n.d.	0.52

Table E. Runs Buffered by Nickel–Nickel Oxide.

Run No.	Starting Material	T°C	Time (hr)	Products	n γ	d(060)	Fe/Fe+Mg (Biotite)
			Runs made at 30,000 p.s.i.				
B1354*	$(FeMix)_{16.93}$	600	92	B	n.d.	1.5379±0.0007	0.169
B1376*	$SB_{16.93}$	600	107	B	1.596±0.003	1.5386±0.0005	0.169
B1370*	$SB_{16.93}$	600	138	B+(S)	1.601	1.5585±0.0005	0.169
B1356*	$(FeMix)_{16.93}$	700	139	B+(S)	1.600	1.5388±0.0005	0.169
B1365*	$SB_{16.93}$	700	117	B+(S)	1.600	1.5363±0.0006	0.169
B1357*	$(FeMix)_{16.93}$	800	92	B+(S)	1.600	1.5388±0.0006	0.169
B1367*	$SB_{16.93}$	800	118	B+(S)	1.600	1.5386±0.0008	0.169
B1353*	$(FeMix)_{35.21}$	600	92	B	n.d.	1.5426±0.0010	0.352
B1372*	$SB_{35.21}$	600	107	B+(S)	1.616	1.5427±0.0006	0.352
B1563*	$SB_{35.21}$	700	113	B+(S)	1.619	n.d.	0.352
B1366*	$SB_{35.21}$	700	117	B+(S)	1.618	1.5440±0.0006	0.352
B1355*	$(FeMix)_{35.21}$	700	139	B	1.616	1.5411±0.0004	0.352
B1361*	$(FeMix)_{35.21}$	800	121	B+(S)	1.619	1.5435±0.0008	0.352

Table E (Cont'd)

Run No.	Starting Material	T°C	Time (hr)	Products	n γ	$d_{(060)}$	Fe/Fe+Mg (Biotite)
B1352*	$(FeMix)_{55.01}$	600	92	B+S	1.641±0.003	1.5467±0.0006	0.550
B1377*	$SB_{55.01}$	600	115	B	1.641	1.5471±0.0009	0.550
B1382*	$SB_{55.01}$	700	118	B+(S)	1.648	1.5471±0.0008	0.550
B1385*	$(FeMix)_{55.01}$	700	179	B+(S)	1.646	1.5472±0.0006	0.550
B1415*	$SB_{55.01}$	800	168	B	1.647	1.5476±0.0005	0.550
B1381*	$SB_{55.01}$	800	168	B	1.646	n.d.	0.550
B1351	$(FeMix)_{76.53}$	600	92	B+S	1.659	1.5517±0.0005	<0.765
B1380	$SB_{76.53}$	600	164.5	B+S	1.661	1.5509±0.0006	<0.765
B1336	$SB_{76.53}$	650	89	B+S	1.653	1.5460±0.0002	<0.765
B1569	$(P+S+M)_{76.53}$	650	829	B+(S)	1.676	1.5497±0.0011	0.765
B1384*	$SB_{76.53}$	700	148	B+(S)	1.676	1.5517±0.0008	0.765
B1391*	$(FeMix)_{76.53}$	700	160	B+(S)	1.675	1.5514±0.0004	0.765
B1564	$(P+S+M)_{76.53}$	700	1000	B+S+M	1.642	n.d.	0.520
B1523	$SB_{76.53}$	750	209	B+S+M	1.660	1.5497±0.0010	0.65/0.66

Table E (Cont'd)

Run No.	Starting Material	T°C	Time (hr)	Products	n ɣ	$d_{(060)}$	Fe/Fe+Mg (Biotite)
B1580	$(P+S+M)_{76.53}$	750	597	B+S+M	1.654±0.003	1.5483±0.0003	0.62/0.60
B1359	$(FeMix)_{76.53}$	800	121	B+S+M	1.648	1.5482±0.0005	0.57/0.60
B1383	$SB_{76.53}$	800	141-1/2	B+S+M	1.649	1.5473±0.0005	0.58/0.55
B1565	$(P+S+M)_{76.53}$	800	786	B+S+M	1.647	1.5471±0.0004	0.57/0.55
B1375*	$SB_{88.01}$	600	132	B+(S)	1.688	1.5530±0.0004	0.880
B1363*	$(FeMix)_{88.01}$	600	139	B+S	1.670	1.5531±0.0008	0.880
B1374	$SB_{88.01}$	700	132	B+S+M	1.688	1.5528±0.0005	0.870
B1390	$(FeMix)_{88.01}$	700	163	B+S+M	1.675	1.5519±0.0005	0.770
B1524	$SB_{88.01}$	750	209	B+S+M	1.660	1.5480±0.0015	0.66/0.58
B1369	$SB_{88.01}$	800	118	B+S+M	1.649	1.5487±0.0010	0.58/0.61
B1358	$(FeMix)_{88.01}$	800	121	B+S+M	1.646	1.5487±0.0004	0.55/0.61
B1392	$SB_{88.01}$	800	154	B+S+M	1.643	1.5468±0.0008	0.530
B1526	$FeMix_{95.93}$	750	209	B+S+M	1.658	n.d.	0.650
B1585	$FeMix_{95.93}$	800	160	B+S+M	1.642	n.d.	0.520

Table E (Cont'd)

Run No.	Starting Material	T°C	Time (hr)	Products	n_γ	d(060)	Fe/Fe+Mg (Biotite)
			Runs made at 15,000 p.s.i.				
B1432*	$FeMix_{35.21}$	850	138	B	1.624±0.003	1.5437±0.0004	0.352
B1462	$SB_{55.01}$	700	92	B+(S)	1.642	1.5465±0.0008	<0.550
B1427*	$FeMix_{55.01}$	700	116	B	n.d.	1.5471±0.0006	0.550
B1453*	$SB_{55.01}$	700	320	B	1.647	1.5487±0.0010	0.550
B1428	$(FeMix)_{55.01}$	800	186	B+S	1.633	1.5458±0.0003	0.45/0.48
B1465	$SB_{76.53}$	700	94	B+S+M	1.666	1.5493±0.0005	0.71/0.64
B1424	$(FeMix)_{76.53}$	750	212	B+S+M	n.d.	1.5496±0.0003	0.65
B1441	$(FeMix)_{76.53}$	800	117	B+S+M	1.640	1.5487±0.0016	0.51/0.57
B1473	$(P+S+M)_{76.53}$	850	823	B+S+M	1.626	n.d.	0.40
B1463	$(FeMix)_{88.01}$	700	94	B+S+M	n.d.	1.5533±0.0003	0.88
B1433	$SB_{88.01}$	700	105	B+S+M	n.d.	n.d.	
B1422	$(FeMix)_{88.01}$	700	116	B+S+M	n.d.	1.5513±0.0006	0.75

Table E (Cont'd)

Run No.	Starting Material	T°C	Time (hr)	Products	n	$d_{(060)}$	Fe/Fe+Mg (Biotite)
B1434	$SB_{88.01}$	750	116	B+S+M	1.650±0.003	1.5480±0.0007	0.58/0.58
B1419	$(FeMix)_{88.01}$	800	167	B+S+M	1.635	1.5499±0.0008	0.47/0.67
B1430	$(FeMix)_{88.01}$	850	92	B+S+M	1.631	1.5452±0.0003	0.43/0.45

Table F. Runs Buffered by Hematite-Magnetite.

Run No.	Starting Materials	T°C	Time (hr)	Products	n_γ	d(060)	Fe/Fe+Mg (Biotite)
				Runs made at 30,000 p.s.i.			
B1318*	$SB_{16.93}$	600	115	B	1.603±0.003	1.5372±0.0005	0.169
B1546	$SB_{16.93}$	700	45	B+(Sa)+(H)	1.609	1.5382±0.0002	< 0.169
B1576A*	$SB_{16.93}$	800	71	B+(S)	1.613	1.5373±0.0002	0.169
B1544*	$SB_{35.21}$	600	73	B	1.629	1.5404±0.0006	0.352
B1245	$SB_{35.21}$	700	118	B+S+H	1.635	1.5379±0.0001	0.300
B1283*	$SB_{35.21}$	700	29	B+(S)	1.630	1.5404±0.0007	0.352
B1543	$SB_{35.21}$	800	73	B+S+H	1.632	1.5396±0.0004	0.300
B1520	$SB_{35.21}$	900	6.5	B+S+M	1.633	1.5388±0.0004	0.250
B1282*	$SB_{55.01}$	520	96	B+(S)	1.645	1.5450±0.0004	0.550
B1121*	$SB_{55.01}$	545	157	B+S	1.640	1.5453±0.0004	0.550
B1082*	$SB_{55.01}$	550	190	B+(S)	1.647	1.5445±0.0004	0.550
B1224	$SB_{55.01}$	580	89	B+(S)	1.635	1.5443±0.0004	0.550
B1041*	$SB_{55.01}$	580	114	B	1.647	1.5447±0.0005	0.550

Table F (Cont'd)

Run No.	Starting Materials	T°C	Time (hr)	Products	n	d(060)	Fe/Fe+Mg (Biotite)
B1321	$SB_{55.01}$	600	94	B+S+H	1.644±0.003	1.5431±0.0007	0.460
B1320	$SB_{55.01}$	650	94	B+S+H	1.646	1.5442±0.0005	0.48/0.50
B1521	$SB_{55.01}$	700	41	B+S+H	1.627	1.5405±0.0010	0.320
B1541	$SB_{55.01}$	700	69	B+S+H+M	1.633	1.5419±0.0004	0.35/0.40
B1566	$SB_{55.01}$	725	67	B+S+H+M	1.628	1.5402±0.0005	0.310
B1554	$SB_{55.01}$	750	62	B+S+H+M	1.634	1.5411±0.0004	0.34/0.35
B1510	$SB_{55.01}$	800	28	B+S+H+M	1.633	1.5394±0.0004	0.31/0.28
B1542	$SB_{55.01}$	800	43	B+S+H+M	1.633	1.5401±0.0005	0.300
B1127*	$SB_{76.53}$	480	141	B+(S)	1.671	1.5512±0.0006	0.765
B1193	$(P+S+M)_{76.53}$	480	250	B+S+M	n.d.	1.5360±0.0007	0.110
B1192	$(P+S+M)_{76.53}$	490	717	B+S+M	n.d.	1.5382±0.0017	0.210
B1204	$SB_{76.53}$	500	69	B+S	1.659	1.5470±0.0007	0.650
B1126	$SB_{76.53}$	500	141	B+S	n.d.	1.5497±0.0004	<0.765
B1042	$SB_{76.53}$	520	72	B+S+H	n.d.	1.5461±0.0009	0.60
B1032	$SB_{76.53}$	550	44-1/2	B+S+H	n.d.	1.5460±0.0004	0.60

Table F (Cont'd)

Run No.	Starting Materials	T°C	Time (hr)	Products	$n\gamma$	$d_{(060)}$	Fe/Fe+Mg (Biotite)
B1037	$SB_{76.53}$	570	65	B+S+H+M	n.d.	1.5471±0.0006	0.65
B1026	$SB_{76.53}$	590	45	B+S+H+M	n.d.	1.5467±0.0003	0.63
B1025	$SB_{76.53}$	620	42	B+S+M	n.d.	1.5453±0.0010	0.57
B1346	$SB_{76.53}$	650	113	B+S+H+M	1.642±0.003	1.5412±0.0010	0.42/0.37
B1018	$SB_{76.53}$	680	42	B+S+H+M	1.641	1.5413±0.0014	0.41/0.37
B1179	$SB_{76.53}$	700	65	B+S+M	1.639	1.5431±0.0013	0.38/0.45
B1004	$SB_{76.53}$	750	42	B+S+M+H	1.635	1.5417±0.0005	0.34/0.38
B1573	$SB_{76.53}$	800	42	B+S+M+H	1.637	1.5396±0.0002	0.33/0.29
B1558	$SB_{88.01}$	450	475	B+S+H	n.d.	1.5498±0.0007	0.78
B1553	$SB_{88.01}$	500	159	B+S+H	n.d.	1.5509±0.0002	0.83
B1585	$SB_{93.93}$	400	140	B+S+H	n.d.	n.d.	-
				Runs made at 15,000 p.s.i. total pressure			
B1547*	$SB_{16.93}$	600	63	B+(S)	1.603	1.5378±0.0005	0.169

Table F (Cont'd)

Run No.	Starting Materials	T°C	Time (hr)	Products	n_γ	$d_{(060)}$	Fe/Fe+Mg (Biotite)
B1570*	$SB_{16.93}$	700	64	B+(Py)	1.602±0.003	1.5379±0.0002	0.169
B1579A*	$SB_{16.93}$	800	66	B+(S)	1.610	1.5381±0.0003	0.169
B1555*	$SB_{35.21}$	600	139	B+(S)+(H)	1.627	1.5410±0.0002	0.352
B1582	$SB_{35.21}$	700	67	B+(S)+(H)+(M)	1.636	1.5407±0.0004	0.352
B1568	$SB_{35.21}$	750	70	B+S+H+M	1.641	1.5397±0.0002	0.37/0.29
B1578	$SB_{35.21}$	775	46	B+S+H+M	1.637	1.5394±0.0005	0.34/0.28
B1578	$SB_{35.21}$	775	61	B+S+H+M	1.633	1.5404±0.0003	0.320
B1574	$SB_{35.21}$	800	45	B+S+H+M	1.635	1.5392±0.0008	0.32/0.27
B1560A	$SB_{35.21}$	850	28.5	B+S+H+M	1.641	1.5396±0.0008	0.30/0.29
B1560	$SB_{35.21}$	875	8	B+S+H+M	1.649	1.5395±0.0004	0.30/0.29
B1073*	$SB_{55.01}$	500	64	B+(S)	1.648	1.5448±0.0005	0.550
B1122*	$SB_{55.01}$	510	159	B+S	1.642	1.5453±0.0004	0.550
B1099*	$SB_{55.01}$	520	142	B+S	1.644	1.5443±0.0002	0.550

Table F (Cont'd)

Run No.	Starting Materials	T°C	Time (hr)	Products	n_γ	$d_{(060)}$	Fe/Fe+Mg (Biotite)
B1557	$SB_{55.01}$	600	93.5	B+S+H	n.d.	1.5395±0.0007	0.29
B1540	$SB_{55.01}$	650	70	B+S+H	n.d.	1.5402±0.0009	0.32
B1575	$SB_{55.01}$	675	69	B+S+H+M	1.636±0.003	1.5411±0.0005	0.38/0.36
B1552	$SB_{55.01}$	700	44	B+S+H+M	1.633	1.5398±0.0012	0.35/0.30
B1556	$SB_{55.01}$	750	38	B+S+H+M	1.626	1.5397±0.0005	0.28/0.29
B1551	$SB_{55.01}$	800	44	B+S+H+M	1.627	1.5390	0.27/0.26
B1205	$SB_{76.53}$	480	69	B+S	1.670	1.5479±0.0003	< 0.765
B1039*	$SB_{76.53}$	485	84	B	1.676	1.5491±0.0008	0.765
B1033*	$SB_{76.53}$	500	42.5	B+(S)	1.678	1.5490±0.0006	0.765
B1027	$SB_{76.53}$	550	43	B+S+H+M	n.d.	1.5470±0.0005	0.65
B1024	$SB_{76.53}$	600	42	B+S+H+M	1.654	1.5441±0.0005	0.53/0.51
B1022	$SB_{76.53}$	620	44	B+S	n.d.	1.5429±0.0003	0.45
B1567	$SB_{76.53}$	650	70	B+S+H+M	1.642	1.5429±0.0008	0.42/0.45
B1548	$SB_{76.53}$	750	42	B+S+H+M	1.630	1.5397±0.0004	0.31/0.29
B1184	$SB_{76.53}$	800	49	B+S+H+M	1.633	1.5405±0.0005	0.31/0.32

Table G. Runs Buffered by Copper–Cuprite.

Run No.	Starting Material	T°C	Time (hr)	Products	n_γ	d(060)	Fe/Fe+Mg (Biotite)
			Runs made at 30,000 p.s.i.				
B1394	$SB_{16.93}$	650	177	B+S+H	1.598±0.003	1.5351±0.0010	0.14/0.07
B1399	$SB_{35.21}$	800	41	B+S+H	1.608	1.5366±0.0010	0.14/0.14
B1397	$SB_{55.01}$	710	164	B+S+H	1.612	1.5377±0.0009	0.22/0.20
B1400	$SB_{55.01}$	800	118	B+S+H	1.625	1.5380±0.0010	0.26/0.21
B1398	$SB_{76.53}$	710	111	B+S+H	1.618	1.5377±0.0005	0.25/0.20

APPENDIX II

Powder X-ray data of biotites on the join phlogopite-annite.

H. Powder X-ray diffraction data for synthetic biotite B1415 ($SB_{55.01}$).

J. Powder X-ray diffraction data for synthetic biotite B1375 ($SB_{88.01}$).

K. Powder X-ray diffraction data for synthetic annite (B1388).

Table H. Powder X-ray Diffraction Data for Synthetic Biotite B1415 ($SB_{55.01}$).

FeKα 2θ obs.	Q x10^5 obs.	hkl 1M	ΔQ	hkl 3T	ΔQ	I	d
10.95	00975	001	-1	0003	-1	>100	10.130
24.175	04676	020	-36	$10\bar{1}0$	-36	10	4.624
33.27	08745	003	+21	0009	+21	80	3.385
43.05	14378	200	-2	$11\bar{2}2$	-25	60	2.641
44.89	15564	004	+20	000(12)	+20	5	2.542
46.57	16675	201	-36	$11\bar{2}5$	-49	0	2.455
52.45	20853	202	-9	$11\bar{2}8$	-7	20	2.190
57.075	24378	005	-28	000(15)	-28	10	2.025
60.275	26895	203	+99	$11\bar{2}(11)$	+20	5	1.929
69.925	35052	006	+12	000(18)	+12	10	1.689
77.500	41752	060	0	$30\bar{3}0$	0	20	1.548
78.450	42693	330	+93	$30\bar{3}3$	+41	10	1.530

Table J. Powder X-ray Diffraction Data for Synthetic Biotite B1375 ($SB_{88.01}$).

FeK_α 2θ obs.	$Q \times 10^5_{obs.}$	hkl (1M)	ΔQ (1M)	hkl (3T)	ΔQ (3T)	I	d
10.95	00975	001	-2	0003	-2	>100	10.130
22.00	03886	002	+6	0006	+6	5	5.073
24.075	04638	020	-30	$10\bar{1}0$	-30	10	4.643
28.20	06334	111	0	$10\bar{1}4$	+2	5	3.973
30.275	07510	121	-26	$10\bar{1}5$	-202	5	3.649
32.650	08441	022	+59	$10\bar{1}6$	+59	5	3.442
33.300	08762	003	-5	0009	-5	80	3.378
35.475	09901	112	-7	$10\bar{1}7$	-1	15	3.178
38.350	11523	$11\bar{3}$	+31	$10\bar{1}8$	-3	10	2.946
41.400	13334	023	+26	$10\bar{1}9$	+22	5	2.739
42.900	14272	200	0	$11\bar{2}2$	-16	70	2.647
44.900	15564	004	+4	000(12)	+4	30	2.535
46.325	16518	201	+9	$11\bar{2}5$	+6	50	2.461
49.225	18518	$22\bar{1}$	+53	$20\bar{2}1$	+22	5	2.324
50.150	19181	$20\bar{3}$	+2	$11\bar{2}7$	-65	10	2.283
52.325	20753	202	-27	$11\bar{2}8$	-19	40	2.195
57.250	24507	$10\bar{5}$ 005	+181 -182	$11\bar{2}(10)$ 000(15)	+117 -182	30	2.020
60.250	26896	203	-24	$11\bar{2}(11)$	-4	5	1.928
69.900	35023	006	+5	000(18)	+5	30	1.690
77.150	41462	060	-	$30\bar{3}0$	-	50	1.553
78.175	42419	330 061	+61 +16	$30\bar{3}3$	+25	20	1.535

Table K. Powder X-ray Diffraction Data for Synthetic Annite (B1388).

FeK_α 2θ obs.	$Q \times 10^5$ obs.	hkl 1M	ΔQ (M1)	hkl (3T)	ΔQ (3T)	I	d
11.000	00980	001	-3	0003	-3	>100	10.100
22.110	03921	002	-13	0006	-13	7	5.050
24.160	04676	020	-72	$10\bar{1}0$	-72	20	4.624
25.140	05053	012	+6	$10\bar{1}2$	-15	10	4.449
28.290	06364	111	+8	$10\bar{1}4$	-23	3	3.964
30.310	07384	$11\bar{2}$	-92	$10\bar{1}5$	-66	0	3.680
32.825	08525	022	-13	$10\bar{1}6$	-13	7	3.453
33.390	08795	102 003	+6 -2	0009	-2	70	3.372
35.580	09937	112	+15	$10\bar{1}7$	-14	10	3.172
38.475	11581	$11\bar{3}$	-69	$10\bar{1}8$	-30	7	2.924
41.580	13437	023	-40	$10\bar{1}9$	-40	5	2.728
42.880	14251	200	0	$11\bar{2}2$	-5	80	2.649
45.040	15651	004	-19	000(12)	-20	30	2.528
46.450	16608	201	-49	$11\bar{2}5$	-84	50	2.454
48.090	17724	211	-14	$11\bar{2}6$	-4	3	2.375
49.200	18494	$22\bar{1}$	+9	$20\bar{2}0$	-78	10	2.325
50.020	19068	$20\bar{3}$	-13	$11\bar{2}7$	+63	10	2.290
51.460	20144	$22\bar{2}$	-40	$20\bar{2}4$	+9	3	2.228
52.420	20828	202	-8	$11\bar{2}8$	-69	30	2.191
57.490	24691	$10\bar{5}$ 005	-29 -266	$11\bar{2}(10)$ 000(15)	-24 -266	20	2.012
60.380	26951	203	+84	$11\bar{2}(11)$	-4	7	1.926
66.380	31977	$20\bar{5}$	+50			3	1.768

Table K (Cont'd)

$2\theta_{obs.}$ (FeKα)	$Q \times 10^5_{obs.}$	hkl 1M	ΔQ (M1)	hkl (3T)	ΔQ (3T)	I	d
70.030	35140	006	+32	000(18)	+32	20	1.687
77.140	41449	060	-	$30\bar{3}0$	-13	50	1.553
78.240	42488	061 330	-62 -62	$30\bar{3}3$	-75	10	1.534

BIOGRAPHICAL SKETCH

David Robert Wones was born in San Francisco, California, July 13, 1932. The third child and second son of Edward Martin Wones and Hannah Pearson Wones, he was brought up in the life of an army family. He attended Punahou School in Honolulu, Hawaii, and Thomas Jefferson High School in San Antonio, Texas, receiving his high school diploma from the latter.

He entered the Massachusetts Institute of Technology in September 1950 as the recipient of an Army-Navy undergraduate scholarship, and received his S. B. in geology in June 1954. He entered the M. I. T. Graduate School in September 1954 and served as a Teaching Assistant until June 1956.

In February 1957 he became the first Vannevar Bush fellow of the M. I. T. Geology Department, and thereupon conducted research on the major portion of this thesis at the Geophysical Laboratory of the Carnegie Institution of Washington until June 1959. In June 1959 he accepted an appointment as geologist with the United States Geological Survey. On November 3, 1959, he entered the Armed Forces as a second lieutenant, USAR, Corps of Engineers, on an abbreviated tour of active duty for training which terminated May 2, 1960.

Mr. Wones is a member of the Geochemical Society, the Mineralogical Society of America, the Geological Society of Washington, and Sigma Xi. He has delivered papers at the Geological Society of America and the American Geophysical Union, and has addressed the Petrologists' Club of Washington, D. C.

He married the former Constance Gilman of Ayer, Massachusetts, on August 24, 1958. They have one child, Edward Martin Wones IV.

BIBLIOGRAPHY

Adams, L. H., 1931, The compressibility of fayalite and the velocity of elastic waves in peridotite with different iron-magnesium rations: Gerl. B. z. Geoph., v. 31, p. 315-321.

Barrow, G., 1893, On an intrusion of muscovite-biotite gneiss in the southeastern highlands of Scotland, and its accompanying metamorphism: Geol. Soc. London Quart Jour., v. 49, p. 330.

Bogatskii, 1938, Investigation of the equilibrium of the reaction NiO + CO = Ni + CO_2: Metallurg., v. 13, no. 2, p. 18.

Boyle, B. J., King, E. G., and Conway, K. C., 1954, Heat of formation of nickel and cobalt oxides (NiO and CoO) of combustion colorimetry: Am. Chem. Soc. Jour., v. 76, p. 3835.

Buddington, A. F., 1929, Granite phacoliths and their contact zones in the northwest Adirondacks: N. Y. State Mus. Bull. 281, p. 51.

Chinner, G. A., 1958, Unpublished Ph.D. thesis, Cambridge University.

Coats, R. R., and Fahey, J. J., 1944, Siderophyllite from Brooks Mountain, Alaska: Am. Mineralogist, v. 29, p. 373.

Coombs, D. S., 1954, Ferriferous orthoclase from Madagascar: Mineralog. Mag., v. 30, p. 409.

Coughlin, J. P., King, E. G., and Bonnickson, K. R., 1951, High temperature heat contents of ferrous oxide, magnetite, and ferric oxide: Am. Chem. Soc. Jour., v. 76, p. 3891.

Crowley, M. S., and Roy, R., 1960, The effect of formation pressures on sheet structures - a possible case of Al-Si ordering: Geochim. et Cosmochim. Acta, v. 18, p. 94.

Darken, L. S., 1948, Melting points of iron oxides on silica: phase equilibria in the system Fe-Si-O as a function of gas composition and temperature: Am. Chem. Soc. Jour., v. 70, p. 2046.

Darken, L. S., and Gurry, R. W., 1945, The system iron-oxygen. I. The wustite field and related equilibria: Am. Chem. Soc. Jour., v. 67, p. 1398.

Darken, L. S., and Gurry, R. W., 1946, The system iron-oxygen. II. Equilibria and thermodynamics of liquid oxides and other phases: Am. Chem. Soc. Jour., v. 68, p. 798.

Donnay, J. D. H., and Nowacki, W., 1954, Crystal data: Geol. Soc. America Memoir 60.

Ernst, W. G., 1957, Alkali amphiboles: Carnegie Inst. Washington, Yearbook 57, p. 119-206.

BIBLIOGRAPHY (Cont'd)

Eugster, H. P., 1957a, Heterogeneous reactions involving oxidation and reduction at high pressures and temperature: Jour. Chem. Physics, v. 26, p. 1760.

Eugster, H. P., 1957b, Stability of annite: Carnegie Inst. Washington Yearbook 57, p. 161.

Eugster, H. P., 1959, Reduction and oxidation in metamorphism, in Abelson, P. H., editor, Researches in geochemistry: New York, John Wiley and Sons, p. 397.

Foster, P. K., and Welch, A. J. E., 1956, Metal-oxide "solid solutions" I. Lattice-constant and phase relationships in ferrous oxide (wustite) and in solid solutions of ferrous oxide and manganous oxide. IV. Activity relationships in solid solutions of ferrous oxide and manganous oxide: Faraday Soc. Transactions, p. 1626 and p. 1636.

Foster, M. D., 1957, Interpretation of the compositions of trioctahedral micas (abs.): U. S. Geol. Survey Bull. 60, p. 1729.

Fyfe, Turner, and Verhoogen, 1958, Metamorphic relations and metamorphic facies: Geol. Soc. America Memoir 73.

Gower, J. A., 1957, X-ray measurement of the iron-magnesium ratio in biotites: Am. Jour. Sci., v. 255, p. 142.

Grout, F. F., 1924, Notes on biotites: Am. Mineralogist, v. 9, p. 159.

Hall, A. J., 1941, The relation between color and chemical compositions in the biotites: Am. Mineralogist, v. 26, p. 29.

Harker, A., 1939, Metamorphism: London, Methuen.

Heinrich, E. W., 1946, Studies in the mica group; the biotite-phlogopite series: Am. Jour. Sci., v. 244, p. 836.

Hellner, E., and Euler, R., 1957, Hydrothermale und rontgeneographische Untersuchungen on gesteins bildenden Meneralen. I. Über ein geologisches Thermometer auf Grund von Untersuchungen au Biotiten /Hydrothermal and X-ray investigations of rock-forming minerals. I. On a geological thermometer of sediments from investigations of biotite/: Geochim. et Cosmochim. Acta, v. 12, p. 47.

Hemley, J. J., 1959, Some mineralogical equilibria in the system K_2O-Al_2O_3-SiO_2-H_2O: Am. Jour. Sci., v. 257, p. 241.

Holland, H. D., 1959, Some applications of thermochemical data to problems of ore deposits. I. Stability relations among the oxides, sulfides, sulfates and carbonates of ore and gangue metals: Econ. Geology, v. 54, p. 184.

BIBLIOGRAPHY (Cont'd)

Holmes, A., 1942, A suite of volcanic rock from south-west Uganda containing kalsilite (a polymorph of $KAlSiO_4$): Mineralog. Mag., v. 2, p. 197.

Holser, William T., 1954, Fugacity of water at high temperatures and pressures: Jour. Phys. Chem., v. 5, p. 316.

Hu, J., and Johnston, H. L., 1951, Low temperature heat capacities of inorganic solids. IX. Heat capacity and thermodynamic properties of cuprous oxide from 140 to 300°C: Am. Chem. Soc. Jour., v. 73, p. 2471.

Humphrey, G. L., and King, E. G., 1952, Heats of formation of quartz and cristobalite: Am. Chem. Soc. Jour., v. 74, p. 2041.

Humphrey, G. L., King, E. G., and Kelley, K. K., 1952, Some thermodynamic values for ferrous oxide: U. S. Bur. Mines Rept. Inv. 4870.

Jakob, J., and Parga-Pondal, G., 1932, Über die Rolle des Titans in den Phlogopiten [On the role of titanium in phlogopite]: Zeitschr. Krist., v. 82, p. 271.

Kelley, K. K., 1949a, Contributions to the data on theoretical metallurgy. IX. Entropies of inorganic substances: U. S. Bur. Mines Bull. 434.

Kelley, K. K., 1949b, Contributions to the data on theoretical metallurgy. X. High temperature heat content, heat capacity, and entropy data for inorganic compounds: U. S. Bur. Mines Bull. 476.

Kelley, K. K., 1950, The entropies of inorganic substances: revision of data: U. S. Bur. Mines Bull. 477.

Kelley, K. K., Barany, R., King, E. G., and Christensen, A. H., 1959, Some thermodynamic properties of flurophlogopite mica: U. S. Bur. Mines Rept. Inv. 5436.

Kelley, K. K., Todd, S. S., Orr, R. L., King, E. G., and Bonnickson, K. R., 1953, Thermodynamic properties of sodium aluminum and potassium aluminum silicates: U. S. Bur. Mines Rept. Inv. 4955.

Kerr, P. K., 1955, Hydrothermal alteration and weathering, in Poldervaart, A., editor, Crust of the earth: Geol. Soc. America Special Paper 62, p. 525-543.

King, E. G., 1952, Heats of formation of manganous metasilicate (rhodonite) and ferrous orthosilicate (fayalite): Am. Chem. Soc. Jour., v. 74, p. 4446.

BIBLIOGRAPHY (Cont'd)

King, E. G., 1957, Heats of formation of manganous metasilicate (rhodonite) and ferrous orthosilicate (fayalite): Am. Chem. Soc. Jour., v. 79, p. 2399.

King, E. G., and Christensen, A. U., Jr., 1958, Heat contents above 298.15°K of oxides of cobalt and nickel: Am. Chem. Soc. Jour., v. 80, p. 1800.

Kiukkola, K., and Wagner, C., 1957, Measurements on galvanic cells involving solid electrolytes: Jour. Electrochem. Soc., v. 104, p. 379.

Kozu, S., and Yoshika, B., 1926, Thermo-optic studies of anomite-basaltic hornblende-quartz-andesite in association with biotite-common hornblende-quartz-andesite which together form the Volcano Sambé in Japan: Tohoku Univ. Sci. Repts., v. 3, p. 177.

Kracek, F. C., Neuvonen, K. J., Burley, G., and Gordon, R. J., 1953, Contributions of thermochemical and X-ray data to the problem of mineral stability; thermochemical properties of minerals: Carnegie Inst. Washington Yearbook 53, p. 69-72.

Krauskopf, K. B., 1959, The use of equilibrium calculations in finding the composition of a magmatic gas phase: Abelson, P. H., editor, Researches in geochemistry: New York, John Wiley and Sons, p. 260.

Kubaschewski, O., and Evans, E. T., 1958, Metallurgical thermochemistry: New York, John Wiley and Sons, Inc.

Kunitz, 1924, Der bezichungen zwischen der chemischen zusammensetzung und den physikalisch-optischen eigenschaften innerhalb der glimmergruppe [The relation between the chemical composition and the physical-optical properties within the mica group]: Neues Jahrb. Geologie u. Palaontologie Abhd., Beil Bd., v. 50, p. 364.

Larsen, E. S., Irving, J., Gonyer, F. A., and Larsen, E. S. 3rd, 1937, Petrological results of a study of the minerals from the Tertiary volcanic rocks of the San Juan region, Colorado: Am. Mineralogist, v. 22, p. 889.

Lovering, T. S., 1949, Rock alteration as a guide to ore—East Tintic District, Utah: Econ. Geology, Monograph 1, p. 65.

Maier, C. G., 1929a, The reduction of cuprous oxide by carbon monoxide: U. S. Bur. Mines Rept. Inv., serial 2926.

Maier, C. G., 1929b, Oxide cells of cadmium, copper, tin and lead: Am. Chem. Soc. Jour., v. 51, p. 194.

Makolkin, I. A., 1942, Electrochemical determination of thermodynamic constants of oxides of several metals: Jour. Phys. Chem. (USSR), v. 16, p. 13-17.

BIBLIOGRAPHY (Cont'd)

Morey, G. W., 1957, The solubility of solids in gases: Econ. Geology, v. 52, p. 225.

Muan, A., 1955, Phase equilibria in the system $FeO-Fe_2O_3-SiO_2$: Jour. Metals, v. 7, Sept. 55, p. 1.

Muan, A., and Osborne, E. F., 1955, Phase equilibria at liquidus temperatures in the system $MgO-FeO-Fe_2O_3-SiO_2$: Jour. Am. Ceram. Soc., v. 39, p. 121.

Newton, Roger H., 1935, Activity coefficients of gases: Indus. and Eng. Chemistry, v. 27, p. 302.

Nockolds, S. R., 1940, The Garabal Hill-Glen Fyne igneous complex: Geol. Soc. London Quart. Jour., v. 96, p. 451.

Nockolds, S. R., 1947, The relation between chemical composition and paragenesis in the biotite micas of igneous rocks: Am. Jour. Sci., v. 245, p. 401.

Nockolds, S. R., and Mitchell, R. L., 1948, The geochemistry of some Caledonian plutonic rocks: a study in the relationship between the major and minor trace elements of igneous rocks and their minerals: Royal Soc. Edinburgh Trans., v. 61, p. 533.

Norton, F. J., 1955, Dissociation pressures of iron and copper oxides: General Electric Res. Lab. Rept. No. 55-RL-1248.

Orr, R. L., 1953, High temperature heat contents of magnesium orthosilicate and ferrous orthosilicate: Am. Chem. Soc. Jour., v. 75, p. 528.

Ostrovskii, I. A., 1954, Experiments in the system biotite-water, fayalite-water. Aspects of the role of hydrogen in granite magma: Dokl. Akad. Nauk /USSR/, v. 108, p. 1164.

Palache, C., Berman, H., and Frondel, C., 1944, Dana's System of mineralogy: New York, John Wiley and Sons, v. 1.

Randall, Merle, Nielsen, Ralph F., and West, George H., 1931, Free energy of some copper compounds: Indust. and Eng. Chem., v. 28, p. 388.

Richardson, F. D., and Jeffes, J. H. E., 1948, The thermodynamics of substances of interest in iron and steel making from 0°C to 2000°C. I. Oxides: Jour. Iron and Steel Institute, v. 160, p. 261.

Rinne, F., 1925, Rontgenographische Diagnostik beins Brennen von Kalkstein, Dolomit, Kaolin, und Glimmer /X-ray analysis of roasted limestone, dolomite, kaolin, and mica/: Zeitschr. Krist., v. 61, p. 113.

BIBLIOGRAPHY (Cont'd)

Roberts, H. S., and Smythe, F. H., 1921, The system copper-cupric oxide-oxygen: Am. Chem. Soc. Jour., v. 43, p. 1061.

Rooksby, H. P., 1951, Oxides and hydroxides of aluminum and iron, in Brindley, G. W., editor, X-ray identification and crystal structure of clay minerals: London, Mineralogical Society.

Roy, R., 1949, Decomposition and resynthesis of the micas: Jour. Am. Ceram. Soc., v. 32, p. 202.

Sales, R. H., and Meyer, C., 1949, Results from preliminary studies of vein formation at Butte, Montana: Econ. Geology, v. 44, p. 465-484.

Schairer, J. F., 1954, The system K_2O-MgO-Al_2O_3-SiO_2: I. Results of quenching experiments on four joins in the tetrahedron cordierite-forsterite-leucite-silica and on the join cordierite-mullite-potash-feldspar: Jour. Am. Ceram. Soc., v. 37, p. 501.

Schenk, R., Franz, H., and Laymann, A., 1932, Gleichgewichtsuntersuchung uber die ruduktions-oxidations-und kohlungsvorgange beim lisen. XI [Equilibrium investigations of the reduction and oxidation reactions of iron and carbon.]: Z. Anorg. allgem. Chemie, v. 206, p. 126.

Schwartz, G. M., 1959, Wall rock alteration: Econ. Geology, v. 54, p.

Smith, J. V., and Yoder, H. S., 1956, Experimental and theoretical studies of the mica polymorphs: Mineralog. Mag., v. 31, p. 209.

Stirland, D. J., Thomas, A. G., and Moore, N. C., 1958, Observations on thermal transformations in alumina: British Ceram. Soc. Trans., v. 57, p. 69.

Thompson, J. B., Jr., 1955, The thermodynamic basis for the mineral facies concept: Am. Jour. Sci., v. 253, p. 65.

Thompson, J. B., Jr., 1957, The graphic analysis of mineral assemblages in pelitic schists: Am. Mineralogist, v. 42, p. 842.

Tilton, G. R., Wetherill, G. W., Davis, G. L., and Hopson, C. A., 1958, Ages of minerals from the Baltimore gneiss near Baltimore, Maryland: Geol. Soc. America Bull., v. 69, p. 1469.

Turner, F. J., 1948, Mineralogical and structural evolution of the metamorphic rocks: Geol. Soc. America, Mem. 30.

Turnock, A. C., and Eugster, H. P., 1958, Magnetite-hercynite relations: Carnegie Inst. Washington Yearbook 58, p. 209.

Tuttle, O. F., 1949, Two pressure vessels for silicate-water studies: Geol. Soc. America Bull., v. 60, p. 1727.

BIBLIOGRAPHY (Cont'd)

Tuttle, O. F., 1953, Optical studies on alkali feldspars: Am. Jour. Sci., Bowen vol., p. 553.

Veres, G. I., Merenkova, T. B., and Ostrovskii, I. A., 1955, Synthetic pure iron hydroxyl mica: Dokl. Akad. Nauk [USSR], v. 101, p. 147.

Wagman, D. D., Kilpatrick, J. E., Taylor, W. J., Pitzer, K. S., and Rossini, F. D., 1945, Heats, free energies and equilibrium constants of some reactions involving O_2, H_2, H_2O, C, CO, CO_2, and CH_4: [U.S.] Natl. Bur. Standards Jour. Research, v. 34, p. 143.

Wagner, C., and Hammen, H., 1938, Bestimmung des Sauerstoff über schuss gebaltes der Kupperoxydulphase [The determination of oxygen above the charge capacity of cuprous oxide (cuprite)]: Zeitschr. Physik. Chemie, v. 40, p. 197.

Winchell, A. N., 1935, The biotite system: Am. Mineralogist, v. 20, p. 773.

Winchell, A. N., 1951, Elements of optical mineralogy. Pt. II. Description of minerals: New York, John Wiley and Sons, Inc., p. 373-377.

Winkler, H. G. F., 1954, Synthese von Hornblende und Biotite [The synthesis of hornblende and biotite]: Naturwissen-schaften, v. 41, p. 574.

Winkler, H. G. F., 1957, Experimentalle Gesteinmetamorphase. I. Hydrothermals Metamorphase karbonst-preier Tone [Hydrothermal metamorphism of carbonate free shale]: Geochim. et Cosmochim. Acta, v. 13, p. 42.

Wyckoff, R. W. G., 1926, The crystal structure of the high temperature modification of quartz: Am. Jour. Sci., v. 211, p. 101.

Wones, D. R., and Eugster, H. P., 1958, Phase relations of hydrous silicates with intermediate Mg/Fe ratios: Carnegie Inst. Washington Yearbook 58, p. 193.

Wones, D. R., and Eugster, H. P., 1959, Biotites on the join phlogopite ($KMg_3AlSi_3O_{10}(OH)_2$-annite ($KFe_3AlSi_3O_{10}(OH)_2$): Carnegie Inst. Washington Yearbook 59, p. 127.

Wrigge, F. W., and Meisel, K., 1932, Die dichte von Kupferoxydul [The density of cuprous oxide]: Zeitschr. Anorg. allgem. Chem., v. 203, p. 312.

BIBLIOGRAPHY (Cont'd)

Wyart, J., and Sabatier, T., 1959, Transformation des sediments pelitiques a 800°C sous une pression d'eau de 1800 bars et granitisations. [Granitization and the transformation of peletic schists at temperatures up to 800°C under water pressure of 1800 bars]: Soc. francaise mineralogie et crystallographie Bull.

Yoder, H. S., 1959, Experimental studies on micas: A synthesis: in Proceedings of the Sixth National Conference on Clays and Clay Minerals: New York, Pergamon Press.

Yoder, H. S., and Eugster, H. P., 1954, Phlogopite synthesis and stability range: Geochim. et Cosmochim. Acta, v. 6, p. 157.

Yoder, H. S., and Eugster, H. P., 1955, Synthetic and natural muscovites: Geochim. et Cosmochim. Acta, v. 8, p. 225.